

Theoretical and experimental study on
local expansion and transformation of
photonic W states

A dissertation submitted to
THE GRADUATE SCHOOL OF ENGINEERING SCIENCE
OSAKA UNIVERSITY
in partial fulfillment of the requirements for the degree of
DOCTOR OF PHILOSOPHY IN SCIENCE

BY

TOSHIYUKI TASHIMA

MARCH 2009

Abstract

In this work, we investigate the preparation and local manipulation of photonic W states, which have interesting structure of forming a weblike structure in which every qubit is entangled with every other qubit with the optimal bipartite entanglement.

The first part of this thesis covers three elementary optical gates we have designed for the preparation, expansion and fusion of W states. In all these operations, we restrict ourselves to local manipulations at a single site and classical communication. The first gate extends an N -photon W state into an $(N + 1)$ -photon W state using a polarization dependent beamsplitter and an ancillary one-photon Fock state. The second gate is composed of two beamsplitters and it uses an ancillary two-photon Fock state. This gate expands an N -photon W state into an $(N + 2)$ -photon W state. The last gate is a fusion gate that receives one photon from each of two arbitrary size W states (W_N and W_M) and when successful it fuses them together to produce a larger W state with $N + M + 2$ photons.

The second part of the thesis contains an experimental demonstration of how two EPR photon pairs can be transformed into a three-photon W state by local operations and classical communication with a high fidelity. The key ingredient in this experiment is a polarization dependent beamsplitter, which has different transmission/reflection characteristics for horizontal and vertical polarized photons. We characterized the final state using quantum state tomography on the three-photon state and on its marginal bipartite states experimentally. The fidelity of the final state to the ideal W state is 0.778 ± 0.043 and the expectation value for its witness operator is -0.111 ± 0.043 implying the success of the proposed local transformation.

Acknowledgments

First of all, I would like to thank my supervisor Prof. Nobuyuki Imoto for allowing me the freedom to explore my interests and giving me great advice and support. It is also a great pleasure for me to thank Assoc. Prof. Masato Koashi for his advice, support, and his excellent lectures on quantum mechanics, quantum information and quantum optics.

This thesis would not be possible were it not for the support of Dr. Takashi Yamamoto and Dr. Şahin Kaya Özdemir. I have always appreciated inspiring discussions with them, their advices on all of my work, and great support through the years of my master course and my PhD course. I would like to say thank you to Dr. Ryo Namiki, Dr. Yuuki Tokunaga, Dr. Jun-ichi Shimamura, Kazuhiro Yokota, Koji Azuma and Yoritoshi Adachi for their friendship, support, and fruitful discussions on various topics. It is also my great pleasure to thank the other members on the group for the enjoyable times spent together.

I would also thank to Prof. Harald Weinfurter at Max-Planck-Institut für Quantenoptik and Ludwig-maximilians Universität München in Germany who kindly accepted my two weeks stay in his group. During this stay, I had the chance to meet and discuss on various topic related with multipartite entanglement with Witlef Wieczorek, Dr. Nikolai Kiesel, Dr. Christian Schmid, Roland Krischek. I thank them for their hospitality and help.

Finally , I would like to dedicate this thesis to my parents, my brother and sister, my friends.

Contents

1	Introduction	11
1.1	Background	11
1.2	Motivation and outline of our work	13
1.2.1	Local expansion and fusion of multipartite W state	13
1.2.2	Local transformation of two EPR pairs into a tripartite W state	15
2	Classification and evaluation of Multipartite entanglement	17
2.1	Brief introduction to quantum information	17
2.1.1	Quantum bits	17
2.1.2	Elements of quantum mechanics	19
2.1.3	Fidelity	21
2.2	Bipartite entanglement	21
2.2.1	Bell basis	23
2.2.2	Concurrence	23
2.2.3	Peres-Horodecki criterion	24
2.3	Multipartite entanglement	25
2.3.1	Classification of tripartite entanglement	25
2.3.2	Entanglement witness	27
3	Engineering and measurement with polarization entangled photons	29
3.1	Spontaneous parametric down conversion	29
3.2	Entangled photon pair generation	31

3.3	Wave plates	32
3.4	Beamsplitters	32
3.5	Quantum state tomography and maximum likelihood estimation	34
4	Local expansion and fusion of a multipartite W state	39
4.1	Local expansion of photonic W state using a polarization dependent beam-splitter	40
4.1.1	Working principle of W state expansion	40
4.1.2	Expansion of polarization entangled W states	43
4.1.3	Practical considerations for preparing W_3 state	44
4.1.4	Brief discussion	48
4.2	Local expansion of photonic W state using two non-polarizing beamsplitters	49
4.2.1	Working principle of the gate	50
4.2.2	Expansion of polarization entangled W states	53
4.2.3	Practical considerations for preparing W_4 state	55
4.2.4	Expansion of polarization entangled GHZ states	60
4.2.5	Brief discussion	61
4.3	Optical fusion gate for two arbitrary-size W states	62
4.3.1	Working principle of fusion gate for W states	62
4.3.2	Linear optics implementation	65
4.3.3	Example of fusing two four-photon W states	67
4.3.4	Brief discussion	68
4.4	Discussion	69
5	Local transformation of two EPR pairs into a tripartite W state	71
5.1	Schematics of local transformation from two EPR photon pairs to a three-photon W state	71
5.1.1	Concept	72
5.1.2	Experimental scheme	72
5.2	Experimental setup	77

5.3	Experimental results	79
5.3.1	Interference of two EPR photon pairs at a PDBS	79
5.3.2	Characterization of initial EPR photon pairs	81
5.3.3	Characterization of the prepared three-photon W state	83
5.4	Discussion	87
6	Conclusion and Future Prospects	91
6.1	Summary	91
6.2	Future Outlook	93
A	Expansion and fusion of polarization entangled GHZ states using a polarizing beamsplitter	95
B	Alignment	99
C	Measurement data	103
	Publications	105
	Activities	107

Chapter 1

Introduction

1.1 Background

In 1935, Albert Einstein, Boris Podolsky and Nathan Rosen (EPR) implied a groundbreaking notion that the counterintuitive features of entanglement, which was named by Erwin Schrödinger [1], cause effects that raise the incompleteness of quantum mechanics [2]. For a long time, most physicists have been enchanted by the notion of entanglement. In 1964, John Bell pointed out that EPR problem indeed leads to gedanken experiment that do not behave according to the predictions of classical physics. His approach has become an important test to determine whether a given physical system abides the rules of classical physics or those of quantum mechanics [3]: If the statistics of the measurement outcomes violate the so-called “*Bell inequalities*” then one can safely conclude the presence of entanglement in the system. In the past years, a number of different Bell inequalities have been proposed and experiments have been performed to check the violation of these inequalities on various systems [4-6]. The reconciliation on the notion of entanglement among the quantum physicists opened an exciting phase in the research of quantum mechanics. Entanglement is now regarded as a purely quantum mechanical resource that plays an essential role in various quantum information processing tasks [7-26]. We can now use entanglement for quantum teleportation [7], quantum key distribution (QKD) [8], quantum computation [9]

and quantum metrology [10].

Research in quantum information science carried out in the past few decades has revealed most of the interesting properties of bipartite entanglement: We know how to prepare, characterize and quantify entanglement between two subsystems of a larger system. In particular, given a single resource of qubits in a maximally entangled state in a bipartite system, which is called an EPR pair, any bipartite qubit state can be prepared using only local operations and classical communication (LOCC). In other words, any bipartite qubit state can be prepared from an EPR pair without direct interaction between the systems located far apart. By contrast, entanglement among three or more systems still remains as a challenge because such qubits have a richer and more complex structure which originates from the existence of different ways the qubits can be entangled with each other such as the Greenberger-Horne-Zeilinger (GHZ)-type state [27], W-type state [28, 29], cluster state [30] and Dicke state [31]. The higher is the number of parties entangled, the more complicated are the preparation, control and manipulation of entanglement, as well as the quantification of its amount in the multipartite system. Thus, it is necessary to study their classification and properties from the standpoint of theory and experiment. In addition, it is also desirable that preparation and manipulation are carried out in an elegant and efficient way, and the characterization of the state is efficiently estimated by a low number of measurement data sets.

In 1997, preparation schemes of a three-photon GHZ state and a four-photon GHZ state were first proposed by Zeilinger *et al.* [32]. In 1999, D. Bouwmeester *et al.*, [33] demonstrated the preparation of a three-photon GHZ state. In the same year, J. G. Rarity *et al.* [34] demonstrated a preparation of a three-photon GHZ state using an EPR photon pair and weak coherent light. In 2005, Resch *et al.* [35] demonstrated a local transformation of two EPR photon pairs into a three-photon GHZ state using a polarizing beamsplitter that performs parity checking. They then characterized the density matrix of the prepared three-photon state by quantum state tomography. Using bell-multiport beamsplitter and four single photon sources, a preparation scheme of a four-photon GHZ state was proposed by Lim *et al.* [36]. In 2007, Walther *et al.* [37] proposed a preparation scheme of a multi-

photon GHZ state. On the other hand, for a W state, Zeilinger *et al.* [38] proposed a scheme using third order optical nonlinearity for three photons entangled in their paths in 1997. In 2002, Yamamoto *et al.* [39] proposed the scheme for preparing a three-photon W state from four photons emitted by parametric down-conversion (PDC). A preparation of three-photon W state were demonstrated by Kiesel *et al.* [40] in 2003 and Eibl *et al.* [41] in 2004. In 2005, Mikami *et al.* [42] demonstrated a preparation of a three-photon W state by using one EPR photon pair and weak coherent light. In the same year, Walther *et al.* [43] demonstrated local conversion of a three-photon GHZ state into an approximate W state. For a four-photon W state, there have been four proposals so far: (i) The scheme introduced by X. Zou *et al.* [44] requires an EPR photon pair from PDC process and two single photons as input modes. (ii) The scheme of Lim *et al.* [36] and B.-S. Shi *et al.* [45] employs 4×4 lossless multiport fiber beam splitter and four single photons. (iii) The scheme proposed by Y. Li *et al.* [46] uses four photons generated by parametric down-conversion (PDC). On the basis of these historical backgrounds, in the next section, we will give the motivation for the present study and the thesis.

1.2 Motivation and outline of our work

In this work, we have focused our research on the preparation and local manipulation of photonic W states due to their interesting structure of forming a weblike structure in which every qubit is entangled with every other qubit with the optimal bipartite entanglement. Our work can be grouped into two sections. Below we give our motivation in carrying out this research.

1.2.1 Local expansion and fusion of multipartite W state

The distinction between GHZ and W states shows up when we consider how one can increase the number of qubits forming W or GHZ states. In the case of GHZ states, there is a systematic way to extend its size without accessing all of the qubits: One can pick the N -th qubit of GHZ state and let it interact with a new qubit to produce the $N + 1$

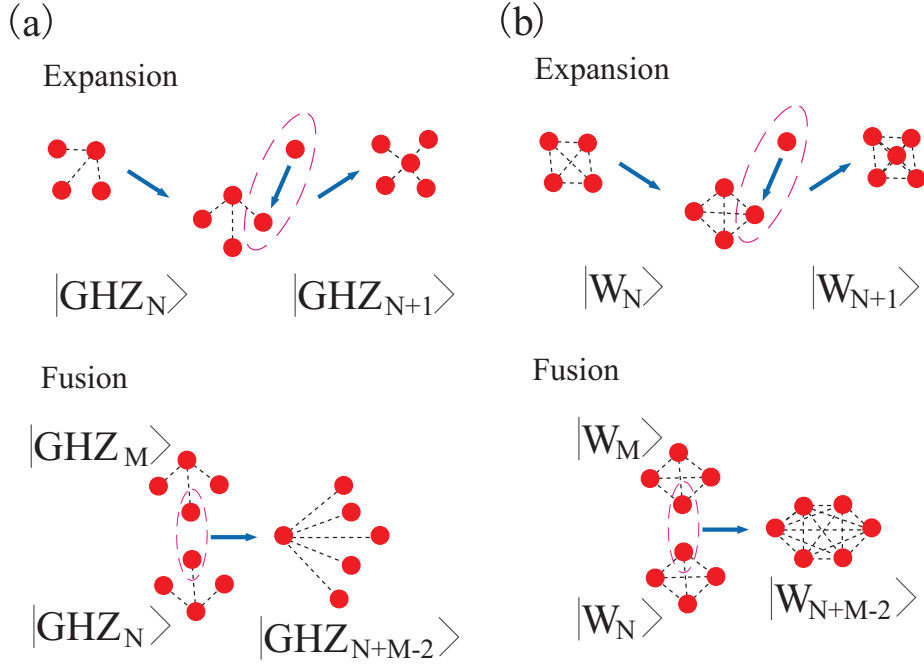


Figure 1.1: Local expansion and fusion of (a) a GHZ-type state and (b) a W-type state.

qubit GHZ state [see Fig. 1.1 (a)]. This is not surprising since (i) the marginal state of the remaining untouched $N - 1$ qubits is the same for the N qubit GHZ state and the $N + 1$ qubit GHZ state, and (ii) the N -th qubit is pivotal such that if we remove and discard it, the rest of the qubits will be disentangled. It has been shown that GHZ state as the initial seeds, quantum parity checking gates [47] can be used to grow large scale GHZ state [see Appendix A]. There are schemes of Resch *et al.* [35] and Zhao *et al.* [17] using a polarizing beamsplitter acting as parity checking gates.

On the other hand, it is not so trivial whether such a local expansion of W states is possible or not. For one thing, the marginal states of $N - 1$ qubits are different for the N -qubit W state and the $(N + 1)$ -qubit W state. Hence no unitary operation on the N -th qubit and a new qubit makes the $(N + 1)$ -qubit W state [see Fig. 1.1 (b)]. In addition, newly added qubits must form the pairwise entanglement with each of the uninteracted $N - 1$ qubits. So far, the study of W states using linear optics have been lagging, and

it begs for efficient elementary-gate-based approach which will enable large scale W-state networks. Current proposals for W states either suffer from low success probability or the requirement of fragile interferometers besides their non-cascadable structures.

In this thesis, we propose two local expansion schemes and one fusion scheme for photonic W states. We first propose the local expansion scheme using one polarization dependent beamsplitter [48] and then introduce another local expansion scheme that uses two non-polarizing beamsplitters [49]. Finally, we propose the fusion scheme of two W states to each other by performing parity checking.

1.2.2 Local transformation of two EPR pairs into a tripartite W state

In quantum communication, it is important to locally prepare and manipulate multipartite entangled states among distantly located parties. The simplest situation is to share tripartite entanglement among three parties. Existence of the distinct classes implies that there is no three-qubit state that can be used as a universal resource for generating arbitrary three-qubit pure states under LOCC. For this purpose, one must look for a resource in larger systems. One of the simplest way is to distribute the resource of an EPR pair between one party (Charlie) and each of the other parties (Alice and Bob). Starting with this resource, it is at least theoretically easy to show that Charlie can prepare three local auxiliary qubits in the desired three-qubit state, which may be an entangled state, and then faithfully send one qubit to Alice and another to Bob by quantum teleportation [7]. Since this scenario involves seven qubits in total, it is hard to carry out in experiments [see Fig. 1.2 (a)]. Thus, a more direct and efficient way of converting EPR pairs to three-qubit states is desired [see Fig. 1.2 (b)]. For the GHZ-type states, it is easy to do this since we can convert the two EPR pairs to a three-photon GHZ state by quantum parity checking [32, 47], which can be done by a polarization beam splitter and post-selection[17, 35]. Any GHZ-type state is then produced with nonzero probability by applying a unitary operation and local filtering on each photon, which can be done with high precision. This line of strategy was further

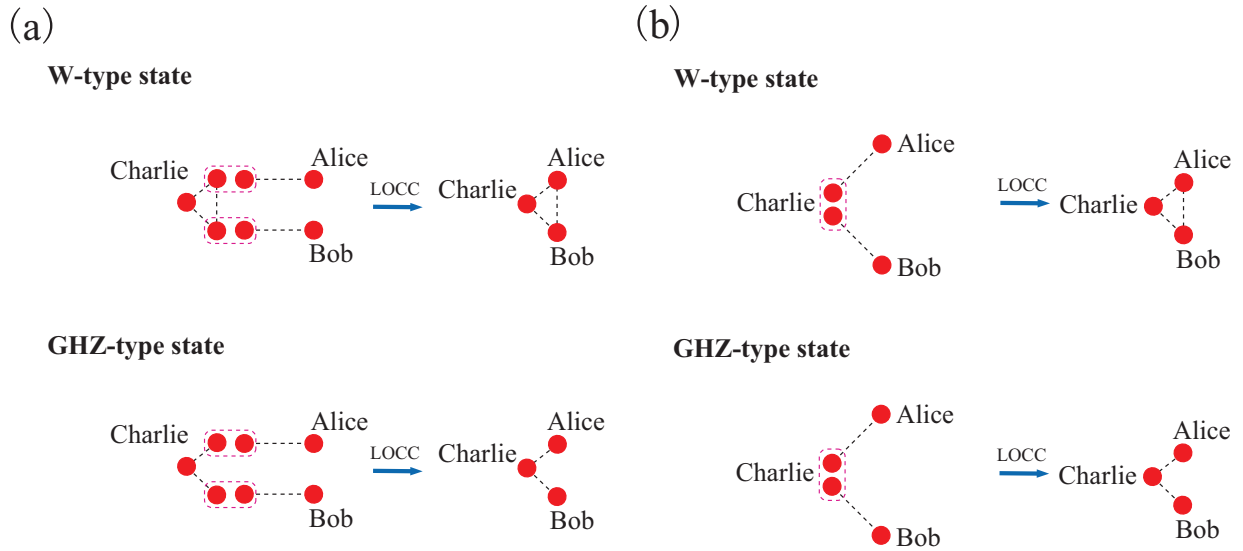


Figure 1.2: Tripartite entanglement preparation schemes using two EPR pairs shared by Alice, Bob and Charlie: (a) Preparing three local auxiliary qubits in the desired three-qubit state on Charlie's side and then faithfully sending one qubit to Alice and another to Bob by quantum teleportation, and (b) converting two EPR pairs to desired three-qubit states directly.

extended for the W -type states by Walther *et al.* [43], who experimentally demonstrated that a three-photon W state can be *approximately* generated from the three-photon GHZ state by LOCC. In this method, there is a trade-off between the success probability and the fidelity of the final state such that the fidelity approaches unity only in the limit of zero success probability, which reflects the fact that the three-photon GHZ and W states belong to distinct classes of states.

In this thesis, we proposed and experimentally demonstrated the missing path of resource conversion, namely, direct transformation of two EPR photon pairs into the three-photon W state [50]. Our scheme simply uses a polarization-dependent beam splitter (PDBS) and a photon detection to realize a desired transformation of Charlie's two photons into one photon.

Chapter 2

Classification and evaluation of Multipartite entanglement

In this Chapter, we will give the fundamental principles of quantum mechanics and the tools for a study of entanglement. In Sec. 2.1, we introduce elements of quantum information. In Sec. 2.2, we introduce a Bell basis and the estimation of the density operator of a bipartite system together with the amount of its entanglement. Sec. 2.3 covers a review of the classification of tripartite entangled states and the concept of entanglement witness.

2.1 Brief introduction to quantum information

In this section, we introduce quantum bit. It is the quantum mechanical counterpart of the classical bit. We also give the fundamental principle in quantum mechanics.

2.1.1 Quantum bits

Quantum states are represented in a Hilbert space known as the state space of the system. The state of the system is described by a unit vector in its state space.

In 1995, Schumacher [51] introduced the notion of quantum bit, “*qubit*”, after the example of classical bit (either 0 or 1) in classical information theory. In this thesis, we define

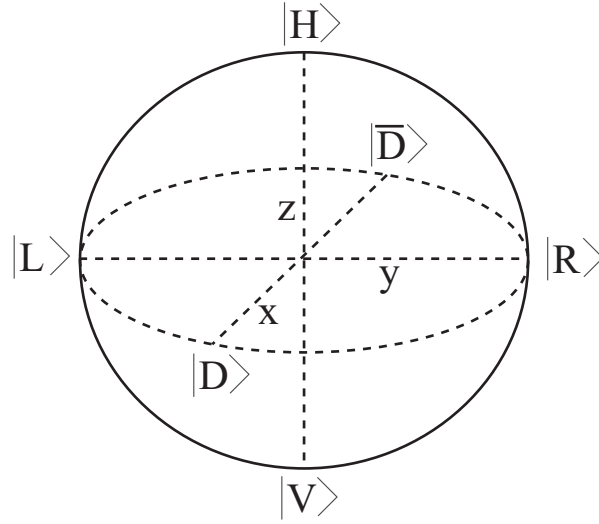


Figure 2.1: Bloch sphere representation of a qubit in Hilbert space. Here $|D/\bar{D}\rangle = (|H\rangle \pm |V\rangle)/\sqrt{2}$ and $|R/L\rangle = (|H\rangle \pm i|V\rangle)/\sqrt{2}$. The eigenstate of the Pauli matrices lie on the corresponding three orthogonal axis (x, y, z) in the example of Sec 2.1.2 (i).

a qubit as polarization states of a photon. A horizontally polarized state and a vertically polarized state are represented by $|H\rangle$ and $|V\rangle$, respectively. The state of single qubit is represented as

$$|\psi\rangle = e^{i\gamma} \left(\cos\left(\frac{\theta}{2}\right)|H\rangle + e^{i\varphi}\sin\left(\frac{\theta}{2}\right)|V\rangle \right), \quad (2.1)$$

where θ , γ , and φ are real numbers. Here we can *ignore* the global phase $e^{i\gamma}$ because it has *no observable effects*. Combining this with the facts, $|\psi\rangle = -|\psi\rangle|_{(\theta \rightarrow \theta + 2\pi)}$, $|\psi\rangle = -|\psi\rangle|_{(\theta \rightarrow 2\pi - \theta, \varphi \rightarrow \varphi + \pi)}$ and $|\psi\rangle = |\psi\rangle|_{(\varphi \rightarrow \varphi + 2\pi)}$, we see that the state $|\psi\rangle$ can be completely parameterized by $0 \leq \theta \leq \pi$ and $0 \leq \varphi \leq 2\pi$. This implies that the state $|\psi\rangle$ can be determined by a unit vector $\mathbf{n} = (\sin(\theta)\cos(\varphi), \sin(\theta)\sin(\varphi), \cos(\theta))$ pointing the surface of a unit sphere. This vector is called Bloch vector, and the sphere is called Bloch sphere [see Fig. 2.1].

2.1.2 Elements of quantum mechanics

In this section, we will briefly introduce the fundamental ingredients in quantum mechanics.

(i) Unitary transformation

The evolution of a closed quantum system is described by a unitary transformation. For example, the state $|\phi(t)\rangle$ of the system at time t is related to the state $|\phi(t + \Delta t)\rangle$ by a unitary operator, U ,

$$|\phi(t + \Delta t)\rangle = U|\phi(t)\rangle. \quad (2.2)$$

Unitary operators that are called the Pauli operators play a fundamental role in quantum information science. The Pauli operators consist of $\{I, \sigma_x, \sigma_y, \sigma_z\}$ where I is the identity operator, σ_x and σ_z respectively represent bit and phase flip operators and σ_y corresponds to a phase flip followed by a bit flip, namely $\sigma_y = i\sigma_x\sigma_z$.

(ii) Measurement

Measurements on quantum states are described by a collection $\{M_m\}$ of the measurement operators acting on the state space being measured. The index m is associated with the measurement outcomes. If the state is given by $|\phi\rangle$, the state after the measurement with the measurement outcome m becomes

$$\frac{M_m|\phi\rangle}{\sqrt{\langle\phi|M_m^\dagger M_m|\phi\rangle}} \quad (2.3)$$

with the probability for result m is given by,

$$p(m) = \langle\phi|M_m^\dagger M_m|\phi\rangle. \quad (2.4)$$

The measurement operators satisfy the completeness equation,

$$\sum_m M_m^\dagger M_m = I, \quad (2.5)$$

which means that the probabilities sum to one.

Projective Measurement

A projective measurement is one of important measurements. A projective measurement is described by an observable M , which is a Hermitian operator on the state being observed. The observable has a spectral decomposition,

$$M = \sum_m m P_m, \quad (2.6)$$

where P_m is the projector onto the eigenspace of M with eigenvalue m , and satisfies $P_m^2 = P_m$. The outcomes of the measurement correspond to the eigenvalues, m , of the observable. If the state is given by $|\phi\rangle$, the probability of getting result m is given by

$$p(m) = \text{Tr}[|\phi\rangle\langle\phi|P_m]. \quad (2.7)$$

POVM Measurement

In quantum mechanics, it is often the case that we are not interested in post-measurement states and our main concern is the probabilities of the respective measurement outcomes. In this case, a mathematical tool which is called Positive operator valued measure (POVM) is used. POVM is defined by a collection of positive operators $\{E_m\}$ with the completeness condition $\sum E_m = I$. The probability of obtaining the measurement outcome m when we measure the state $|\phi\rangle$ is given by

$$p(m) = \text{Tr}[|\phi\rangle\langle\phi|E_m]. \quad (2.8)$$

(iii) Density matrices

A convenient alternative formulation for representing the states is the so-called density operator formulation which is mathematically equivalent to the pure state approach given in the previous section. Given an ensemble of states $\{|\phi_1\rangle, |\phi_2\rangle, |\phi_3\rangle \cdots, |\phi_n\rangle\} \in H$ with each state $|\phi_i\rangle$ taking place with probability p_i , the density matrix for this ensemble, which represents a mixture of all the states $\{|\phi_i\rangle\}$, is defined as

$$\rho = \sum_{i=1}^n p_i |\phi_i\rangle\langle\phi_i|. \quad (2.9)$$

The evolution of a density operator is described by

$$\rho(t + \Delta t) = U\rho(t)U^\dagger. \quad (2.10)$$

The density operator after the measurement $\{M_m\}$ is given by

$$\frac{M_m\rho M_m^\dagger}{\text{Tr}[M_m\rho M_m^\dagger]} \quad (2.11)$$

where $\text{Tr}[M_m\rho M_m^\dagger]$ gives the probability of the measurement outcome m . Moreover, the probability of outcome m in the measurement specified by POVM $\{E_m\}$ is written by

$$p(m) = \text{Tr}[\rho E_m]. \quad (2.12)$$

2.1.3 Fidelity

Fidelity is an important distance measure that is used to quantify how close two given states are. In 1976, Uhlmann [52] proposed the fidelity of two mixed states ρ and σ , which is represented by

$$F = \left(\text{Tr} \left[\sqrt{\sqrt{\sigma}\rho\sqrt{\sigma}} \right] \right)^2. \quad (2.13)$$

In special case of the fidelity between a pure state $|\phi\rangle$ and an arbitrary state ρ , the expression in Eq. (2.13) simplifies to

$$F = \text{Tr}[\rho|\phi\rangle\langle\phi|] = \langle\phi|\rho|\phi\rangle. \quad (2.14)$$

2.2 Bipartite entanglement

In this section, we will review the basic properties of bipartite entanglement and the methods of quantifying the amount of entanglement in bipartite systems.

In quantum world, there is a property that cannot be described in classical world. To define this new feature, we introduce a paradigm where distantly located parties Alice and Bob are permitted to use local operations (LO) and classical communication (CC) channel

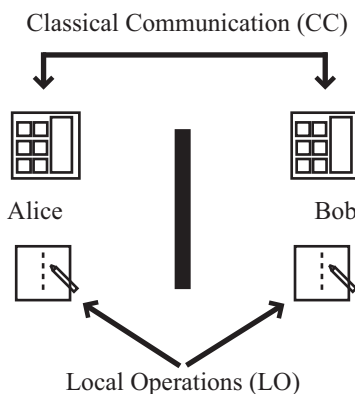


Figure 2.2: Local operations and classical communication (LOCC).

such as telephone [see Fig. 2.2]. This paradigm is called LOCC. The correlation made in this paradigm should be called classical. For example, a state in the form of

$$\rho = \sum_i p_i \rho_A^{(i)} \otimes \rho_B^{(i)} \quad (2.15)$$

can be freely created by LOCC. This type of state is called separable state. Conversely, correlation that cannot be created by LOCC should be called non-classical or quantum. Such correlation is dubbed entanglement.

A famous example of a state holding entanglement, so called an EPR pair, is

$$|\Phi^+\rangle = \frac{1}{\sqrt{2}}(|H\rangle_A |H\rangle_B + |V\rangle_A |V\rangle_B). \quad (2.16)$$

General entangled states are not restricted in this form.

To quantify entanglement of a system, entanglement measures were introduced by the effort of quantum information theory. For example, entanglement measure of pure states is

$$E_S(|\psi_{AB}\rangle) = S(\text{Tr}_{A(B)}[|\psi\rangle\langle\psi|_{AB}]) \quad (2.17)$$

where S is the von Neumann entropy defined by

$$S(\rho) = -\text{Tr}[\rho \log_2(\rho)]. \quad (2.18)$$

One of the entanglement measures for mixed states is entanglement of formation E_F :

$$E_F(\rho) \equiv \min_{\{p_i, |\phi_i\rangle\}} \sum_i p_i E_S(|\phi_i\rangle), \quad (2.19)$$

where the minimum is taken over all ensembles $\{p_i, |\phi_i\rangle\}$ satisfying $\rho = \sum_i p_i |\phi_i\rangle\langle\phi_i|$. In general, it is hard to quantify the value of $E_F(\rho)$. However, for two qubits, Wootters [53] has found the formula of E_F enabling easy calculations. In Sec. 2.2.2, we review shortly this formula.

2.2.1 Bell basis

A Bell basis is defined as

$$|\Phi^+\rangle = \frac{1}{\sqrt{2}}(|H\rangle_1|H\rangle_2 + |V\rangle_1|V\rangle_2), \quad (2.20)$$

$$|\Phi^-\rangle = \frac{1}{\sqrt{2}}(|H\rangle_1|H\rangle_2 - |V\rangle_1|V\rangle_2), \quad (2.21)$$

$$|\Psi^+\rangle = \frac{1}{\sqrt{2}}(|H\rangle_1|V\rangle_2 + |V\rangle_1|H\rangle_2), \quad (2.22)$$

$$|\Psi^-\rangle = \frac{1}{\sqrt{2}}(|H\rangle_1|V\rangle_2 - |V\rangle_1|H\rangle_2), \quad (2.23)$$

where the subscripts, 1 and 2 represent the subsystems. Each of four states is also called an EPR pair. These states are related with local unitary operations as follows:

$$|\Phi^+\rangle = (I \otimes \sigma_z)|\Phi^-\rangle = (I \otimes \sigma_x)|\Psi^+\rangle = (I \otimes (\sigma_z\sigma_x))|\Psi^-\rangle. \quad (2.24)$$

2.2.2 Concurrence

In this subsection, we introduce concurrence, which is useful in determining the amount of entanglement in a bipartite system [54]. The concurrence is defined as the fidelity of a given state to its spin-flipped counterpart. For a pure state of a single qubit after the spin flip, the state is defined as

$$|\tilde{\chi}\rangle = \sigma_y|\chi^*\rangle, \quad (2.25)$$

where $|\chi^*\rangle$ is the complex conjugate of $|\chi\rangle$ and $\hat{\sigma}_y$ expressed in that same basis is the matrix

$$\begin{bmatrix} 0 & -i \\ i & 0 \end{bmatrix}. \quad (2.26)$$

For example, the spin-flipped state of a general state ρ of two qubit is

$$\tilde{\rho} = (\sigma_y \otimes \sigma_y) \rho^* (\sigma_y \otimes \sigma_y). \quad (2.27)$$

For a pure state of two qubits, we obtain the concurrence C as

$$C = |\langle \chi | \tilde{\chi} \rangle|. \quad (2.28)$$

The function for calculating entanglement of formation (EOF) is given by

$$E_F(C) = h\left(\frac{1 + \sqrt{1 - C^2}}{2}\right), \quad (2.29)$$

where $h(x) = -x \log_2 x - (1 - x) \log_2 (1 - x)$. $E_F(C)$ is monotonically increasing, and it ranges from 0 to 1 as C goes from 0 to 1. For a Bell state, both C and $E_F(C)$ are equal to 1. For an unentangled pure state, C and $E_F(C)$ are equal to zero. For a mixed state ρ , the concurrence is obtained by

$$C(\rho) = \max\{0, \sqrt{\lambda_1} - \sqrt{\lambda_2} - \sqrt{\lambda_3} - \sqrt{\lambda_4}\}, \quad (2.30)$$

where λ_j 's are the eigenvalues of $\rho \tilde{\rho}$, and $\lambda_1 \geq \lambda_2 \geq \lambda_3 \geq \lambda_4 \geq 0$. The entanglement of formation is then given by

$$E_F(\rho) = h\left(\frac{1 + \sqrt{1 - C^2(\rho)}}{2}\right). \quad (2.31)$$

2.2.3 Peres-Horodecki criterion

In 1996, Peres [55] proved that a necessary condition for the separability of a state is the positivity of its partial transposition (PPT). Horodecki *et al.* [56] then gave the necessary and sufficient condition of the separability for 2×2 (bipartite two-level system-qubit) and 2×3 (bipartite three-level system-qutrit) systems. However, in general case, it is noted that the PPT of the state is not always a sufficient condition for the separability of a state. For example, there exists entangled states which are PPT. Such states are referred to as bound entangled states (BES) [66].

2.3 Multipartite entanglement

Compared to entanglement in bipartite systems, multipartite entanglement is complex and difficult to understand. In this section, we review the classification and detection of entanglement in multipartite systems. In particular, we focus on the classification of tripartite entanglement and its detection using entanglement witness.

2.3.1 Classification of tripartite entanglement

It is known that entanglement cannot increase under local operations and classical communication (LOCC). This does not mean that when two states have the same amount of entanglement, they can necessarily be converted into one another via LOCC. If two states cannot be converted into each other via LOCC, it is interpreted that these two states belong to different classes or they are inequivalent.

In 2000, Dür *et al.* [58] proved that there are six equivalence classes for pure states of three qubits via stochastic LOCC (SLOCC). Their idea behind this classification is that a three-qubit state $|a\rangle$ can be locally converted into another three-qubit state $|b\rangle$ with a non zero probability iff there exists an invertible local operator (ILO) $A \otimes B \otimes C$ such that

$$|a\rangle = A \otimes B \otimes C |b\rangle. \quad (2.32)$$

This implies that the states $|a\rangle$ and $|b\rangle$ are equivalent under SLOCC if an ILO relating them exists. The classification is shown in Figure 2.3 (a). The classes consist of one completely separable state (A-B-C), three biseparable states where two qubits are entangled but separated from the third one (A-BC, C-AB and B-AC), two genuine tripartite entangled states, namely GHZ- and W- type states. The GHZ and W states for polarization entangled photons are represented as

$$|\text{GHZ}_3\rangle = \frac{1}{\sqrt{2}}(|\text{H}\rangle|\text{H}\rangle|\text{H}\rangle + |\text{V}\rangle|\text{V}\rangle|\text{V}\rangle) \quad (2.33)$$

and

$$|\text{W}_3\rangle = \frac{1}{\sqrt{3}}(|\text{H}\rangle|\text{H}\rangle|\text{V}\rangle + |\text{H}\rangle|\text{V}\rangle|\text{H}\rangle + |\text{V}\rangle|\text{H}\rangle|\text{H}\rangle). \quad (2.34)$$

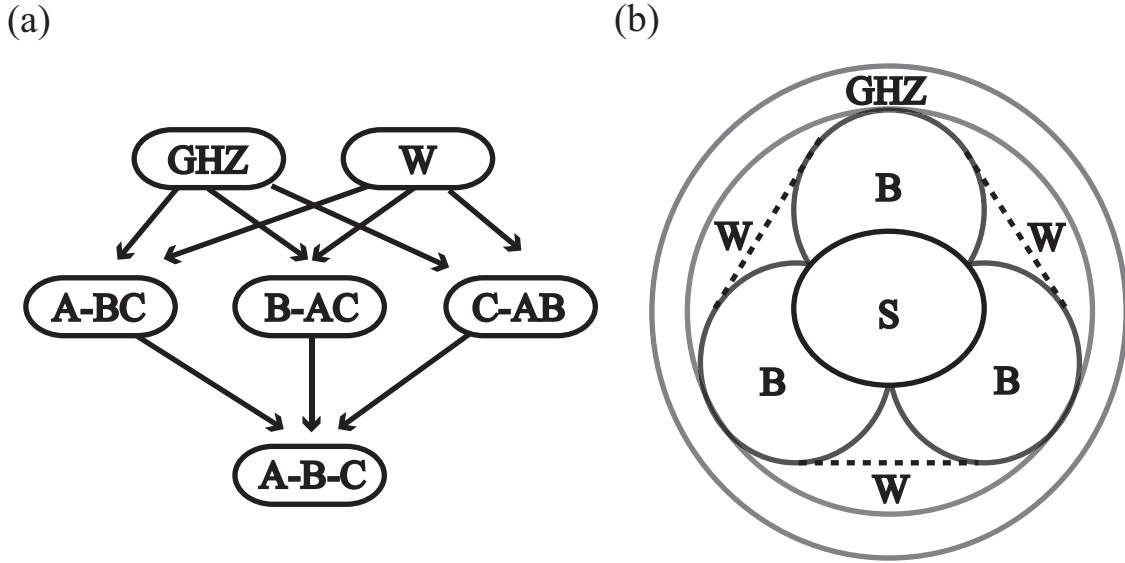


Figure 2.3: (a) The classification of pure states. Its classification consists of three hierarchies: Genuinely tripartite entangled states (GHZ-type states and W-type states), biseparable states (A-BC and its permutations) and separable states (A-B-C). (b) The classification of mixed states. It starts from the smallest class consisting of convex combinations of separable state (S), and adds the class of biseparable states(B) and W-type states (W). Finally the class of GHZ-type states includes all embedded subclasses.

The distinction between these two types of entanglement becomes clearer if we consider their generalizations to the N -qubit case: $|W_N\rangle = |N-1, 1\rangle/\sqrt{N}$ and $|\text{GHZ}_N\rangle = (|N, 0\rangle + |0, N\rangle)/\sqrt{2}$ where $|N-k, k\rangle$ is the sum over all the terms with $N-k$ modes in $|H\rangle$ and k modes in $|V\rangle$. In $|W_N\rangle$, every pair of qubits are entangled with each other directly, namely, the pairwise entanglement survives even after the rest of the qubits are discarded [28, 29, 59]. In fact, it was shown that the state $|W_N\rangle$ has the maximum amount of such pairwise entanglement shared by every pair [28]. It looks as if forming a web-like structure in which every qubit has a bond with every other qubit. On the other hand, the entanglement in $|\text{GHZ}_N\rangle$ is sustained by all of the N qubits, and loss of only one particle

destroys the entanglement completely. But if access to every qubit is allowed, it shows a maximal violation of local realism [60].

On the other hand, the classification for mixed states introduced by Acín *et al.* [61] is different from that for pure states in a generalization of the SLOCC. This classification is shown in Figure 2.3 (b). The class of separable states (A-B-C) contains all states that can be decomposed as a convex combination of pure separable states. The class of biseparable mixed states (A-BC, C-AB and B-AC) is formed by all states that can be expressed as a convex combination of separable or any kind of biseparable states. Convex combinations of states from separable states, biseparable and pure W-type states constitute the class of mixed W-type states. Finally, the class of GHZ-type states includes all physical three-qubit states.

2.3.2 Entanglement witness

A tool for detection of entanglement is the entanglement witness that is an hermitian operator \mathcal{W} detecting the entangled state ρ_e . All of separable states ρ_{sep} satisfy $\text{Tr}[\mathcal{W}\rho_{sep}] \geq 0$. $\text{Tr}[\mathcal{W}\rho_e] < 0$ is satisfied by at least one entangled state ρ_e . If a negative expectation value of \mathcal{W} is observed for a state ρ , it clearly shows that ρ is entangled.

A witness operator that detects genuine multipartite entanglement around a pure state $|\phi\rangle$ is given by

$$\mathcal{W} = \alpha \mathbf{1} - |\phi\rangle\langle\phi|, \quad (2.35)$$

where $\mathbf{1}$ is the identity operator, and α is calculated by

$$\alpha = \max_{|\psi_b\rangle \in B} |\langle\psi_b|\phi\rangle|^2, \quad (2.36)$$

with B denoting the set of biseparable states. This guarantees that $\text{Tr}[\mathcal{W}\rho_b] \geq 0$ for all biseparable states ρ_b , and that $\text{Tr}[\mathcal{W}\rho_e] < 0$ for at least one entangled state. Thus, a negative expectation value of the observable \mathcal{W} clearly signifies that the state is entangled.

For tripartite entanglement, the generic witness [62, 63] that detects states close to

$|\text{GHZ}_3\rangle$ is given by

$$\mathcal{W}_{\text{GHZ}} = \frac{3}{4}\mathbf{1} - |\text{GHZ}_3\rangle\langle\text{GHZ}_3|, \quad (2.37)$$

and one of generic W_3 witness is given by

$$\mathcal{W}_W = \frac{2}{3}\mathbf{1} - |W_3\rangle\langle W_3|. \quad (2.38)$$

Expectation values of the above witness operators are positive for biseparable states including the fully separable states and negative for at least one states belonging to the GHZ and W states respectively.

Chapter 3

Engineering and measurement with polarization entangled photons

In this chapter, we review tools in linear optical quantum processing. In Sec. 3.1, We start with the creation of photon pairs from spontaneous parametric down conversion (SPDC). In Sec. 3.2, we then introduce entangled photon pair generation from SPDC. In Sec. 3.3 and Sec. 3.4, we introduce birefringent crystals and beamsplitters which are basic elements in linear optics. Finally, in Sec. 3.5, we will give a quantum state tomography and introduce a maximally likelihood method for reconstructing physical density matrix.

3.1 Spontaneous parametric down conversion

A photon pair cannot be generated by a linear effect. However, it is possible to prepare photon pairs using spontaneous parametric down conversion (SPDC) with a second order nonlinear effect. When a strong pump beam with wavenumber \mathbf{k} and frequency ω is incident to a nonlinear crystal such as β -barium borate (BBO), photon pairs are probabilistically generated in a signal and an idler mode when the phase matching conditions determined

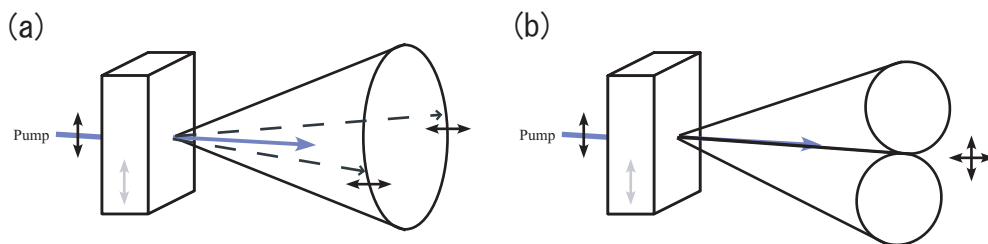


Figure 3.1: Photon pair generation by spontaneous parametric down conversion (SPDC) process. (a) In Type I process, a generated signal and idler photons have the same polarization which is orthogonal to the polarization of the pump field. (b) In Type II, signal and idler photons are orthogonally polarized to each other.

by

$$\begin{aligned}
 \mathbf{k} &= \mathbf{k}_s + \mathbf{k}_i \\
 \omega &= \omega_s + \omega_i
 \end{aligned} \tag{3.1}$$

are satisfied. In Eq. (3.1), \mathbf{k}_s and \mathbf{k}_i are the wavenumbers, and ω_s and ω_i are the frequencies of the photons in the signal and idler modes, respectively. Vacuum component, that is no photon pair generation, occurs with the highest probability dominating the output of the SPDC process; and hence the probability of a photon pair generation is low. Although the probability is much smaller, there may exist cases where multiple-photon pairs are generated. Multiple-photon pair generation can be reduced by using a low intensity pump field with the cost of reduced one-photon pair generation rate.

There are two types of SPDC process: In Type I process, the generated signal and idler photons have the same polarization which is orthogonal to the polarization of the pump field [see fig. 3.1 (a)]. In Type II process, on the other hand, the signal and idler photons are orthogonally polarized to each other [see fig. 3.1 (b)].

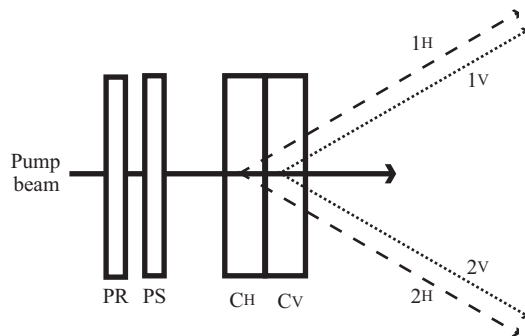


Figure 3.2: Entangled photon pair generation from SPDC. Photon pairs in mode 1 and 2 are generated on stacked nonlinear crystals (C_H and C_V). PR is a polarization rotator and PS is a phase shifter.

3.2 Entangled photon pair generation

In 1999, Kwiat, *et al.* [64] demonstrated a simple scheme of entangled photon pair generation using a non-linear crystal, which is formed by stacking together two Type I phase matched β -barium borate (BBO) crystals with their optical axes orthogonal to each other. In our experiment, we use this photon pair generation scheme for photon pair generations.

The setup of a photon pair generation scheme is shown in Fig. 3.2. When a V-polarized pump is incident on this BBO, the H-polarized photon pairs are generated. The generated state is written as

$$|\Psi\rangle_{12} = \sqrt{g}(|vac\rangle_{12} + \gamma e^{i\phi_p} |1_H\rangle_1 |1_H\rangle_2 + \gamma^2 e^{2i\phi_p} |2_H\rangle_1 |2_H\rangle_2 \dots), \quad (3.2)$$

where subscripts 1 and 2 denote the spatial mode of each output after SPDC, $|vac\rangle$ stands for the vacuum state, $g = 1 - \gamma^2$, and $\gamma e^{i\phi_p}$ is proportional to the complex amplitude of the pump field. On the other hand, when arbitrarily polarized pump controlled by a polarization rotator (PR) and a phase shifter (PS) is incident on this BBO, entangled photon pairs are generated. The generated state is given by

$$|\Psi\rangle_{12} = \sqrt{g_1}(|vac\rangle_{12} + \gamma e^{i\phi_p} |\Lambda_0\rangle_{12} + \gamma^2 e^{2i\phi_p} |\Lambda_1\rangle_{12} \dots), \quad (3.3)$$

where α and β are complex numbers satisfying $|\alpha|^2 + |\beta|^2 = 1$, $|\Lambda_0\rangle_{12} = \alpha |1_H\rangle_1 |1_H\rangle_2 +$

$\beta|1_V\rangle_1|1_V\rangle_2$, and $|\Lambda_1\rangle_{12} = \alpha\beta|1_H1_V\rangle_1|1_H1_V\rangle_2 + \beta^2|2_V\rangle_1|2_V\rangle_2 + \alpha^2|2_H\rangle_1|2_H\rangle_2$ is unnormalized, and $g_1 = (1 - \gamma^2|\alpha|^2)(1 - \gamma^2|\beta|^2)$. For example, when α and β are $1/\sqrt{2}$, The generated state is given by

$$|\Psi\rangle_{12} = \sqrt{g_1}(|vac\rangle_{12} + \gamma e^{i\phi_p}|\Lambda_0\rangle_{12} + \frac{1}{2}\gamma^2 e^{2i\phi_p}|\Lambda_1\rangle_{12} \dots), \quad (3.4)$$

where $|\Lambda_0\rangle_{12} = (|1_H\rangle_1|1_H\rangle_2 + |1_V\rangle_1|1_V\rangle_2)/\sqrt{2}$, and $|\Lambda_1\rangle_{12} = |1_H1_V\rangle_1|1_H1_V\rangle_2 + |2_V\rangle_1|2_V\rangle_2 + |2_H\rangle_1|2_H\rangle_2$, and $g_1 = (1 - \gamma^2/2)^2$.

3.3 Wave plates

In linear optics, unitary operations on a single qubit encoded on the polarization degree of freedom of a single photon can be easily implemented by using birefringent crystals such as half wave plates (HWP) and quarter wave plates (QWP). These plates are used to change the polarization state of light. If the plane of polarization of the incident light is at an angle θ with respect to the fast axis of HWP, the incident light polarization will rotate through an angle of 2θ after passing through the HWP. For example, setting $\theta = \pi/4$ will rotate an H-polarized incident light to V-polarized light. Setting $\theta = \pi/8$ will rotate an H-polarized incident light to a diagonally polarized light. Setting $\theta = \pi/2$ will induce a π -phase shift on the V-polarized light. Quarter wave plates, on the other hand, are used to turn linearly-polarized light into circularly polarized light. This can be achieved by sending the incident light at an angle of $\pi/4$ to the slow or fast axis of the QWP. Conversely, a circularly polarized light is converted to a linearly polarized light by a QWP.

3.4 Beamsplitters

In order to make joint or single operations on photon pairs, we often use a beamsplitter [see Fig. 3.3 (a)]. The transformation of a general beamsplitter (BS) is written as

$$\begin{aligned} \hat{a}_1^\dagger &= \sqrt{1-\mu} \hat{a}_3^\dagger - \sqrt{\mu} \hat{a}_4^\dagger \\ \hat{a}_2^\dagger &= \sqrt{\mu} \hat{a}_3^\dagger + \sqrt{1-\mu} \hat{a}_4^\dagger, \end{aligned} \quad (3.5)$$

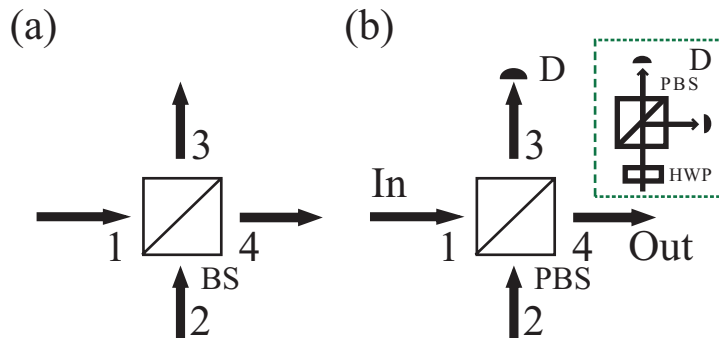


Figure 3.3: Schematic diagram of (a) a general beamsplitter (BS) and (b) a quantum parity checking gate using a polarizing beamsplitter with a discriminating detector (D). Input modes are 1 and 2, and output modes are 3 and 4.

where \hat{a}_j^\dagger denotes the creation operator of mode j . μ and $1 - \mu$ are the transmission and the reflection coefficient, respectively. Subscripts 1 and 2 are the input modes, and subscripts 3 and 4 are the output modes. A beamsplitter can be designed to have polarization dependent or independent transmission and reflection coefficients. In particular, we often use a polarizing beamsplitter (PBS) and a 50:50 beamsplitter in linear optical experiments. A PBS has the property that completely transmit H-polarized photons and totally reflect V-polarized photons. A 50:50 BS is represented from Eq. (3.5) as follows;

$$\begin{aligned}\hat{a}_1^\dagger &= \frac{1}{\sqrt{2}} \hat{a}_3^\dagger - \frac{1}{\sqrt{2}} \hat{a}_4^\dagger \\ \hat{a}_2^\dagger &= \frac{1}{\sqrt{2}} \hat{a}_3^\dagger + \frac{1}{\sqrt{2}} \hat{a}_4^\dagger.\end{aligned}\quad (3.6)$$

Here we show an example of application using a polarizing beamsplitter. In 2001, Pittman *et al.*[47] proposed a quantum parity checking gate [see fig. 3.3 (b)]. The gate is composed of a polarizing beamsplitter (PBS) and a polarization discriminating detector(D). This discriminating detector is composed of a HWP, a PBS and two photodetectors and enables the measurements in the diagonal polarization bases $|D\rangle = (|H\rangle + |V\rangle)/\sqrt{2}$ and

$|\bar{D}\rangle = (|H\rangle - |V\rangle)/\sqrt{2}$. The operation of the gate counts the photon number in the mode 3: When the two inputs are both H-polarized photons (V-polarized photons), the detector in mode 3 detects one H-polarized photon (one V-polarized photon), resulting in an H-polarized photon (a V-polarized photon) in mode 4. When the inputs are an H-polarized photon in mode 1 and a V-polarized photon in mode 2, the detector in mode 3 detects no photons, resulting in an H-polarized photon and a V-polarized photon in mode 4. When the inputs are a V-polarized photon in mode 1 and an H-polarized photon in mode 2, the detector in mode 3 detects both of the H-polarized photon and the V-polarized photon, resulting in zero photon in mode 4.

3.5 Quantum state tomography and maximum likelihood estimation

(i) Quantum state tomography

Quantum state tomography is used to obtain a complete density matrix of a quantum state from measured data. From a decomposition of the density matrix into projectors one can easily express the density matrix in terms of probabilities for detecting a certain coincidence. Relative frequencies obtained in a measurement are subject to poissonian counting statistics caused by slight deviations from the real probabilities. Therefore, the estimated density matrices are not necessarily physical. In such a case, maximum likelihood estimation (MLE) approach is employed. With MLE, it becomes possible to construct a physical density matrix which gives the closest counting statistics to those obtained in the experiments.

An n -qubit state can be characterized by a density matrix which is written by

$$\rho = \frac{1}{2^n} \sum_{i_1, i_2, \dots, i_n=0}^3 r_{i_1, i_2, \dots, i_n} \sigma_{i_1} \otimes \sigma_{i_2} \otimes \dots \otimes \sigma_{i_n} \quad (3.7)$$

where the 4^n parameters r_{i_1, i_2, \dots, i_n} are real numbers and $\{\sigma_0 = I, \sigma_1 = \sigma_x, \sigma_2 = \sigma_y, \sigma_3 = \sigma_z\}$. The normalization property of the density matrices requires that $r_{0,0,\dots,0} = 1$, and so the

density matrix is specified by $4^n - 1$ real parameters. The values of r_{i_1, i_2, \dots, i_n} can be calculated from the expectation values obtained from the measurement of various combinations of pauli operators, $\{I, \sigma_x, \sigma_y, \sigma_z\}$. Then we obtain density matrix ρ .

James *et al.* [65] discussed tomographic sets for polarization qubits and showed how to generally deduce the density matrix from measurement data when a certain tomographic set is available.

Using polarization states, $\{I, \sigma_x, \sigma_y, \sigma_z\}$ are represented by

$$\begin{aligned}
I &= \begin{bmatrix} 1 & 0 \\ 0 & 1 \end{bmatrix} = |\text{H}\rangle\langle\text{H}| + |\text{V}\rangle\langle\text{V}| = |\text{D}\rangle\langle\text{D}| + |\bar{\text{D}}\rangle\langle\bar{\text{D}}| = |\text{L}\rangle\langle\text{L}| + |\text{R}\rangle\langle\text{R}|, \\
\sigma_x &= \begin{bmatrix} 0 & 1 \\ 1 & 0 \end{bmatrix} = |\text{H}\rangle\langle\text{V}| + |\text{V}\rangle\langle\text{H}| = |\text{D}\rangle\langle\text{D}| - |\bar{\text{D}}\rangle\langle\bar{\text{D}}| = i(|\text{R}\rangle\langle\text{L}| - |\text{L}\rangle\langle\text{R}|), \\
\sigma_y &= \begin{bmatrix} 0 & -i \\ i & 0 \end{bmatrix} = -i|\text{H}\rangle\langle\text{V}| + i|\text{V}\rangle\langle\text{H}| = i(|\text{D}\rangle\langle\bar{\text{D}}| - |\bar{\text{D}}\rangle\langle\text{D}|) = |\text{L}\rangle\langle\text{L}| - |\text{R}\rangle\langle\text{R}|, \\
\sigma_z &= \begin{bmatrix} 1 & 0 \\ 0 & -1 \end{bmatrix} = |\text{H}\rangle\langle\text{H}| - |\text{V}\rangle\langle\text{V}| = |\text{D}\rangle\langle\bar{\text{D}}| + |\bar{\text{D}}\rangle\langle\text{D}| = |\text{R}\rangle\langle\text{L}| + |\text{L}\rangle\langle\text{R}|,
\end{aligned} \tag{3.8}$$

where $\{|\text{H}\rangle, |\text{V}\rangle, |\text{D}\rangle, |\bar{\text{D}}\rangle, |\text{R}\rangle, |\text{L}\rangle\}$ is given by

$$\begin{aligned}
|\text{H}\rangle &= \begin{bmatrix} 1 \\ 0 \end{bmatrix}, & |\text{V}\rangle &= \begin{bmatrix} 0 \\ 1 \end{bmatrix}, \\
|\text{D}\rangle &= \frac{1}{\sqrt{2}} \begin{bmatrix} 1 \\ 1 \end{bmatrix}, & |\bar{\text{D}}\rangle &= \frac{1}{\sqrt{2}} \begin{bmatrix} 1 \\ -1 \end{bmatrix}, \\
|\text{L}\rangle &= \frac{1}{\sqrt{2}} \begin{bmatrix} 1 \\ i \end{bmatrix}, & |\text{R}\rangle &= \frac{1}{\sqrt{2}} \begin{bmatrix} 1 \\ -i \end{bmatrix}.
\end{aligned} \tag{3.9}$$

Here we define the operator for projection measurement as $|\psi_\nu\rangle\langle\psi_\nu|$. For example, for a two-qubit case, we can define the operator by $|\psi_1\rangle = |\text{HH}\rangle_{12}$, $|\psi_2\rangle = |\text{HV}\rangle_{12}$, $|\psi_3\rangle = |\text{VH}\rangle_{12}$, $|\psi_4\rangle = |\text{VV}\rangle_{12}$, $|\psi_5\rangle = |\text{RH}\rangle_{12}$, $|\psi_6\rangle = |\text{RV}\rangle_{12}$, $|\psi_7\rangle = |\text{DV}\rangle_{12}$, $|\psi_8\rangle = |\text{DH}\rangle_{12}$,

$|\psi_9\rangle = |\text{DR}\rangle_{12}$, $|\psi_{10}\rangle = |\text{DD}\rangle_{12}$, $|\psi_{11}\rangle = |\text{RD}\rangle_{12}$, $|\psi_{12}\rangle = |\text{HD}\rangle_{12}$, $|\psi_{13}\rangle = |\text{VD}\rangle_{12}$,
 $|\psi_{14}\rangle = |\text{VL}\rangle_{12}$, $|\psi_{15}\rangle = |\text{HL}\rangle_{12}$, $|\psi_{16}\rangle = |\text{RL}\rangle_{12}$.

In optical experiments, for n -photon states, measurements are performed by the coincidence detection. The average number of coincidence counts that will be observed in a given experimental run is

$$n_\nu = \mathcal{N} \langle \psi_\nu | \rho | \psi_\nu \rangle \quad (\nu = 1, 2, \dots, 4^n) \quad (3.10)$$

where ρ is the density matrix describing the ensemble of qubits, and \mathcal{N} is a constant dependent on the photon flux and detector efficiencies.

The mapping for the tomographic reconstruction of the density matrices is given by

$$\rho = \frac{\sum_{\nu=1}^{4^n} M_\nu n_\nu}{\mathcal{N}}, \quad (3.11)$$

where the value of the unknown parameter \mathcal{N} in experiments is given by

$$\mathcal{N} = \sum_{\nu=1}^{2^n} \text{Tr}[M_\nu] n_\nu. \quad (3.12)$$

The set of M_ν is given by

$$M_\nu = \sum_{\mu=1}^{4^n} (B^{-1})_{\nu,\mu} \Gamma_\mu. \quad (3.13)$$

where Γ_μ is a $2^n \times 2^n$ matrix in a set of 4^n linearly independent $2^n \times 2^n$ matrices $\{\Gamma_\mu\}$, constructed from pauli matrices as in Eq. (3.7). $B_{\nu,\mu}$ is $4^n \times 4^n$ matrix given by $B_{\nu,\mu} = \langle \psi_\nu | \Gamma_\mu | \psi_\nu \rangle$.

(ii) Maximum likelihood estimation

Density matrices for all physical states ρ must have the property that all of the eigenvalues must lie in the interval $[0, 1]$ and their sum being equal to 1. However, the density matrices reconstructed from sets of data obtained by linear tomography often violate this condition. To avoid this problem, the maximum likelihood (ML) estimation of density matrices is used [66, 67, 68, 69].

The probability of obtaining the outcome $|y_i\rangle$ when the state ρ is measured, is given by

$$p_j = \langle y_j | \rho | y_j \rangle, \quad (3.14)$$

where $\sum_j |y_j\rangle\langle y_j| = I$. The empirical probability calculated from measurement data in a experiment is defined as f_j given by

$$f_j = \frac{n_j}{\sum_j n_j}, \quad (3.15)$$

where n_j is a count obtained by measurement in the experiment and $\sum_j n_j$ is a total count obtained by all of measurement in the experiment. Then the likelihood function is defined as

$$\mathcal{L}(\rho) = \prod_j \langle y_j | \rho | y_j \rangle^{f_j}, \quad (3.16)$$

which should be maximized over ρ . One of methods for obtaining the maximum of the likelihood function is to use an iterative algorithm.

The density matrix can be parameterized as

$$\rho = \sum_k r_k |\phi_k\rangle\langle\phi_k|, \quad \rho |\phi_k\rangle = r_k |\phi_k\rangle, \quad (3.17)$$

where r_k are eigenvalues of ρ . Keeping the normalization condition $\text{Tr}[\rho] = 1$ satisfied, maximization conditions is defined by

$$\frac{\partial}{\partial r_k} [\ln \mathcal{L}(\rho) - \Lambda \text{Tr}[\rho]] = 0, \quad (3.18)$$

$$\frac{\partial}{\partial |\phi_k\rangle} [\ln \mathcal{L}(\rho) - \Lambda \text{Tr}[\rho]] = 0, \quad (3.19)$$

where Λ is Lagrange multiplier. When $\ln \mathcal{L}(\rho)$ is maximized with a diagonal matrix ρ , $R\rho = \rho R = \rho$ is satisfied, where the operator R is defined by

$$R = \sum_j \frac{f_j}{p_j} |y_j\rangle\langle y_j|. \quad (3.20)$$

This operator R , which is generally referred to as the *update operator*, depends on the old density matrix. To maximize the likelihood, the operation, $\rho^{(l+1)} = R^{(l)}\rho^{(l)}$ is done

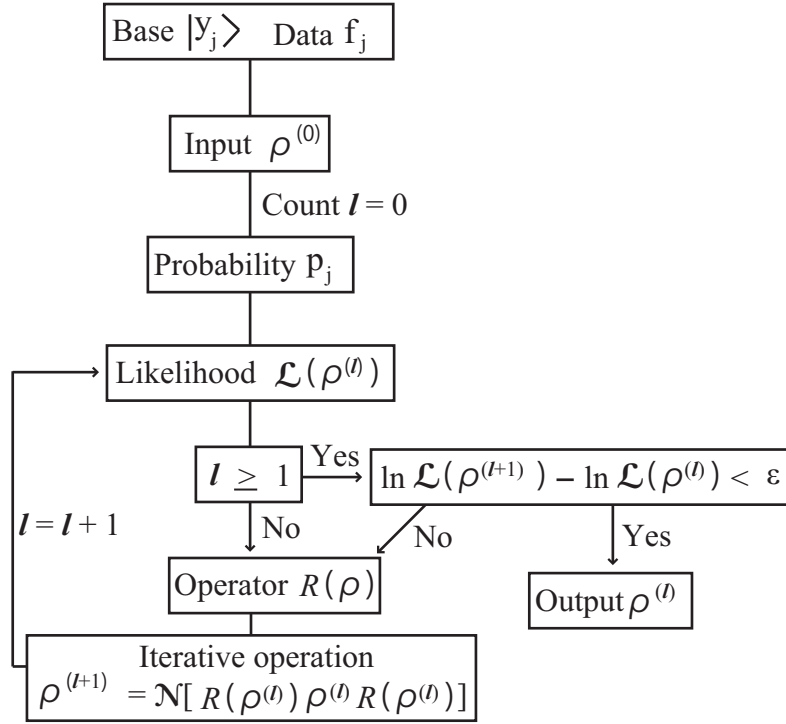


Figure 3.4: Flowchart of iterative maximum likelihood (IML) estimation for density matrices.

repeatedly until the condition $\ln \mathcal{L}_{l+1} - \ln \mathcal{L}_l < \epsilon$ is satisfied [see Fig. 3.4]. Here, when ρ is not a diagonal matrix, this operation can be done by replacing $\rho^{(l+1)} = R^{(l)} \rho^{(l)}$ by $\rho^{(l+1)} = \mathcal{N}[R^{(l)} \rho^{(l)} R^{(l)}]$ where \mathcal{N} is a normalization constant. It is noted that when $\sum_j |y_j\rangle\langle y_j| \neq I$, maximization can be done by $R \rightarrow G^{-1/2} R G^{-1/2}$ where $G \equiv \sum_j |y_j\rangle\langle y_j| / \sum_j p_j$.

Chapter 4

Local expansion and fusion of a multipartite W state

In this chapter, we propose two local expansion schemes and one fusion scheme for photonic W states. In Sec. 4.1, we propose a simple probabilistic optical gate to prepare and expand polarization entangled W states. The gate uses one polarization-dependent beamsplitter (PDBS) and a horizontally polarized single photon as an ancilla. The gate post-selectively expands N -photon W states to $(N + 1)$ -photon W states. In Sec. 4.2, we introduce an elementary optical gate for preparing and expanding polarization entangled W state using commercial 50:50 beamsplitters, which have no polarization dependence. The gate is composed of a pair of 50:50 beamsplitters and a phase shifter, and it requires a two-photon ancillary state. When the input is a photon from an N -photon W state, the gate produces an $(N + 2)$ -photon W state for post-selected events. Moreover, we show that this gate can be used to prepare and expand GHZ states by a simple modification of the ancillary state. In Sec. 4.3, we propose a fusion gate for two arbitrary W states. The operation of this gate corresponds to parity checking. The gate is composed of a polarizing beamsplitter (PBS), three half wave plates (HWP) and two polarization discriminating detectors. The gate post-selectively fuses N - and M -photon W states to prepare a $(N + M - 2)$ -photon W state. In Sec. 4.4, we give a brief summary and conclusions.

4.1 Local expansion of photonic W state using a polarization dependent beamsplitter

This section is organized as follows: In Sec. 4.1.1, we describe the principles of the gate operation. Sec. 4.1.2 includes a discussion of how this basic gate structure can be used to expand any polarization entangled W state. In Sec. 4.1.3, we give a scheme for the experimental realization of this gate and carry out a feasibility analysis under realistic conditions. Finally, in Sec. 4.1.4, we give a brief summary and conclusions.

4.1.1 Working principle of W state expansion

The details of the proposed gate are shown in Fig. 4.1 (a). The key component in this gate is the PDBS whose reflection and transmission coefficients depend on the polarization of the input light. The action of a PDBS for H-polarized photons and V-polarized photons can be written as

$$\hat{a}_{1\text{H}}^\dagger = \sqrt{1-\mu} \hat{a}_{3\text{H}}^\dagger - \sqrt{\mu} \hat{a}_{4\text{H}}^\dagger, \quad \hat{a}_{2\text{H}}^\dagger = \sqrt{\mu} \hat{a}_{3\text{H}}^\dagger + \sqrt{1-\mu} \hat{a}_{4\text{H}}^\dagger, \quad (4.1)$$

and

$$\hat{a}_{1\text{V}}^\dagger = \sqrt{1-\nu} \hat{a}_{3\text{V}}^\dagger - \sqrt{\nu} \hat{a}_{4\text{V}}^\dagger, \quad \hat{a}_{2\text{V}}^\dagger = \sqrt{\nu} \hat{a}_{3\text{V}}^\dagger + \sqrt{1-\nu} \hat{a}_{4\text{V}}^\dagger \quad (4.2)$$

where $\hat{a}_{j\text{H}}^\dagger$ ($\hat{a}_{j\text{V}}^\dagger$) denotes the creation operator of H (V)-polarized photon in the j -th mode of PDBS, and μ (ν) is the transmission coefficient for H (V)-polarization. The gate uses an H-polarized photon as the ancilla in mode 2, and a photon in mode 1 with an arbitrary polarization as the input. The successful operation of the gate is signalled by a coincidence detection which occurs when there is one photon in each of the output modes 3 and 4. In order to understand the working principle of this gate for W-state preparation and expansion, it is enough to consider its action on two possible cases: $|1_{\text{H}}\rangle_1 |1_{\text{H}}\rangle_2 = \hat{a}_{1\text{H}}^\dagger \hat{a}_{2\text{H}}^\dagger |vac\rangle_{12}$ and $|1_{\text{V}}\rangle_1 |1_{\text{H}}\rangle_2 = \hat{a}_{1\text{V}}^\dagger \hat{a}_{2\text{H}}^\dagger |vac\rangle_{12}$, where $|vac\rangle$ stands for the vacuum state. Using the relations given in Eqs. (4.1) and (4.2) for the PDBS, we find that these input states are transformed

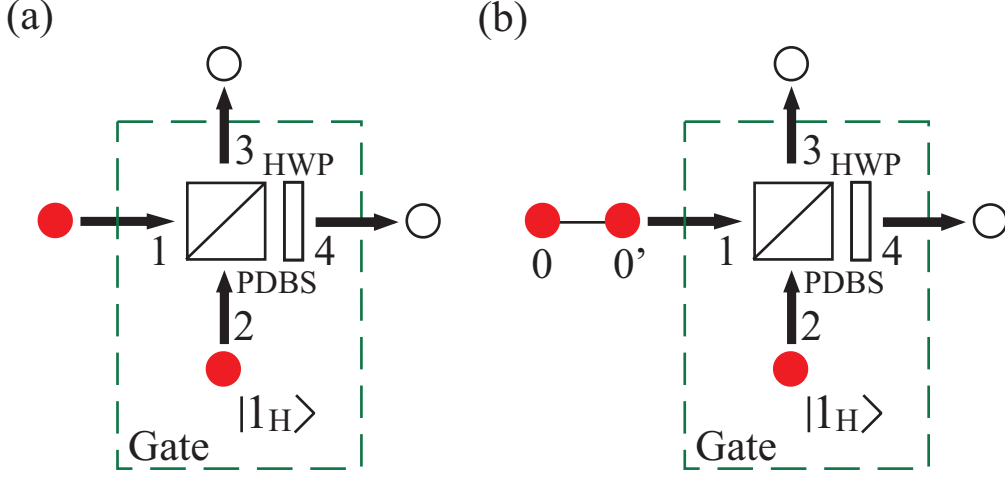


Figure 4.1: (a) The optical gate proposed for the local expansion of W states. The gate uses a polarization-dependent beamsplitter (PDBS), a half wave plate (HWP) and a horizontally (H) polarized single-photon as an ancilla in input mode 2. The photon in the input mode 1 comes from the W state to be expanded. (b) An example of expansion of state $|W_2\rangle$ to state $|W_3\rangle$.

into

$$|1_H\rangle_1 |1_H\rangle_2 \rightarrow \sqrt{2\mu(1-\mu)} |2_H\rangle_3 |0\rangle_4 + \underline{(1-2\mu) |1_H\rangle_3 |1_H\rangle_4} - \sqrt{2\mu(1-\mu)} |0\rangle_3 |2_H\rangle_4, \quad (4.3)$$

and

$$|1_V\rangle_1 |1_H\rangle_2 \rightarrow \sqrt{\mu(1-\nu)} |1_V 1_H\rangle_3 |0\rangle_4 + \sqrt{(1-\nu)(1-\mu)} |1_V\rangle_3 |1_H\rangle_4 - \sqrt{\mu\nu} |1_H\rangle_3 |1_V\rangle_4 - \sqrt{\nu(1-\mu)} |0\rangle_3 |1_V 1_H\rangle_4. \quad (4.4)$$

In the above equations, only the underlined terms lead to successful gate operation and we will focus only on those terms. It is seen that when the input photon is in V-polarization, the coincidence detection will postselect the state $\sqrt{(1-\nu)(1-\mu)} |1_V\rangle_3 |1_H\rangle_4 - \sqrt{\mu\nu} |1_H\rangle_3 |1_V\rangle_4$ which is an EPR pair if the PDBS parameters are chosen such that $\mu + \nu = 1$. This implies that this gate works as an “entangling gate”. The probability of this event is $2\mu\nu$.

Next, let us assume that we have an EPR pair in modes 0 and 0' given as $|W_2\rangle = (|1_V\rangle_0|1_H\rangle_{0'} + |1_H\rangle_0|1_V\rangle_{0'})/\sqrt{2}$. If the photon in mode 0' is input to mode 1 of the gate [see Fig. 4.1 (b)], a triple coincidence at modes 0, 3 and 4 will postselect the state

$$\frac{1}{\sqrt{2}}[(1-2\mu)|1_V\rangle_0|1_H\rangle_3|1_H\rangle_4 + \sqrt{(1-\nu)(1-\mu)}|1_H\rangle_0|1_V\rangle_3|1_H\rangle_4 - \sqrt{\mu\nu}|1_H\rangle_0|1_H\rangle_3|1_V\rangle_4]. \quad (4.5)$$

If the weights of the components of this superposition state in Eq. (4.5) are made equal, then Eq. (4.5) will be of the form $|W_3\rangle$ except a π -phase shift which can be compensated using a HWP in mode 4. The equalization of the weights occurs when

$$1-2\mu = \sqrt{(1-\nu)(1-\mu)} = \sqrt{\mu\nu}. \quad (4.6)$$

Second equality in Eq. (4.6) imposes the condition $\mu + \nu = 1$ which is the same condition obtained above for EPR pair preparation. Solving the remaining equalities under the condition $\mu + \nu = 1$, we find that one should choose $\mu = (5 - \sqrt{5})/10$ and $\nu = (5 + \sqrt{5})/10$. Inserting these values of μ and ν into Eqs. (4.3) - (4.4), and imposing the coincidence detection, we find that the successful gate operation is characterized by the following transformations

$$\begin{aligned} |1_H\rangle_1|1_H\rangle_2 &\rightarrow \frac{1}{\sqrt{5}}|1_H\rangle_3|1_H\rangle_4, \\ |1_V\rangle_1|1_H\rangle_2 &\rightarrow \frac{1}{\sqrt{5}}|1_V\rangle_3|1_H\rangle_4 + \frac{1}{\sqrt{5}}|1_H\rangle_3|1_V\rangle_4, \end{aligned} \quad (4.7)$$

where we have included the effect of the HWP in mode 4. Putting all together, we conclude that this gate can prepare the EPR pair $|W_2\rangle$ with a probability of 2/5 starting with a V-polarized photon in mode 1, and the $|W_3\rangle$ state with a probability of 3/10 starting with the EPR pair $|W_2\rangle$ in modes 0 and 0'. This success probability for $|W_3\rangle$ state preparation is a significant improvement over other linear optics schemes existing in the literature. Among the previously proposed schemes, the one in Ref. [45] has the highest success probability given as 1/9 which is less than that of the present scheme.

4.1.2 Expansion of polarization entangled W states

We show that the same gate can be used to prepare and expand arbitrary W states. In the following, we will represent an N -partite W state $|W_N\rangle$ as

$$|W_N\rangle = [|(N-2)_{\text{H}}, 1_{\text{V}}\rangle_{\tilde{1}} \otimes |1_{\text{H}}\rangle_1 + |(N-1)_{\text{H}}, 0_{\text{V}}\rangle_{\tilde{1}} \otimes |1_{\text{V}}\rangle_1] / \sqrt{N}, \quad (4.8)$$

where the subscript 1 denotes the spatial mode of the photon that is input to the gate and $\tilde{1}$ denotes the remaining $N-1$ modes of $|W_N\rangle$, and $|l_{\text{H}}, k_{\text{V}}\rangle$ is the sum over all the terms with l modes in $|H\rangle$ and k modes in $|V\rangle$. Using this notation, the transformation in Eq. (4.7) can be represented as $|1_{\text{H}}\rangle_1 |1_{\text{H}}\rangle_2 \rightarrow \sqrt{1/5} |2_{\text{H}}, 0_{\text{V}}\rangle$ and $|1_{\text{V}}\rangle_1 |1_{\text{H}}\rangle_2 \rightarrow \sqrt{1/5} |1_{\text{H}}, 1_{\text{V}}\rangle$. Thus, we find that upon the selection of the successful events, the action of the gate is given as

$$\begin{aligned} |(N-2)_{\text{H}}, 1_{\text{V}}\rangle_{\tilde{1}} |1_{\text{H}}\rangle_1 &\rightarrow \frac{1}{\sqrt{5}} |(N-2)_{\text{H}}, 1_{\text{V}}\rangle_{\tilde{1}} \otimes |2_{\text{H}}, 0_{\text{V}}\rangle, \\ |(N-1)_{\text{H}}, 0_{\text{V}}\rangle_{\tilde{1}} |1_{\text{V}}\rangle_1 &\rightarrow \frac{1}{\sqrt{5}} |(N-1)_{\text{H}}, 0_{\text{V}}\rangle_{\tilde{1}} \otimes |1_{\text{H}}, 1_{\text{V}}\rangle. \end{aligned} \quad (4.9)$$

Using these relations, it is straightforward to show that the successful gate operation performs the following transformation on an initial $|W_N\rangle$:

$$\begin{aligned} |W_N\rangle &\rightarrow \frac{1}{\sqrt{5N}} [|(N-2)_{\text{H}}, 1_{\text{V}}\rangle_{\tilde{1}} \otimes |2_{\text{H}}, 0_{\text{V}}\rangle + |(N-1)_{\text{H}}, 0_{\text{V}}\rangle_{\tilde{1}} \otimes |1_{\text{H}}, 1_{\text{V}}\rangle] \\ &= \sqrt{\frac{N+1}{5N}} |W_{N+1}\rangle. \end{aligned} \quad (4.10)$$

Thus we conclude that the gate expands a given W state $|W_N\rangle$ to $|W_{N+1}\rangle$ by one photon with a success probability of $(N+1)/5N$. The success probability will approach the constant $1/5$ when N becomes large. This analysis clearly shows that the proposed gate can be used in two different ways: (i) A given arbitrary-size W state $|W_N\rangle$ can be expanded by one at each successful operation of the gate which takes place with the probability $(N+1)/5N$, e.g., a probability of $4/15$ for the expansion of $|W_3\rangle$ to $|W_4\rangle$, and (ii) starting from a V-polarized input photon, an arbitrary-size W state can be prepared by cascade application of the gate. For example, cascading k of this gate will prepare the state $|W_{k+1}\rangle$ with a probability of $(k+1)5^{-k}$.

4.1.3 Practical considerations for preparing W_3 state

We introduce an experimental scheme for the implementation of this gate to expand the EPR pair $|W_2\rangle$ to the three-photon W state $|W_3\rangle$, and discuss the effects of realistic conditions on the performance of the gate. We will focus on the effects of imperfections in (a) the preparation of the state $|W_2\rangle$ and the ancillary state, $|1_H\rangle$, (b) the detection of the successful events, and (c) the deviations of the parameters of PDBS from its optimal values.

(a) Basic scheme

We propose the scheme given in Fig. 4.2 for the practical implementation of the proposed gate. In this scheme, the output of a pulsed laser (PL) with angular frequency ω_0 in the visible range of the spectrum is frequency doubled in a nonlinear crystal to produce pulses of ultraviolet (UV) light of angular frequency $2\omega_0$. These UV pulses are then used to pump twice in forward and backward directions a pair of nonlinear crystals, which are stacked together such that their optical axes are orthogonal to each other [64]. The crystals are for Type I spontaneous parametric down conversion (SPDC) to produce photon pairs in two modes (idler and signal) with the same polarization and at half the frequency of the pump beam. In the forward pumping direction, the polarization of the UV beam is set to vertical so that an H-polarized photon pair in modes 2 and 2' are generated from which the required ancillary state $|1_H\rangle$ in mode 2 can be prepared. The remaining (non-down-converted) portion of the UV beam first passes through a quarter wave plate (QWP) which changes its polarization into an ellipsoidal polarization. A mirror placed after the QWP back-reflects this beam and sends it through the QWP again which further changes the polarization of the beam into diagonal polarization. This diagonally polarized beam pumps the crystals in the backward direction creating the entangled photon pair $(|1_H\rangle_0|1_H\rangle_{0'} + |1_V\rangle_0|1_V\rangle_{0'})/\sqrt{2}$. Changing the polarization of the photon in the mode 0 (idler) of the SPDC output will prepare the $|W_2\rangle$ in the spatial modes 0 and 0'. Then the ancillary photon in mode 2 and the photon in mode 1 of $|W_2\rangle$ are combined at the PDBS. The successful events are

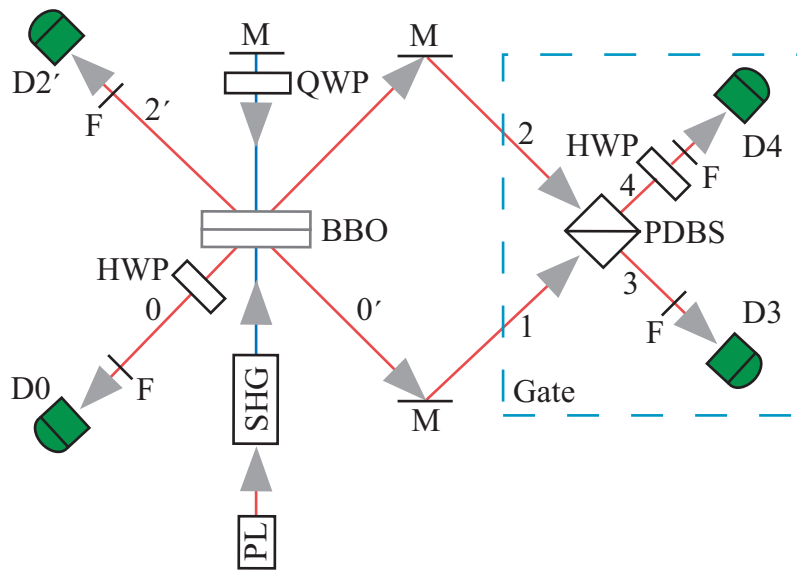


Figure 4.2: Experimental setup for realizing the proposed gate. PL, pulsed laser; SHG, second harmonic generator; Type I BBO, phase matched β -barium borate crystal for spontaneous parametric down conversion (SPDC); PDBS, polarization dependent beamsplitter; D_j , photodetectors; QWP, quarter-wave plate; HWP, half-wave plate; F, narrow-band interference filter; M, mirror.

selected by a four-fold coincidence detection by ON/OFF detectors placed at the modes 0, 2', 3 and 4 as seen in Fig. 4.2. In order to have a high fidelity, it is crucial that the information on the source of the photons in modes 3 and 4 is erased. This can be done by placing narrowband interference filters, whose coherence times are much longer than the duration of the pump pulse, in front of the detectors [70, 71]. Indistinguishability of these photons can be further enhanced by spatial filters, which can be implemented using single-mode fiber-coupled photodetectors. It is to be noted that there is a trade-off between the indistinguishability and the success probability. The tighter is the spectral and spatial filtering the higher is the indistinguishability and hence the fidelity, but the lower is the efficiency. In the following analysis of the effects of imperfections in photon generation, photon detection and the PDBS on the performance of the gate, we assume for the sake of

simplicity that the photons are perfectly matched and they are indistinguishable.

(b) Effects of SPDC and imperfect detection

Imperfections in the photon detectors affect the gate in two ways: (i) Recording some of the successful events as the failure due to non-unit quantum efficiency, and (ii) reporting some of the failures as the successful ones due to dark counts and/or due to the fact that detectors cannot resolve the photon number. In the following, without loss of generality, we neglect the errors due to dark counts. This is acceptable as the dark counting rates of current detectors are very low [72]. Moreover, the requirement of four-fold coincidence detection in our scheme significantly reduces the probability of false events caused by dark counts. Neglecting the dark counts, the positive operator valued measure (POVM) elements for ON/OFF photodetectors become

$$\Pi_0 = \sum_{m=0}^{\infty} (1 - \eta)^m |m\rangle\langle m|, \quad (4.11)$$

$$\Pi_1 = 1 - \Pi_0 = \sum_{m=1}^{\infty} [1 - (1 - \eta)^m] |m\rangle\langle m|, \quad (4.12)$$

where Π_0 and Π_1 are, respectively, the elements for no click (OFF) and for a click (ON) [71]. Returning back to our gate, we see that if there is only one photon in each of the modes 1 and 2, then the success probability of detecting one photon in each of modes 3 and 4 becomes $3\eta^4/10$. Note that the error due to (ii) occurs when there are more than one photon in either or both of the modes 3 and 4. This takes place when either or both of the backward and forward SPDC processes prepare two or more photon pairs. In practical settings, SPDC suffers from the non-deterministic nature of the process: The output of the SPDC contains vacuum with high probability and the probability of a photon pair generation is low. Moreover, although the probability is much lower, there are cases when multiple pairs of photons are generated. The generated state in the forward direction becomes

$$|\Psi\rangle_{22'} = \sqrt{g}(|vac\rangle_{22'} + \gamma e^{i\phi_p} |1_H\rangle_2 |1_H\rangle_{2'} + \gamma^2 e^{2i\phi_p} |2_H\rangle_2 |2_H\rangle_{2'} \dots), \quad (4.13)$$

where $g = 1 - \gamma^2$ and $\gamma e^{i\phi_p}$ is proportional to the complex amplitude of the pump field. Assuming that the losses in the forward and backward pumping are negligible, the state in the backward direction can be written as

$$|\Psi\rangle_{01} = \sqrt{g_1}(|vac\rangle_{01} + \gamma e^{i\phi_p} |W_2\rangle_{01} + \frac{1}{2}\gamma^2 e^{2i\phi_p} |\Lambda\rangle_{01} \dots), \quad (4.14)$$

where $|\Lambda\rangle_{01} = |1_H 1_V\rangle_0 |1_H 1_V\rangle_1 + |2_V\rangle_0 |2_H\rangle_1 + |2_H\rangle_0 |2_V\rangle_1$ is unnormalized and $g_1 = (1 - \gamma^2/2)^2$. Combining the above expressions, we find that four-fold coincidence detection postselects the state,

$$\begin{aligned} |\Psi\rangle_{0122'} &= \sqrt{gg_1} [\gamma^2 e^{2i\phi_p} |W_2\rangle_{01} |1_H\rangle_2 |1_H\rangle_{2'} \\ &\quad + \gamma^3 e^{3i\phi_p} (|W_2\rangle_{01} |2_H\rangle_2 |2_H\rangle_{2'} + \frac{1}{2} |\Lambda\rangle_{01} |1_H\rangle_2 |1_H\rangle_{2'})] + \mathcal{O}(\gamma^4) \\ &= \sqrt{gg_1} [\frac{1}{\sqrt{2}} \gamma^2 e^{2i\phi_p} (\hat{a}_{0V}^\dagger \hat{a}_{1H}^\dagger + \hat{a}_{0H}^\dagger \hat{a}_{1V}^\dagger) \hat{a}_{2H}^\dagger \hat{a}_{2'H}^\dagger \\ &\quad + \frac{1}{2\sqrt{2}} \gamma^3 e^{3i\phi_p} (\hat{a}_{0V}^\dagger \hat{a}_{1H}^\dagger + \hat{a}_{0H}^\dagger \hat{a}_{1V}^\dagger) (\hat{a}_{2H}^\dagger)^2 (\hat{a}_{2'H}^\dagger)^2 \\ &\quad + \frac{1}{4} \gamma^3 e^{3i\phi_p} \{ 2\hat{a}_{0H}^\dagger \hat{a}_{0V}^\dagger \hat{a}_{1H}^\dagger \hat{a}_{1V}^\dagger + (\hat{a}_{0V}^\dagger)^2 (\hat{a}_{1H}^\dagger)^2 \\ &\quad + (\hat{a}_{0H}^\dagger)^2 (\hat{a}_{1V}^\dagger)^2 \} \hat{a}_{2H}^\dagger \hat{a}_{2'H}^\dagger] |vac\rangle_{0122'} + \mathcal{O}(\gamma^4), \end{aligned} \quad (4.15)$$

where we have focused on the terms up to γ^3 by considering that in practice, $\gamma^2 \sim \mathcal{O}(10^{-4})$ is very small. The PDBS transforms modes 1 and 2 of $|\Psi\rangle_{0122'}$ according to the relations given in Eqs. (4.1) and (4.2). Defining the state after the transformation as $|\Psi'\rangle_{0342'}$ and using POVM given in Eq. (4.12), the four-fold coincidence detection probability p_c can be calculated as

$$\begin{aligned} p_c &= {}_{0342'} \langle \Psi' | \Pi_1^0 \Pi_1^3 \Pi_1^4 \Pi_1^2 | \Psi' \rangle_{0342'} \\ &= \underbrace{\frac{1}{2} gg_1 \gamma^4 \eta^4 [2\mu(\mu - 1) + 1]}_{p_t} \\ &\quad + \underbrace{\frac{1}{2} gg_1 \gamma^6 \eta^4 (2 - \eta)^2 + \frac{1}{2} gg_1 \gamma^6 \eta^4 (2 - \eta)^2 [\mu(\mu - 1) + 1]}_{p_f} + \mathcal{O}(\gamma^8), \end{aligned} \quad (4.16)$$

where Π_1^j is the POVM for “click” events at the detection in mode j , and p_t and p_f respectively corresponds to the probability of true and false coincidences. We see in Eq. (4.16)

two contributions, p_t and p_f . The true coincidences (p_t) are due to the $|W_2\rangle_{01}|1_H\rangle_2|1_H\rangle_{2'}$ term in $|\Psi\rangle_{0122'}$ and the false coincidences (p_f) originates from multiple pairs of photons. Plugging the value $\mu = (5 - \sqrt{5})/10$ in these terms, we find that the ratio of the true coincidences to the total coincidence events becomes

$$p = \frac{p_t}{p_t + p_f} = 1 - 3\gamma^2(\eta - 2)^2 + \mathcal{O}(\gamma^4). \quad (4.17)$$

It is clearly seen that almost all of the four-fold coincidence detections are true coincidences within the range of realistic values of η and γ .

(c) Effect of deviation in the PDBS parameter

We consider the effect of deviations in the parameters of PDBS from its ideal values of $\mu = (5 - \sqrt{5})/10$ and $\nu = (5 + \sqrt{5})/10$ on the probability and the fidelity of expanding the state $|W_2\rangle$ into the state $|W_3\rangle$. Let us assume that the reflection coefficients of PDBS for H- and V-polarized photons are deviated from the ideal values by δ and Δ , respectively. Then the action of the imperfect PDBS on H-polarized light and V-polarized light becomes

$$\hat{a}_{1H}^\dagger = \sqrt{1 - \mu - \delta} \hat{a}_{3H}^\dagger - \sqrt{\mu + \delta} \hat{a}_{4H}^\dagger, \quad \hat{a}_{2H}^\dagger = \sqrt{\mu + \delta} \hat{a}_{3H}^\dagger + \sqrt{1 - \mu - \delta} \hat{a}_{4H}^\dagger, \quad (4.18)$$

and

$$\hat{a}_{1V}^\dagger = \sqrt{1 - \nu - \Delta} \hat{a}_{3V}^\dagger - \sqrt{\nu + \Delta} \hat{a}_{4V}^\dagger, \quad \hat{a}_{2V}^\dagger = \sqrt{\nu + \Delta} \hat{a}_{3V}^\dagger + \sqrt{1 - \nu - \Delta} \hat{a}_{4V}^\dagger, \quad (4.19)$$

where $-\mu \leq \delta \leq \nu$ and $-\nu \leq \Delta \leq \mu$. Using these expressions, we calculated the probability of coincidence detection and the fidelity of the output state to the desired one. We omit the analytic expressions since they are rather lengthy and complicated. Instead, we depict the constant fidelity and constant probability contours as a function of δ and Δ in Fig. 4.3. We see that the effect of δ on the fidelity is much larger than that of Δ . We can thus tolerate larger deviations from the ideal value for Δ .

4.1.4 Brief discussion

In this section, we have proposed a simple probabilistic optical gate for expanding polarization entangled W states and analyzed its feasibility taking into account the imperfections

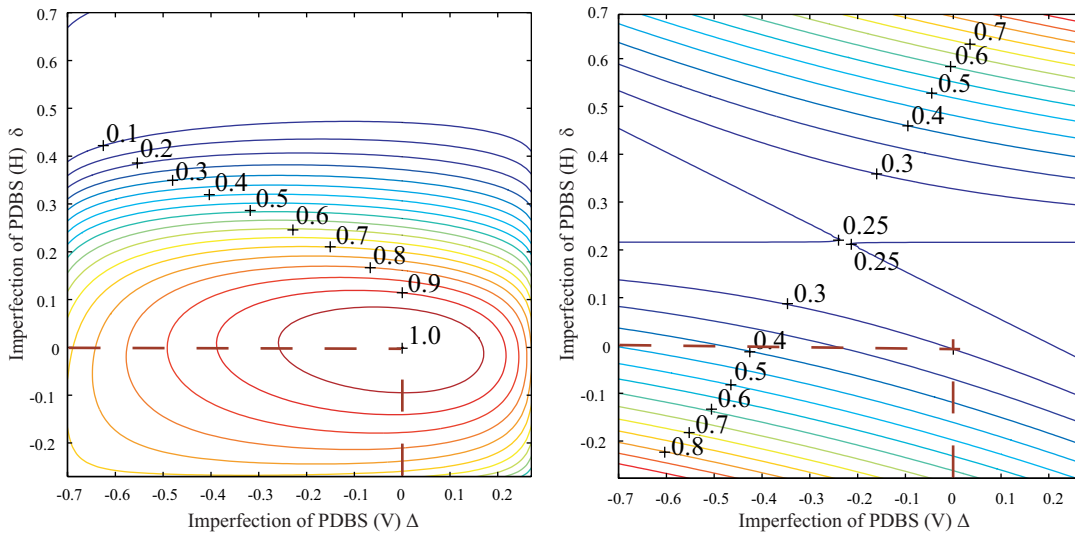


Figure 4.3: Constant fidelity (left) and constant probability (right) contour plots as a function of δ and Δ , which are deviations of the parameters μ and ν of PDBS from their ideal values, respectively.

encountered in practice. The proposed gate expands $|W_N\rangle$ by one qubit into $|W_{N+1}\rangle$ by locally acting on one of its qubits. A remarkable feature of this gate is that starting with a EPR pair, it can prepare tripartite entangled W state with a success probability of $3/10$ which is the highest among all the proposed schemes so far. Moreover, the gate does not need stabilization of optical paths and does not employ sub-wavelength adjustments. Our feasibility analysis shows that the proposed gate can be implemented by the current experimental technologies.

4.2 Local expansion of photonic W state using two non-polarizing beamsplitters

This section is organized as follows: In Sec. 4.2.1, we give the working principle of the proposed gate (T_{+2}^W gate). Sections 4.2.2 and 4.2.3 include, respectively, the use of this gate

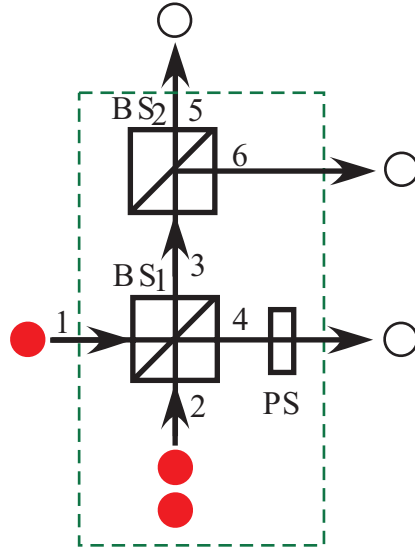


Figure 4.4: Schematic diagram of the proposed elementary optical gate.

in the preparation and expansion of polarization entangled W states, and the feasibility analysis for $|W_4\rangle$ preparation. In Sec. 4.2.4, we show that by changing the state of the ancilla photons, this gate can be used for the expansion of GHZ states, and finally Sec. 4.2.5 will contain a summary of this work.

4.2.1 Working principle of the gate

In Fig. 4.4, we show the schematic of the proposed gate. The gate receives one photon from mode 1 as the input, and combines it by a 50:50 beamsplitter (BS_1) with two ancilla photons in the state $|2_H\rangle_2$ where H stands for the horizontal polarization and the subscript number signifies the spatial mode. One of the output modes of BS_1 is further divided into two modes by another 50:50 beamsplitter (BS_2). The gate is successful when one photon is found in each of the output modes 4, 5, and 6. The phase shifter (PS) placed in mode 4 is a half-wave plate which introduces a π -phase shift between H and V polarizations to keep the final W state in the standard symmetric form.

First we analyze the operation of this gate for H-polarized ($|1_H\rangle_1$) or V-polarized ($|1_V\rangle_1$)

seed states in mode 1. The action of the polarization-independent BS₁ on H (V) polarization is represented by the transformation

$$\begin{aligned}\hat{a}_{1\text{H(V)}}^\dagger &= (\hat{a}_{3\text{H(V)}}^\dagger - \hat{a}_{4\text{H(V)}}^\dagger)/\sqrt{2}, \\ \hat{a}_{2\text{H(V)}}^\dagger &= (\hat{a}_{3\text{H(V)}}^\dagger + \hat{a}_{4\text{H(V)}}^\dagger)/\sqrt{2},\end{aligned}\quad (4.20)$$

where $\hat{a}_{j\text{H(V)}}^\dagger$ is the photon creation operator for mode j in H(V) polarization. Using these relations we find that with the action of BS₁, the initial states $|1_{\text{H(V)}}\rangle_1 \otimes |2_{\text{H}}\rangle_2 = 2^{-1/2}\hat{a}_{1\text{H(V)}}^\dagger(\hat{a}_{2\text{H}}^\dagger)^2|0\rangle$ evolve as

$$\begin{aligned}|1_{\text{H}}\rangle_1|2_{\text{H}}\rangle_2 &\rightarrow \frac{\sqrt{3}}{2\sqrt{2}}|3_{\text{H}}\rangle_3|0\rangle_4 + \frac{1}{2\sqrt{2}}\underline{|2_{\text{H}}\rangle_3|1_{\text{H}}\rangle_4} - \frac{1}{2\sqrt{2}}|1_{\text{H}}\rangle_3|2_{\text{H}}\rangle_4 \\ &\quad - \frac{\sqrt{3}}{2\sqrt{2}}|0\rangle_3|3_{\text{H}}\rangle_4, \\ |1_{\text{V}}\rangle_1|2_{\text{H}}\rangle_2 &\rightarrow \frac{1}{2\sqrt{2}}|1_{\text{V}}2_{\text{H}}\rangle_3|0\rangle_4 + \frac{1}{2}\underline{|1_{\text{H}}1_{\text{V}}\rangle_3|1_{\text{H}}\rangle_4} + \frac{1}{2\sqrt{2}}|1_{\text{V}}\rangle_3|2_{\text{H}}\rangle_4 \\ &\quad - \frac{1}{2\sqrt{2}}\underline{|2_{\text{H}}\rangle_3|1_{\text{V}}\rangle_4} - \frac{1}{2}|1_{\text{H}}\rangle_3|1_{\text{H}}1_{\text{V}}\rangle_4 - \frac{1}{2\sqrt{2}}|0\rangle_3|1_{\text{V}}2_{\text{H}}\rangle_4.\end{aligned}\quad (4.21)$$

The underlined terms, in which there are two photons in mode 3 and one photon in mode 4, are the only ones leading to the successful gate operation. Hence we are interested only in the underlined terms. The states $|2_{\text{H}}\rangle_3$ and $|1_{\text{H}}1_{\text{V}}\rangle_3$ appearing in the underlined terms are transformed at BS₂ as

$$\begin{aligned}|2_{\text{H}}\rangle_3 &\rightarrow \frac{1}{2}|2_{\text{H}}\rangle_5|0\rangle_6 + \frac{1}{\sqrt{2}}\underline{|1_{\text{H}}\rangle_5|1_{\text{H}}\rangle_6} + \frac{1}{2}|0\rangle_5|2_{\text{H}}\rangle_6, \\ |1_{\text{H}}1_{\text{V}}\rangle_3 &\rightarrow \frac{1}{2}|1_{\text{H}}1_{\text{V}}\rangle_5|0\rangle_6 + \frac{1}{2}\underline{|1_{\text{H}}\rangle_5|1_{\text{V}}\rangle_6} + \frac{1}{2}\underline{|1_{\text{V}}\rangle_5|1_{\text{H}}\rangle_6} + \frac{1}{2}|0\rangle_5|1_{\text{H}}1_{\text{V}}\rangle_6.\end{aligned}\quad (4.22)$$

Since successful gate operation requires that there is one photon in each of the modes 4, 5 and 6, it is apparent that only the underlined terms in Eq. (4.22) has contribution. If we postselect these terms with a coincidence detection scheme, the operation of the gate will

	$ 1_V\rangle_1 2_H\rangle_2$			$ 1_H\rangle_1 2_H\rangle_2$		
output modes	4	5	6	4	5	6
Classical case	H	H	V	H	H	H
	H	V	H	H	H	H
	V	H	H	H	H	H
Quantum case	H	H	V	H	H	H
	H	V	H			
	V	H	H			

minus sign

↓

-	H	H	H
	H	H	H

Table 4.1: Input-output relation for the intuitive understanding of gate operations.

be given by the following state transformations:

$$|1_H\rangle_1|2_H\rangle_2 \rightarrow \frac{1}{4}|1_H\rangle_4|1_H\rangle_5|1_H\rangle_6, \quad (4.23)$$

$$|1_V\rangle_1|2_H\rangle_2 \rightarrow \frac{1}{4}|1_H\rangle_4|1_H\rangle_5|1_V\rangle_6 + \frac{1}{4}|1_H\rangle_4|1_V\rangle_5|1_H\rangle_6 + \frac{1}{4}|1_V\rangle_4|1_H\rangle_5|1_H\rangle_6, \quad (4.24)$$

where we have included the effect of the PS in mode 4. All the four terms appearing in Eq. (4.23) and Eq. (4.24) have the same amplitude implying that the success probability is $1/16$ for the $|1_H\rangle_1$ input and $3/16$ for the $|1_V\rangle_1$ input. If the seed photon is a part of a polarization entangled system, we will have a coherent superposition of the above two cases. It is interesting to see here that the gate performs a symmetrization among the input and the ancillary states. The insight into the above equations can be gained as follows [see Table 4.1]: When the seed is a V-polarized photon, we have a classical situation where two H-polarized photons are distributed among three output modes in three different ways and the remaining one port is occupied by the V-polarized photon from the seed. These three cases are $|1_H\rangle_4|1_H\rangle_5|1_V\rangle_6$, $|1_H\rangle_4|1_V\rangle_5|1_H\rangle_6$, $-|1_V\rangle_4|1_H\rangle_5|1_H\rangle_6$. Note that the last term with the minus sign corresponds to the situation where there are two H-polarized

photons at the input of BS_2 . On the other hand, when the seed is an H-polarized photon, we have three indistinguishable particles and quantum effects come into play. Contrary to the expectation with distinguishable particles, we end up with only one term because the three possible cases to distribute the particles among the output modes correspond exactly to the same state $|1_H\rangle_4|1_H\rangle_5|1_H\rangle_6$ with one having a minus sign. This minus sign leads to destructive interference resulting in only one term, $|1_H\rangle_4|1_H\rangle_5|1_H\rangle_6$. This is the important feature of the gate which will be exploited in expanding the symmetrically shared entanglement in W state.

4.2.2 Expansion of polarization entangled W states

We observe that the expression on the right hand side of Eq. (4.24) corresponds to $|W_3\rangle$ which implies that the gate prepares polarization entangled $|W_3\rangle$ state with a success probability of $3/16$ if the seed $|W_1\rangle$ is a V-polarized single photon. Equations (4.23) and (4.24) also tell that if the input photon in mode 1 has formed an EPR pair $|W_2\rangle = (|1_H\rangle_0|1_V\rangle_1 + |1_V\rangle_0|1_H\rangle_1)/\sqrt{2}$ with another photon in mode 0, the output state for the post-selected events are given by

$$\begin{aligned} |W_2\rangle &\rightarrow \frac{1}{4\sqrt{2}} [|1_H\rangle_0|1_H\rangle_4|1_H\rangle_5|1_V\rangle_6 + |1_H\rangle_0|1_H\rangle_4|1_V\rangle_5|1_H\rangle_6 \\ &\quad + |1_H\rangle_0|1_V\rangle_4|1_H\rangle_5|1_H\rangle_6 + |1_V\rangle_0|1_H\rangle_4|1_H\rangle_5|1_H\rangle_6] \\ &\rightarrow \frac{1}{\sqrt{8}} |W_4\rangle, \end{aligned} \tag{4.25}$$

which means that the $|W_4\rangle$ state is produced with probability $1/8$.

The success probability $1/8$ for the preparation of $|W_4\rangle$ is significant improvements over the other linear optics-based schemes proposed for these states. For instance, the most efficient schemes so far are those in Ref [44] for $|W_4\rangle$ with the corresponding success probability of $2/27$ which is lower than that of our proposal. For the preparation of $|W_3\rangle$, the success probability $3/10$ of our proposed gate in Sec. 4.1 is higher than the success probability $3/16$ of this proposed gate.

If the input photon is from a general W state $|W_N\rangle$, the application of the gate will

result in the transformation:

$$\begin{aligned} |W_N\rangle &\rightarrow [|(N-2)_H, 1_V\rangle \otimes |3_H, 0\rangle + |(N-1)_H, 0\rangle \otimes |2_H, 1_V\rangle]/4\sqrt{N} \\ &= |N+1_H, 1_V\rangle/4\sqrt{N}, \end{aligned} \quad (4.26)$$

implying that $|W_{N+2}\rangle$ is prepared with a success probability of $(N+2)/(16N)$ where $|l_H, k_V\rangle$ is the sum over all the terms with l modes in $|H\rangle$ and k modes in $|V\rangle$. When N becomes large, the success probability will approach to the constant $1/16$.

An interesting feature of this gate is that it can be cascaded to prepare any desired size of W state. Starting with an input state of $|1_V\rangle_1$ to the first gate in the cascaded series of k proposed gates, a $2k+1$ -photon polarization entangled W state, $|W\rangle_{2k+1}$, can be prepared provided that coincidence detection is observed at $2k+1$ output spatial modes. The success probability of such an event scales as $p_{\text{success}} = (2k+1)2^{-4k}$. Similarly, starting with a photon from a EPR pair and cascading k gates, one can prepare $2(k+1)$ -photon polarization entangled W state, $|W\rangle_{2(k+1)}$ with a success probability of $p_{\text{success}} = (k+1)2^{-4k}$.

In comparison to the gate proposed in Sec. 4.1, this gate which adds two photons here tends to have a better success probability of producing a specific W state. For example, For preparation of $|W_5\rangle$ from a V-polarized photon. the gate in Sec. 4.1 requires cascading of four gates and the success probability becomes $5/5^4 = 1/125$. On the other hand, this gate requires cascading of two gates and the success probability is $5/16^2 = 5/256$. In general, when the number of photons, are large, the gate in Sec. 4.1 needs a cascade of two gates for addition of two photons, which reduces the success probability by a factor of $1/5^2 = 1/25$. Whereas this gate which adds two photons reduces the success probability by a factor of $1/16$. For the case of starting from an initial state and preparing a desired state, this is the reason why the proposed gate which adds two photons has a greater advantage than the proposed gate in Sec. 4.1.

Besides our current proposal, the scheme based on $N \times N$ multiport interferometers [36, 45] is so far the only proposal encompassing generation of $|W_N\rangle$ with arbitrary N . This scheme requires a different multiport device for each N . In addition, numerical calculation up to $N = 7$ shows that our proposal has better efficiency, e.g., for $N = 5$ our proposal

succeeds with a probability 12 times higher than that of the multiport interferometer. Note also that $N \times N$ interferometer cannot generate the $|W_6\rangle$ state because of the zero probability of coincidence detection due to destructive interference.

4.2.3 Practical considerations for preparing W_4 state

We introduce an experimental scheme for the implementation of this gate to expand the EPR pair $|W_2\rangle$ to $|W_4\rangle$, and discuss the effects of realistic conditions on the performance of the gate. We will analyze the effects of imperfections in (a) the preparation of the $|W_2\rangle$ and the ancillary state, $|2_H\rangle$, (b) the detection of the successful events, and (c) the deviations of the parameters of 50:50 BS from its optimal values.

(a) Basic scheme

So far, several linear optical schemes for preparing the state $|W_4\rangle$ have been proposed [44, 45, 46], but no experiments have been done yet. It is thus important to consider the feasibility of our scheme with practical photon sources, namely, parametric down-conversion (PDC) and/or weak coherent pulses (WCP) obtained by attenuating laser pulses. We give a schematic configuration of a possible experimental scheme in Fig. 4.5.

In this scheme, the light from a mode-locked Ti:sapphire laser (wavelength 790nm; pulse width 90fs; repetition rate 82MHz) is frequency-doubled to a wavelength of 395nm with a second harmonic generator (SHG) to prepare ultraviolet (UV) light. Then the UV light is divided into two parts one of which is used to prepare the EPR photon pair and the other to prepare the H-polarized two-photon ancillary state using spontaneous parametric down conversion (SPDC). For EPR photon pair generation the polarization of the UV pulse is set to diagonal polarization, and it is used to pump BBO_1 , which is formed by stacking together two Type I phase matched 1.5mm thick β -barium borate (BBO) crystals with their optical axes orthogonal to each other [64]. For the ancilla state preparation, the UV pulse is set to vertical polarization and then it is used to pump a Type I BBO_2 to prepare two photons in H-polarization collinearly. Then one photon of the EPR photon pair is sent to the proposed

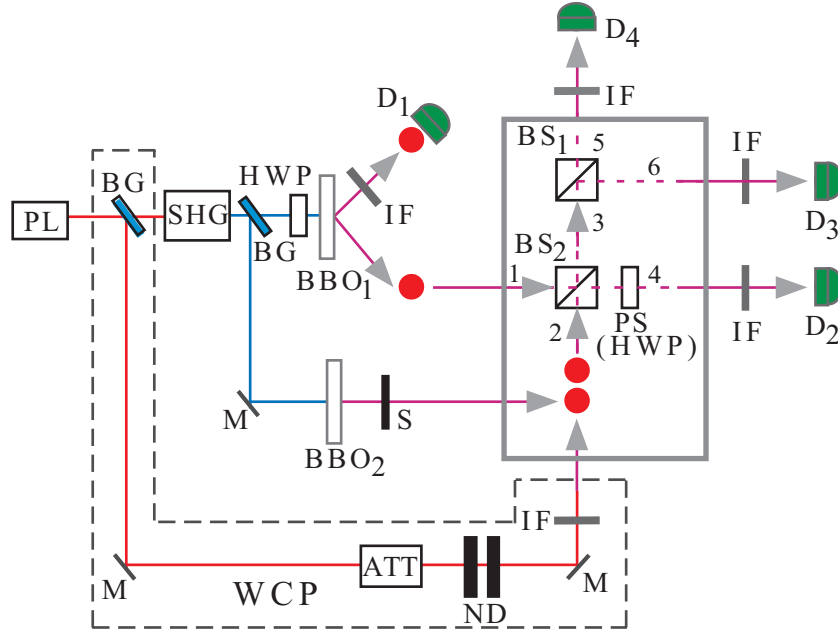


Figure 4.5: Schematic configuration of experimental setup for realizing the proposed gate. PL, pulsed laser; SHG, second harmonic generator; BG, brewster window; BBO_{1,2}, Type I phase matched 1.5mm thick β -barium borate crystal for spontaneous parametric down conversion (SPDC); BS₁ and BS₂, 50:50 symmetric beamsplitters; PS, phase shifter implemented using half wave plate (HWP); IF, interference filter with central wavelength $\lambda = 790\text{nm}$ and full-width at half-maximum bandwidth $\Delta\lambda = 2.7\text{nm}$; ND, neutral density filter; ATT, optical attenuator; D_j, photodetectors; M, mirror. The H-polarized two-photon ancilla state can be prepared by either using SPDC or weak coherent pulse (WCP). When it is prepared using SPDC, the part of the figure in dashed box is not used, and the shutter (S) is open. On the other hand, when it is prepared from WCP then the dashed part will be used and the shutter will be closed.

gate where it is mixed with the ancilla photons. The correct events are post-selected by a four-fold coincidence detection at silicon avalanche photodiodes, $D_{j=1,2,3,4}$, (EG&G single photon counting module- SPCM with quantum efficiency $\eta_d \sim 0.55$ and dark count rate 50 count/s).

(b) Imperfect detection

We discuss the effect of imperfections of detectors and the photon source on our scheme. The errors due to dark counts of the detectors cannot be eliminated even by post-selection, but the dark count rates of current detectors are pretty low for multi-photon coincidence measurements (e.g., in a detection window of 2.5ns, there will be 1.25×10^{-6} count/window), and thus errors due to them can be neglected [71, 72]. Hence, the errors in the post-selected state are mainly caused by multi-photon pairs from the SPDC. The probability of correct events in this scheme is $\mathcal{O}(\eta^4 \gamma^4)$ where $\gamma^2 \sim 10^{-4}$ is the photon pair generation rate per pulse in a typical SPDC process, and $\eta \sim 10^{-1}$ is the overall system efficiency which takes into account the detector efficiency and losses due to coupling and optical components [72]. On the other hand, the probability of false events due to generation of excess pairs scales as $\mathcal{O}(\eta^4 \gamma^n)$ with $n \geq 6$. Thus the contribution of false events in the post-selected events is $\mathcal{O}(10^{-4})$, and hence it can be neglected.

Alternatively, we may also use WCP instead of SPDC for the ancillary photons in mode 2. In this case, the experimental setup will be modified as follows: The light pulses from Ti:sapphire laser is divided into two unequal parts by a beamsplitter. The stronger portion will go to SHG to prepare the UV used for EPR photon pair generation at the Type I BBOs. The weak part will be further attenuated through a combination of HWPs, polarizers and neutral density (ND) filters to obtain a WCP with mean photon number ν . Then the desired events occur with a rate $\mathcal{O}(\eta^4 \gamma^2 \nu^2)$. If we assume that $\nu \ll 1$, then the main source of error will be the two-pair production at SPDC which leads to two photons in the input mode 1. Then even one photon in the WCP will lead to triple coincidence at modes 4, 5, and 6 with a rate $\mathcal{O}(\eta^4 \gamma^4 \nu)$. The contribution of false events in the post-selected events is $\mathcal{O}(\gamma^2/\nu)$ so the error is small if $\gamma^2 \ll \nu \ll 1$. Another possible case which may lead to

error is the presence of three photons in WCP while an EPR photon pair is generated at the SPDC. In that case the fourfold coincidence will occur with the rate $\mathcal{O}(\eta^4\gamma^2\nu^3)$, thus the contribution of the false events to the post-selected events will be $\mathcal{O}(\nu)$ which can be safely neglected if we choose $\nu \sim \mathcal{O}(10^{-2})$.

Mode mismatch, which decreases the fidelity of the prepared states, can be minimized by proper spectral and spatial filtering as discussed in Ref. [73]. However, this will reflect itself as reduced rate of post-selected events. Thus, there is a trade-off between the efficiency and the fidelity.

(c) Effect of deviation in the 50:50 BS parameter

We consider the effect of imperfections in the beamsplitters. We assume that the reflection coefficients of the beamplitters BS₁ and BS₂ are deviated from their ideal values of $1/\sqrt{2}$ by a value of x and y , respectively. Then the action of imperfect BS₁ on H (V) polarization is represented by the transformation:

$$\hat{a}_{1\text{H(V)}}^\dagger = \sqrt{(1-x)/2} \hat{a}_{3\text{H(V)}}^\dagger - \sqrt{(1+x)/2} \hat{a}_{4\text{H(V)}}^\dagger \quad (4.27)$$

and

$$\hat{a}_{2\text{H(V)}}^\dagger = \sqrt{(1+x)/2} \hat{a}_{3\text{H(V)}}^\dagger + \sqrt{(1-x)/2} \hat{a}_{4\text{H(V)}}^\dagger, \quad (4.28)$$

where $-1 < x < 1$. Similar expressions can be written for BS₂ by considering the corresponding modes and by replacing x with y where $-1 < y < 1$. After some straightforward but lengthy calculations, we find that the fidelity of the prepared state upon a four-fold coincidence detection becomes

$$F = \frac{(x+1)^2}{3x^2 + 2x + 1}, \quad (4.29)$$

where we see that the fidelity is dependent on the imperfection of only the BS₁. On the other hand, the probability of four-fold coincidence detection which is found as

$$p = \frac{(1-x)(1-y^2)}{8(3x^2 + 2x + 1)} \quad (4.30)$$

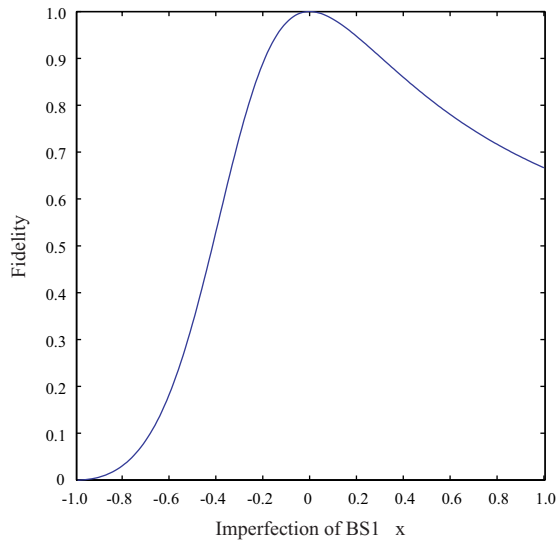


Figure 4.6: Effect of deviation in the parameters of beamsplitters (BS) on fidelity of the prepared W_4 . Fidelity is dependent only on the error x in BS_1 reflection coefficient.

depends on the imperfections of both beamsplitters. This can be simply understood if we notice that BS_1 decides the weight of the components forming the W state: If there is a deviation from $1/\sqrt{2}$ in BS_1 , the superposition will not be equally weighted which will result in lower fidelity since we accept the events whenever we have a four-fold coincidence. On the other hand, if BS_1 is ideal, then the probability of four-fold detection will be determined by the imperfections in BS_2 . The plots of the dependence of fidelity and the probability of four-fold coincidence are depicted in Figs. 4.6 and 4.7. It is worth noting here that if we know the amount of imperfection in BS_1 , we can compensate its effect by introducing losses on only V-polarized photons. In that case, we can obtain a unit fidelity state generation but with a lower success probability. For $x < 0$, the success probability becomes $(1 + 3x)^2(1 - x)(1 - y^2)/32$; for $x > 0$ it becomes $(1 - x)^2(1 - x)(1 - y^2)/32$.

Putting all together, we conclude that the proposed elementary gate is easy to implement and feasible with the current experimental technologies.

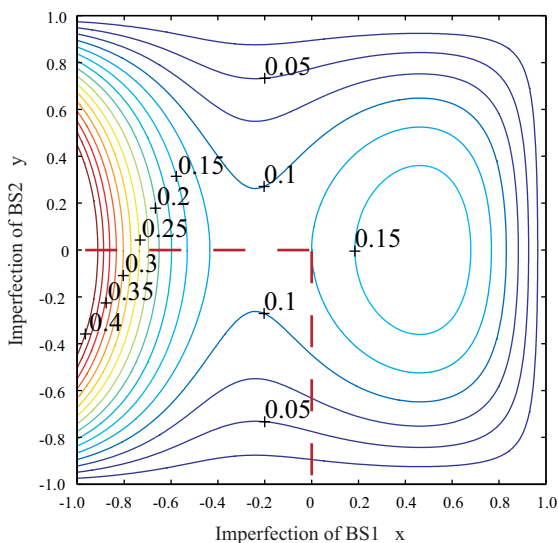


Figure 4.7: Effect of imperfect 50:50 beamsplitters (BS) on the probability of four-fold coincidence detection. Deviations of reflection coefficients of BS₁ and BS₂ are represented by x and y , respectively.

4.2.4 Expansion of polarization entangled GHZ states

In our proposed gate, a polarization entangled state is prepared or expanded using only passive polarization-independent components. (The phase shifter PS is used only for the purpose of making the output state in the standard form.) The polarization dependence of the gate comes from the polarization of the ancilla photons. This may suggest the possibility of expanding states other than W states by modifying the polarization of the ancilla photons. Let us consider the case in which, instead of the H-polarized two-photon ancilla state $|2_H\rangle_2$, we choose the state $|1_H1_V\rangle_2$ as the state of the two ancillary photons. We still require that one photon is present in each of the output spatial modes. As we will see, it turns out that this modified gate can be used for the expansion of GHZ states.

Suppose that a V-polarized photon is present at the input mode 1. This photon undergoes two-photon interference at BS₁ with the V-polarized photon from the ancilla mode 2, resulting in either both photons emerging at mode 3 or both photons emerging at mode 4. Since mode 4 must have exactly one photon for the post-selection, only the former case

leads to the post-selection. In addition, the remaining H-polarized ancilla photon must go to mode 4. Hence the transformation leading to post-selection is written by

$$|1_V\rangle_1 |1_H 1_V\rangle_2 \rightarrow \frac{1}{2\sqrt{2}} |1_H\rangle_4 |1_V\rangle_5 |1_V\rangle_6. \quad (4.31)$$

Similarly, an H-polarized photon at the input is transformed as

$$|1_H\rangle_1 |1_H 1_V\rangle_2 \rightarrow \frac{1}{2\sqrt{2}} |1_V\rangle_4 |1_H\rangle_5 |1_H\rangle_6. \quad (4.32)$$

If we rotate the polarization of the photon in mode 4 by $\pi/2$, all the photons in the output modes should have the same polarization as the input, namely,

$$|1_V\rangle_1 |1_H 1_V\rangle_2 \rightarrow \frac{1}{2\sqrt{2}} |1_V\rangle_4 |1_V\rangle_5 |1_V\rangle_6 \quad (4.33)$$

and

$$|1_H\rangle_1 |1_H 1_V\rangle_2 \rightarrow \frac{1}{2\sqrt{2}} |1_H\rangle_4 |1_H\rangle_5 |1_H\rangle_6. \quad (4.34)$$

From the above discussion, we see that if the input photon is an equal superposition of H- and V-polarized photons, $(|1_H\rangle_1 + |1_V\rangle_1)/\sqrt{2}$, it will evolve into a superposition state $|\text{GHZ}_3\rangle = (|1_H\rangle_4 |1_H\rangle_5 |1_H\rangle_6 + |1_V\rangle_4 |1_V\rangle_5 |1_V\rangle_6)/\sqrt{2}$ with a success probability of $1/8$. Similarly, it transforms any size of GHZ state $|\text{GHZ}_N\rangle$ to $|\text{GHZ}_{N+2}\rangle$ with the same probability. Hence the use of a different polarization state for the two photons in the ancillary mode enables us to expand a different class of multipartite entangled states. Here we need to mention that it is already known that a parity check gate with an single-photon ancilla state will extend GHZ states by one with a probability of $1/2$ [17, 35, 47]. In order to extend a GHZ state by 2, the gate should be applied twice leading to an overall probability of $1/4$ which is twice as high as that of our gate.

4.2.5 Brief discussion

In this section, we have proposed an elementary optical gate for both preparing and expanding the symmetrically shared entanglement in polarization entangled W states. It has a larger success probability than other preparation methods proposed so far [see Table 4.2].

Scheme	Probability	Fidelity
Our scheme	1/8	1
X. Zou et al [44]	2/27	1
B. -S. Shi et al [45]	1/16	1
Y. Li et al [46]	3/200	0.985

Table 4.2: Comparison of our scheme and other schemes in the literature for the preparation of W_4 . It is seen that our scheme has a higher probability of success.

We believe that the proposed gate provides an easy-to-implement scheme which is feasible with the current experimental technologies. In our gate, polarization-dependent components play no essential role, and the desired transformation is achieved by multi-photon interference between the input photon and the ancilla photons. In fact, we were able to show that just by changing the state of the ancilla photons, the gate can be used for the preparation and extension of GHZ states.

4.3 Optical fusion gate for two arbitrary-size W states

In this section, we introduce an optical gate to fuse two W states to prepare a larger W state by accessing only one qubit from each of the input W states. This section is organized as follows: In Sec. 4.3.1, we introduce the scenario and the basic assumptions. In Sec. 4.3.2, we describe the structure of the fusion gate. In sec. 4.3.3, we give an example of fusing two four-photon W states. Finally, in Sec. 4.3.4, we give a brief summary and conclusions.

4.3.1 Working principle of fusion gate for W states

Let us assume that two spatially separated parties, Alice and Bob, decide to merge their local W states $|W_n\rangle_A$ and $|W_m\rangle_B$ into a larger entangled web $|W_\gamma\rangle_{AB}$ with the help of a trusted third party Claire [see Fig. 4.8]. In order to do this, each of Alice and Bob transmits

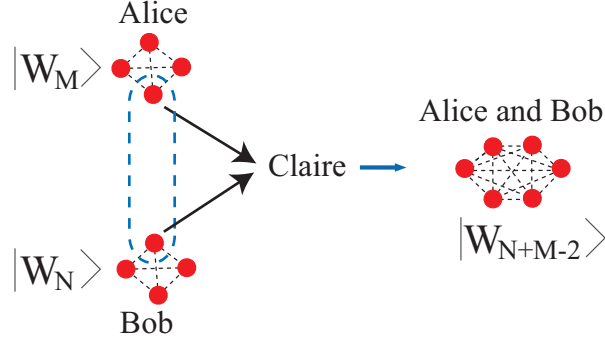


Figure 4.8: Schematic of our concept. Two spatially separated Alice and Bob decide to merge their small scale W-state networks $|W_N\rangle$ and $|W_M\rangle$ into a larger one $|W_{N+M-2}\rangle$ by acting locally on the received two qubits and communicating classically the outcome to Alice and Bob.

one qubit from his/her W state to Claire who will operate locally on the received two qubits and inform Alice and Bob whether the task is successful or not. The question is whether such a local manipulation is possible or not, and if possible then how the operation of Claire can be realized within the linear optics realm. The polarization entangled W states of Alice and Bob can be represented by

$$\begin{aligned}
 |W_N\rangle_A &= \frac{1}{\sqrt{N}} |(N-1)_H, 1_V\rangle_A = \frac{1}{\sqrt{N}} (|(N-1)_H, 0\rangle_{a'} |1_V\rangle_a + |(N-2)_H, 1_V\rangle_{a'} |1_H\rangle_a), \\
 |W_M\rangle_B &= \frac{1}{\sqrt{M}} |(M-1)_H, 1_V\rangle_B = \frac{1}{\sqrt{M}} (|(M-1)_H, 0\rangle_{b'} |1_V\rangle_b + |(M-2)_H, 1_V\rangle_{b'} |1_H\rangle_b),
 \end{aligned}
 \tag{4.35}$$

where the photons denoted by the subscripts $a(b)$ are sent to Claire by Alice (Bob) and those denoted by $a'(b')$ are the rest of the qubits in the initial W states, and $|l_H, k_V\rangle$ is the sum over all the terms with l modes in $|H\rangle$ and k modes in $|V\rangle$. After Claire receives the

qubits, the state of the whole system shared by Alice, Bob and Claire becomes

$$\begin{aligned}
|W_N\rangle_A \otimes |W_M\rangle_B \rightarrow & \frac{1}{\sqrt{NM}} |(N-1)_{\text{H}}, 0\rangle_{a'} |(M-1)_{\text{H}}, 0\rangle_{b'} \underline{|1_{\text{V}}\rangle_a |1_{\text{V}}\rangle_b} \\
& + \frac{1}{\sqrt{NM}} |(N-1)_{\text{H}}, 0\rangle_{a'} |(M-2)_{\text{H}}, 1_{\text{V}}\rangle_{b'} \underline{|1_{\text{V}}\rangle_a |1_{\text{H}}\rangle_b} \\
& + \frac{1}{\sqrt{NM}} |(N-2)_{\text{H}}, 1_{\text{V}}\rangle_{a'} |(M-1)_{\text{H}}, 0\rangle_{b'} \underline{|1_{\text{H}}\rangle_a |1_{\text{V}}\rangle_b} \\
& + \frac{1}{\sqrt{NM}} |(N-2)_{\text{H}}, 1_{\text{V}}\rangle_{a'} |(M-2)_{\text{H}}, 1_{\text{V}}\rangle_{b'} \underline{|1_{\text{H}}\rangle_a |1_{\text{H}}\rangle_b},
\end{aligned} \tag{4.36}$$

where the system formed by the underlined terms belong to Claire. It is easy to see that if Claire counts the number of V-polarized photons and finds that the outcome is two, the state of the remaining qubits in the modes a' and b' becomes $|(N-1)_{\text{H}}\rangle_{a'} |(M-1)_{\text{H}}\rangle_{b'}$ which is a product state containing only H-polarized photons. Such an event takes place with a probability of $1/NM$. On the other hand, if her outcome is zero, then the state of the remaining qubits becomes

$$\frac{1}{\sqrt{NM}} |(N-2)_{\text{H}}, 1_{\text{V}}\rangle_{a'} |(M-2)_{\text{H}}, 1_{\text{V}}\rangle_{b'} = \frac{\sqrt{(N-1)(M-1)}}{\sqrt{NM}} |W_{N-1}\rangle_{a'} |W_{M-1}\rangle_{b'}, \tag{4.37}$$

which implies that the outcome is two W states, each of which has one qubit less than the original state. Such an event takes place with a probability of $(N-1)(M-1)/NM$. Now if Claire's outcome is one, the remaining qubits will be either in the state $|(N-1)_{\text{H}}, 0\rangle_{a'} |(M-2)_{\text{H}}, 1_{\text{V}}\rangle_{b'}$ or in the state $|(N-2)_{\text{H}}, 1_{\text{V}}\rangle_{a'} |(M-1)_{\text{H}}, 0\rangle_{b'}$. Now if Claire can count the number of V-polarized photons without revealing the source of the V-photon, that is, if the information of whether the detected V polarized photon is from Alice or from Bob could be erased, then the resultant state will be a coherent superposition of the above two terms,

$$\frac{1}{\sqrt{NM}} (|(N-1)_{\text{H}}, 0\rangle_{a'} |(M-2)_{\text{H}}, 1_{\text{V}}\rangle_{b'} + |(N-2)_{\text{H}}, 1_{\text{V}}\rangle_{a'} |(M-1)_{\text{H}}, 0\rangle_{b'}). \tag{4.38}$$

Eq. (4.38) can be shown to be equal to

$$\frac{\sqrt{N+M-2}}{\sqrt{NM}} |W_{N+M-2}\rangle_{a'b'} \quad (4.39)$$

which implies that Claire's outcome of one fuses the systems of Alice and Bob into a $(N+M-2)$ -partite W state with a probability of $(N+M-2)/NM$. To conclude, we see that if Claire can count the number of V-polarized photons without revealing their source, she can fuse the W-state systems of Alice and Bob with the loss of two qubits destroyed by the detection to signal the successful fusion. It is also seen that when Claire's outcome is zero, upon communicating this result from Claire, Alice and Bob can send new qubits to Claire to attempt a second round of fusion, which we call as recycling process. Therefore, we classify Claire's outcome as successful when the outcome is one, recyclable when the outcome is zero, and failure when the outcome is two.

4.3.2 Linear optics implementation

Next, we discuss how the measurement process of Claire can be implemented in linear optics. It turns out that Claire's action corresponds to quantum parity checking which is a very common and well-known concept in linear optics based quantum information science. In Fig. 4.9, we show the detail of the proposed fusion gate which is composed of a polarizing beamsplitter (PBS), half wave plates (HWP) and two polarization discriminating detectors (D_1 and D_2). This discriminating detector, which is composed of a HWP, a PBS and two photon detectors, enables the measurements in the diagonal polarization bases $|D\rangle = (|H\rangle + |V\rangle)/\sqrt{2}$ and $|\bar{D}\rangle = (|H\rangle - |V\rangle)/\sqrt{2}$. The HWPs in mode b changes the polarization of the incoming photon as $|H\rangle \leftrightarrow |V\rangle$.

Writing the photons in the diagonal bases $|1_D\rangle = (|1_H\rangle + |1_V\rangle)/\sqrt{2}$ and $|1_{\bar{D}}\rangle = (|1_H\rangle - |1_V\rangle)/\sqrt{2}$, the state of Claire's photons after the first PBS and just before the detectors

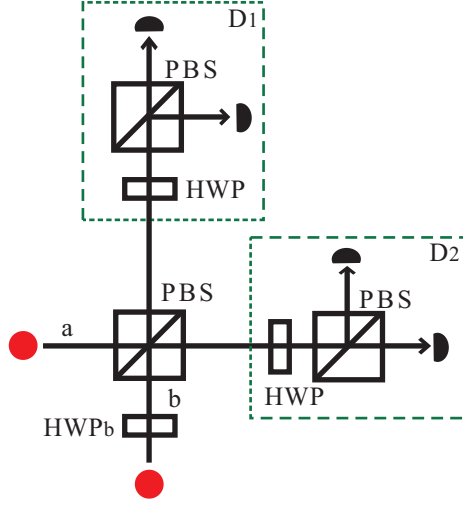


Figure 4.9: Schematic diagram of the proposed optical fusion gate. The gate is composed of a polarizing beamsplitter (PBS), half wave plates (HWP) and two polarization discriminating detectors (D_1 and D_2). This discriminating detector is composed of a HWP, a PBS and two photon detectors, and enables the measurements in the diagonal polarization bases $|D\rangle = (|H\rangle + |V\rangle)/\sqrt{2}$ and $|\bar{D}\rangle = (|H\rangle - |V\rangle)/\sqrt{2}$.

shown in Fig. 4.9 becomes

$$\begin{aligned}
|1_V\rangle_a |1_V\rangle_b &\rightarrow |1_H 1_V\rangle_{D_1} \\
&= \frac{|1_H 1_H\rangle_{D_1} - |1_V 1_V\rangle_{D_1}}{\sqrt{2}} \\
|1_H\rangle_a |1_H\rangle_b &\rightarrow |1_H 1_V\rangle_{D_2} \\
&= \frac{|1_H 1_H\rangle_{D_2} - |1_V 1_V\rangle_{D_2}}{\sqrt{2}} \\
|1_H\rangle_a |1_V\rangle_b &\rightarrow |1_H\rangle_{D_1} |1_H\rangle_{D_2} \\
&= \frac{(|1_D\rangle_{D_1} |1_D\rangle_{D_2} + |1_{\bar{D}}\rangle_{D_1} |1_{\bar{D}}\rangle_{D_2}) + (|1_D\rangle_{D_1} |1_{\bar{D}}\rangle_{D_2} + |1_{\bar{D}}\rangle_{D_1} |1_D\rangle_{D_2})}{2} \\
|1_V\rangle_a |1_H\rangle_b &\rightarrow |1_V\rangle_{D_1} |1_V\rangle_{D_2} \\
&= \frac{(|1_D\rangle_{D_1} |1_D\rangle_{D_2} + |1_{\bar{D}}\rangle_{D_1} |1_{\bar{D}}\rangle_{D_2}) - (|1_D\rangle_{D_1} |1_{\bar{D}}\rangle_{D_2} + |1_{\bar{D}}\rangle_{D_1} |1_D\rangle_{D_2})}{2}
\end{aligned} \tag{4.40}$$

where the subscripts D_1 and D_2 denote the spatial modes where the Claire's two detectors are placed. Substituting Eq. (4.40) in Eq. (4.36) and arranging the terms, we immediately see that if Claire's detectors D_1 and D_2 both detects a photon in the state $|1_D\rangle$ or in the state $|1_{\bar{D}}\rangle$, then the initially separate W states become a single fused W state with $N + M - 2$ photons. If one of the detectors detects a photon in the state $|1_D\rangle$ and the other in the state $|1_{\bar{D}}\rangle$, either Alice or Bob should employ a π -phase shift to obtain the fused W state. Thus, the overall success probability becomes $p_s = (N + M - 2)/NM$. The gate fails to fuse the W states into a larger one if both photons are channeled into the same output of the PBS. If D_1 detects two photons in total, the remaining photons are all H-polarized and both W states are completely destroyed. This failure event takes place with probability $p_f = 1/NM$. On the other hand, if both photons are detected by D_2 , Alice and Bob will have smaller W states with $N - 1$ and $M - 1$ photons. This last case occurs with the probability $p_r = (N - 1)(M - 1)/NM$, and can be recycled which means that they can attempt fusing again until either of the W state are destroyed.

4.3.3 Example of fusing two four-photon W states

In Fig. 4.10, we show an example of fusing two four-photon W states, $|W_4\rangle_A \otimes |W_4\rangle_B$. Using the expressions derived in the previous paragraphs, we find that four-photon W state can be fused together to form a $|W_6\rangle$ with a success probability of $3/8$. Failure probability is $1/16$, and the probability of obtaining a recyclable outcome that leads to the reduced W states $|W_3\rangle_A \otimes |W_3\rangle_B$ is $9/16$. If we attempt to fuse $|W_3\rangle$'s of Alice and Bob, we obtain a successful event which leads to $|W_4\rangle$ with a success probability of $1/4$. The failure probability becomes $1/16$, and with a probability of $1/4$, Alice and Bob will have reduced W states $|W_2\rangle_A \otimes |W_2\rangle_B$. It is important that if either Alice or Bob ends up with a $|W_2\rangle$, trials for fusing should be stopped as fusing any arbitrary size W state with a $|W_2\rangle$ will not increase the size of the W state even for the successful outcome.

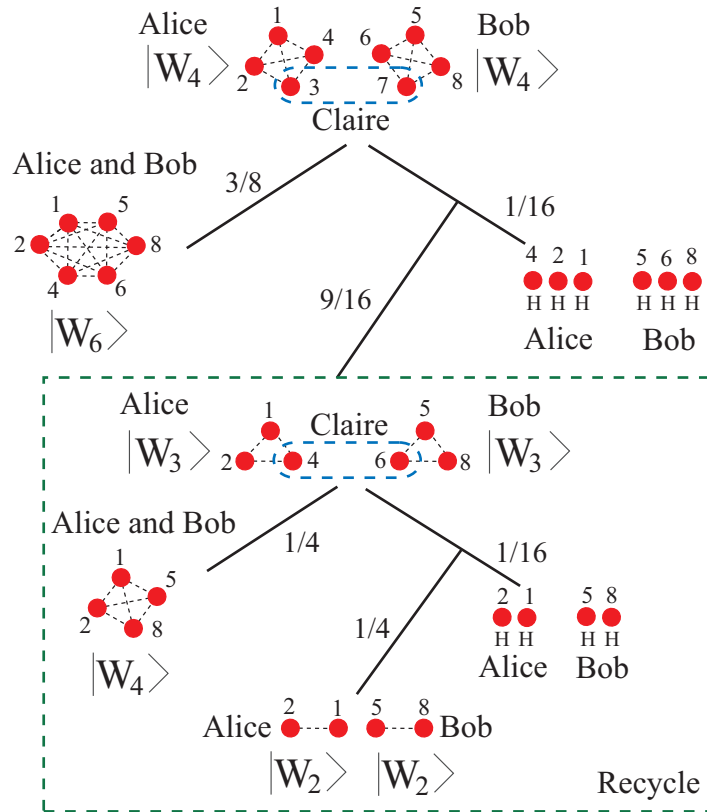


Figure 4.10: Example of fusing two four-photon W states.

4.3.4 Brief discussion

In this section, we have proposed an optical gate for fusing two polarization entangled W states. This proposed gate has the property that the larger W states become, the smaller the probability of complete failure becomes. For example, attempt to fuse two $|W_{10}\rangle$ will completely fail only with a probability of 1%. Thus, we envision the following scenario: The elementary optical gates introduced in the previous sections are used to prepare W states and expand them to moderate sizes. Once a set of such moderate size W states are prepared, then the fusion gate is applied to pairs of W states until all the states in the set are fused to each other. The remaining photons in a complete failure situation and the pairs in $|W_2\rangle$ obtained in a recyclable situation can be used in the preparation and expansion gates introduced earlier. Our preliminary calculations show that the cost of preparing a W

state of size N scales at most sub-exponentially. On the other hand, we still do not know whether a polynomial scaling is possible or not. Moreover, the optimal strategy in fusing W states when a set of W states with various sizes are given remains as an open problem.

4.4 Discussion

In this Chapter, we considered how one can increase the number of qubits forming W state using local operations. We proposed two simple probabilistic optical gates for expanding a polarization W state, and one fusion gate, which performs a parity checking to fuse two W states to obtain a larger W state. We also performed a feasibility analysis for practical implementation of the proposed expansion gates, and showed that they are within the reach of the current technologies. Interestingly, for the preparation of $|W_3\rangle$, the success probability $3/10$ of the former expansion gate is higher than the success probability $3/16$ of the latter expansion gate. However in order to prepare large scale W states, if these gates is cascaded, a success probability of the former expansion gate is larger than one of the latter expansion gate. The latter expansion gate has the property that can be used for expansion of GHZ states. The fusion gate requires a further study, and there is room for further research to improve its performance and to determine the cost of preparing a large scale W state with a desired size.

Chapter 5

Local transformation of two EPR pairs into a tripartite W state

In this Chapter, we propose and experimentally demonstrate a transformation of two EPR photon pairs distributed among three parties into a three-photon W state using local operations and classical communication (LOCC). In Sec. 5.1, we will give a brief concept and an experimental scheme for converting two EPR photon pairs to a three photon W state. In Sec. 5.2 and 5.3, we show our experimental setup and results. Finally, in Sec. 5.4, we give a summary of this chapter.

5.1 Schematics of local transformation from two EPR photon pairs to a three-photon W state

This section is organized as follows: In Sec. 5.1.1, we briefly describe the concept of local conversion from two EPR photon pairs to a three-photon W state and Sec. 5.1.2 includes the experimental scheme.

5.1.1 Concept

What we want to do here is a local transformation of two EPR pairs distributed among three parties (Alice, Bob and Charlie) into a three-photon W state using local operations and classical communication [See Fig. 5.1]. In this approach, Charlie, who has two qubits, one from each EPR pair, first performs a local operation on the qubits and then uses one of them as a trigger for confirming the successful events. The remaining qubit becomes one qubit of the state $|W_3\rangle$ shared between Alice, Bob and Charlie.

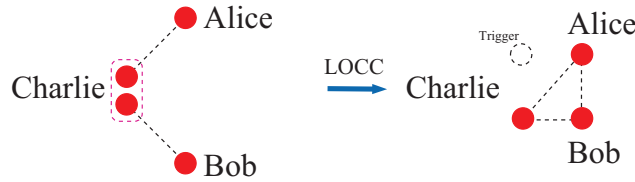


Figure 5.1: The concept of a local transformation from two EPR pairs to the W state. Two EPR pairs are shared by Alice-Charlie and Bob-Charlie. Charlie's operation is performed on his two qubit.

5.1.2 Experimental scheme

Our scheme simply uses a polarization-dependent beam splitter (PDBS) and photon detection to realize the desired transformation of Charlie's two photons into one photon. In the following, we discuss the working principle.

Let us assume that four photons in state $|EPR\rangle_{12}|EPR\rangle_{34} = (|HHHH\rangle_{1234} + |HHVV\rangle_{1234} + |VVHH\rangle_{1234} + |VVVV\rangle_{1234})/2$ are distributed such that Alice has the photon in mode 1, Bob has mode 4, and Charlie has modes 2 and 3. Charlie sends his two photons to a PDBS, whose output modes are labelled as 5 and 6 [see Fig. 5.2]. The transformation of a PDBS for H- and V-polarized photons can be written as

$$\hat{a}_{2H}^\dagger = \sqrt{1-\mu} \hat{a}_{5H}^\dagger - \sqrt{\mu} \hat{a}_{6H}^\dagger, \quad \hat{a}_{3H}^\dagger = \sqrt{\mu} \hat{a}_{5H}^\dagger + \sqrt{1-\mu} \hat{a}_{6H}^\dagger, \quad (5.1)$$

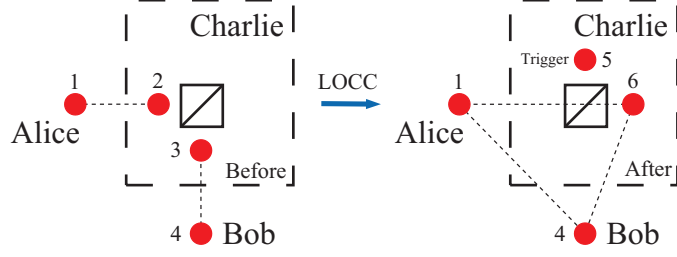


Figure 5.2: Local transformation from two EPR photon pairs to the W state using a polarization dependent beamsplitter. Two EPR photon pairs are shared by Alice-Charlie and Bob-Charlie.

and

$$\hat{a}_{2V}^\dagger = \sqrt{1-\nu} \hat{a}_{5V}^\dagger - \sqrt{\nu} \hat{a}_{6V}^\dagger, \quad \hat{a}_{3V}^\dagger = \sqrt{\nu} \hat{a}_{5V}^\dagger + \sqrt{1-\nu} \hat{a}_{6V}^\dagger \quad (5.2)$$

where \hat{a}_{jH}^\dagger (\hat{a}_{jV}^\dagger) denotes the creation operator of H (V)-polarized photon in the j -th mode of PDBS, and μ (ν) is the transmission coefficient for H (V)-polarization. We consider its action on four possible cases: $|1_H\rangle_2|1_H\rangle_3 = \hat{a}_{2H}^\dagger\hat{a}_{3H}^\dagger|vac\rangle_{23}$, $|1_H\rangle_2|1_V\rangle_3 = \hat{a}_{2H}^\dagger\hat{a}_{3V}^\dagger|vac\rangle_{23}$, $|1_V\rangle_2|1_H\rangle_3 = \hat{a}_{2V}^\dagger\hat{a}_{3H}^\dagger|vac\rangle_{23}$ and $|1_V\rangle_2|1_V\rangle_3 = \hat{a}_{2V}^\dagger\hat{a}_{3V}^\dagger|vac\rangle_{23}$, where $|vac\rangle$ stands for the vacuum state. Using the relations given in Eqs. (5.1) and (5.2) for the PDBS, we find that these input states are transformed into

$$\begin{aligned} |1_H\rangle_2|1_H\rangle_3 &\rightarrow \sqrt{2\mu(1-\mu)} |2_H\rangle_5|0\rangle_6 + \underline{(1-2\mu)|1_H\rangle_5|1_H\rangle_6} - \sqrt{2\mu(1-\mu)} |0\rangle_5|2_H\rangle_6, \\ |1_H\rangle_2|1_V\rangle_3 &\rightarrow \sqrt{\nu(1-\mu)} |1_V1_H\rangle_5|0\rangle_6 - \underline{\sqrt{\nu\mu} |1_V\rangle_5|1_H\rangle_6} \\ &\quad + \sqrt{(1-\mu)(1-\nu)} |1_H\rangle_5|1_V\rangle_6 - \sqrt{\mu(1-\nu)} |0\rangle_5|1_V1_H\rangle_6, \\ |1_V\rangle_2|1_H\rangle_3 &\rightarrow \sqrt{\mu(1-\nu)} |1_V1_H\rangle_5|0\rangle_6 + \underline{\sqrt{(1-\nu)(1-\mu)} |1_V\rangle_5|1_H\rangle_6}, \\ &\quad - \underline{\sqrt{\mu\nu} |1_H\rangle_5|1_V\rangle_6} - \sqrt{\nu(1-\mu)} |0\rangle_5|1_V1_H\rangle_6, \\ |1_V\rangle_2|1_V\rangle_3 &\rightarrow \sqrt{2\nu(1-\nu)} |2_V\rangle_5|0\rangle_6 + \underline{(1-2\nu)|1_V\rangle_5|1_V\rangle_6} - \sqrt{2\nu(1-\nu)} |0\rangle_5|2_V\rangle_6. \end{aligned} \quad (5.3)$$

Here, we are only interested in the case where a photon is present in each of the modes 1,

4, 5 and 6. Keeping only such terms, the state after the PDBS is written as

$$\begin{aligned} & \frac{1}{2} \left[(2\mu - 1) |HHH\rangle_{146} + \sqrt{(1-\mu)(1-\nu)} |HV V\rangle_{146} - \sqrt{\mu\nu} |VHV\rangle_{146} \right] |H\rangle_5 \\ & + \frac{1}{2} \left[(2\nu - 1) |VVV\rangle_{146} - \sqrt{\mu\nu} |HVH\rangle_{146} + \sqrt{(1-\mu)(1-\nu)} |VHH\rangle_{146} \right] |V\rangle_5. \end{aligned} \quad (5.4)$$

If Charlie has detected an H-polarized photon (a V-polarized photon) in mode 5, he announces it and switches the polarization mode 6 as $|H\rangle_6 \leftrightarrow |V\rangle_6$. At this point, the three parties share the following states

$$\frac{1}{2} \left[(2\mu - 1) |HHV\rangle_{146} + \sqrt{(1-\mu)(1-\nu)} |HVH\rangle_{146} - \sqrt{\mu\nu} |VHH\rangle_{146} \right] \quad (5.5)$$

and

$$\frac{1}{2} \left[(2\nu - 1) |VVH\rangle_{146} - \sqrt{\mu\nu} |HV V\rangle_{146} + \sqrt{(1-\mu)(1-\nu)} |VHV\rangle_{146} \right], \quad (5.6)$$

respectively for H- and V- polarization detection in mode 5. If the phases and amplitudes in Eqs. (5.5) and (5.6) are not equal, they can be adjusted by introducing phase shift and attenuation for V-polarized photons in each mode. Then the three parties share the W state $|W\rangle_3$. The overall success probability is given by

$$p_H \equiv \frac{3}{4} \min\{(2\mu - 1)^2, (1-\mu)(1-\nu), \mu\nu\} \quad (5.7)$$

and

$$p_V \equiv \frac{3}{4} \min\{(2\nu - 1)^2, (1-\mu)(1-\nu), \mu\nu\}. \quad (5.8)$$

Now, we want to know the values μ and ν for obtaining the largest success probability. Let us assume that $\mu\nu$ is the minimum of $\{(2\mu - 1)^2, (1-\mu)(1-\nu), \mu\nu\}$, that is, $\mu\nu \leq (2\mu - 1)^2$, and $\mu\nu \leq (1-\mu)(1-\nu)$. From $\mu\nu \leq (1-\mu)(1-\nu)$, we have $\nu \leq 1-\mu$, and hence $\mu\nu \leq \mu(1-\mu)$. By solving $\mu(1-\mu) = (2\mu - 1)^2$, the parameter (μ, ν) of the PDBS for the largest success probability p_H are found to be $\mu = (5 + \sqrt{5})/10$ and $\nu = (5 - \sqrt{5})/10$ or vice versa. Then the amplitudes of three terms satisfy

$$2\mu - 1 = \sqrt{(1-\mu)(1-\nu)} = \sqrt{\mu\nu}. \quad (5.9)$$

In this case, p_V also takes the largest value. Here, even if we assume that $(2\mu - 1)^2$ or $(1 - \mu)(1 - \nu)$ is the minimum of $\{(2\mu - 1)^2, (1 - \mu)(1 - \nu), \mu\nu\}$, we will obtain the same result, that is, $\mu = (5 + \sqrt{5})/10$ and $\nu = (5 - \sqrt{5})/10$ or vice versa, for the largest success probability p_H . It is noted that when we assume that $(2\mu - 1)^2$ is the minimum, we need to consider the cases of both $\mu\nu \leq (1 - \mu)(1 - \nu)$ and $\mu\nu \geq (1 - \mu)(1 - \nu)$.

For this choice, Eqs. (5.5) and (5.6) after locally compensating phase shift on mode 1 are represented by

$$\frac{1}{2\sqrt{5}} \left[|\text{HHV}\rangle_{146} + |\text{HVH}\rangle_{146} + |\text{VHH}\rangle_{146} \right] \quad (5.10)$$

and

$$\frac{1}{2\sqrt{5}} \left[|\text{VVH}\rangle_{146} + |\text{HVV}\rangle_{146} + |\text{VHV}\rangle_{146} \right]. \quad (5.11)$$

Hence, both probabilities take their optimal values $p_H = p_V = 3/20 = 15\%$ without introducing local attenuations and the total success probability becomes $p = p_H + p_V = 3/10 = 30\%$.

In this work, in order to convert two EPR photon pairs to a three-photon W state, we use a PDBS. However, it is noted that if we restrict ourselves to polarization-independent beamsplitters ($\mu = \nu$), the optimal choice is $\mu = \nu = 2/3$. Using this BS, the output state is obtained as

$$\begin{aligned} & \frac{1}{6} \left[|\text{HHH}\rangle_{146} + |\text{HVV}\rangle_{146} - 2|\text{VHV}\rangle_{146} \right] |\text{H}\rangle_5 \\ & + \frac{1}{6} \left[|\text{VVV}\rangle_{146} + |\text{VHH}\rangle_{146} - 2|\text{HVH}\rangle_{146} \right] |\text{V}\rangle_5. \end{aligned} \quad (5.12)$$

If Charlie has detected an H-polarized photon (a V-polarized photon) in mode 5, he announces it and switches the polarization of mode 6 as $|\text{H}\rangle_6 \leftrightarrow |\text{V}\rangle_6$. Upon hearing Charlie's outcome, Alice applies local phase shift and attenuations. The resulting state becomes the W state $|\text{W}\rangle_3$ with a total success probability of $p = p_H + p_V = 1/6$ with $p_H = p_V = 1/12$.

In our experiment, we made a sub-optimal choice of the PDBS parameters, $\mu = (7 + \sqrt{17})/16$ and $\nu = 1/2$. One of the reasons for this choice is that the two-photon interference for the V polarization is observed directly, which makes the alignment easier and gives us a

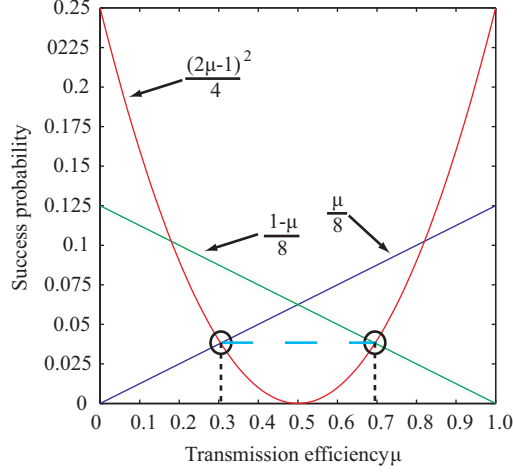


Figure 5.3: Success probability of each terms by detecting H-polarized photon on Charlie's side. The circle gives $\mu = (9 - \sqrt{17})/16$ and $\mu = (7 + \sqrt{17})/16$.

clue about how well the two photons from different pairs are overlapped at the PDBS. We show the derivation of optimal value for μ when $\nu = 1/2$. Setting $\nu = 1/2$ in Eq. (5.4), we obtain

$$\begin{aligned} & \frac{1}{2} \left[(2\mu - 1) |HHH\rangle_{146} + \sqrt{\frac{1-\mu}{2}} |HVV\rangle_{146} - \sqrt{\frac{\mu}{2}} |VHV\rangle_{146} \right] |H\rangle_5 \\ & + \frac{1}{2} \left[-\sqrt{\frac{\mu}{2}} |HVH\rangle_{146} + \sqrt{\frac{1-\mu}{2}} |VHH\rangle_{146} \right] |V\rangle_5, \end{aligned} \quad (5.13)$$

where we see that if Charlie has detected a V-polarized photon in mode 5, three parties share the bi-separable state $(\sqrt{\mu}|HV\rangle_{14} + \sqrt{1-\mu}|VH\rangle_{14})|H\rangle_6/2\sqrt{2}$. On the other hand, if Charlie has detected an H-polarized photon in mode 5 and Alice introduces a phase shift locally, they will end up with a W-like state from which $|W_3\rangle$ can be prepared by equalizing the weights of the components. Thus they should choose μ such that $(\mu - 1/2)^2 = (1 - \mu)/8$ or $(\mu - 1/2)^2 = \mu/8$ is satisfied to obtain the largest minimum weight [see Fig. 5.3]. These equations, respectively, give $\mu = (7 + \sqrt{17})/16$ and $\mu = (9 - \sqrt{17})/16$, both of which lead to the same weight, hence either of them can be used. Substituting $\mu = (7 + \sqrt{17})/16$ in Eq. (5.13), and keeping only the terms leading to coincidence detection triggered by an

H-photon detection in mode 5, the post-selected state in modes 1, 4 and 6 becomes

$$\frac{\sqrt{9 - \sqrt{17}}}{8\sqrt{2}} \left[|HHV\rangle + |HVV\rangle + \frac{\sqrt{7 + \sqrt{17}}}{\sqrt{9 - \sqrt{17}}} |VHH\rangle \right]_{146}, \quad (5.14)$$

after Charlie compensates phase shift locally and changes the polarization of his photon in mode 6. We see that the component VHH is the only one with a V in mode 1; thus its weight can be equalized to the others by introducing polarization dependent losses in mode 1. Then the final state becomes $\sqrt{3(9 - \sqrt{17})/128} |W_3\rangle_{146}$ implying that local conversion of two EPR pairs into a $|W_3\rangle$ is achieved with unit fidelity at a success probability of $3(9 - \sqrt{17})/128 \sim 11.4\%$.

5.2 Experimental setup

The details of our experimental setup are shown in Figs. 5.4 (a) and 5.5. The ultraviolet (UV) pulses (wavelength 395nm, average power 380mW, diagonal polarization) from a frequency-doubled mode-locked Ti:Sapphire laser (wavelength 790nm; pulse width 90fs; repetition rate 82MHz) make two passes through a pair of Type I phase matched β -barium borate (BBO) crystals (thickness 1.5mm) stacked with their optical axes orthogonal to each other to produce two EPR photon pairs via spontaneous parametric down conversion (SPDC) [see Appendix B]. Extra BBOs with thickness 1.65mm (comp) are placed on the path of the each photon to compensate for walk-off effects. Nominal values of PDBS (Showa Optronics Co., Ltd) used in experiment are $\mu \cong 7/10$ and $\nu \cong 1/2$. It is noted that $\mu = (7 + \sqrt{17})/16$ is near to 0.695. The spectral filtering of the photons is done by a narrow-band interference filter (IF, wavelength: 790nm; bandwidth: 2.7nm). All the detectors D_1 , D_4 , D_5 and D_6 are silicon avalanche photodiodes placed after single-mode optical fibers to achieve high fidelity.

Charlie's local operations are performed as follows. Modes 2 and 3 are overlapped at the PDBS, and polarizing beamsplitter (PBS) placed at the output mode 5 selects only the H-polarized photons. A half-wave plate (HWPc) at mode 6 interchanges H and V polarizations. On Alice's side, a set of glass plates (GP) are placed in mode 1, which can be

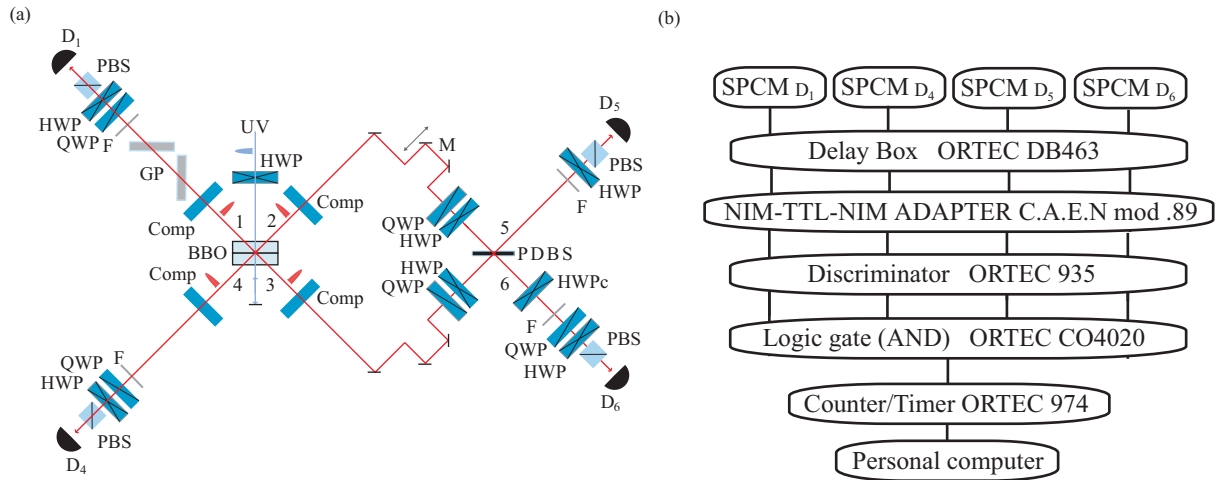


Figure 5.4: Schematics of the experiment. (a) The experimental setup. UV; ultra-violet pulses (wavelength 395nm, average power 380mW, Model 3980, Spectra physics) from a frequency-doubled mode-locked Ti:Sapphire laser (wavelength 790nm; pulse width 90fs; repetition rate 82MHz, Tsunami, Spectra physics), BBO; Type I phase matched β -barium borate (BBO) crystals (thickness 1.5mm) stacked with their optical axes orthogonal to each other. Comp; extra BBO with thickness 1.65mm to compensate for walk-off effects. PDBS; a polarization dependent beamsplitter, GP; glass plate to compensate for amplitude, QWP; quarter wave plate, HWP; half wave plate, PBS; polarizing beamsplitter, F; narrow-band interference filter (IF, wavelength: 790nm; bandwidth: 2.7nm). $D_{j=1,4,5,6}$; silicon avalanche photodiode (SPCM-AQR, Perkin Elmer). (b) The coincidence counting system. A delay box DB463 (EG&G ORTEC) compensate the electrical delay of signals from the SPCMs. We convert the TTL signals from SPCMs to NIM using NIM-TTL-NIM ADAPTER C.A.E.N mod.89 (EG&G ORTEC). The NIM signals are then converted to short pulses using a discriminator 935 (EG&G ORTEC). The output pulses of the discriminators are input to logic gate module to perform AND operation on them. The output of the AND gate is counted using Counter/Timer 974 (EG&G ORTEC). Finally, the coincidence count of the Counter is sent to a personal computer.

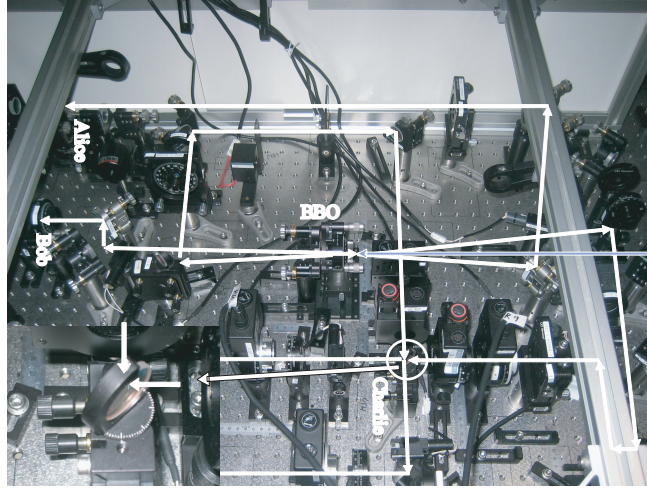


Figure 5.5: Picture of the experimental setup. When the ultraviolet pulse is incident on BBO in forward pass, one EPR photon pair is generated and Bob and Charlie share this EPR photon pair. Returning UV pulse, another EPR photon pair is generated. Alice and Charlie share this EPR photon pair. PDBS is in Circle.

tilted to adjust the amount of the polarization dependent loss. The two plates are tilted in opposite directions such that the beam passing through experiences a minimal transverse shift. Successful events are signalled by four-photon coincidences using photon detectors in modes 1, 4, 5 and 6. The quarter wave plates (QWP), HWPs and PBSs in front of the detectors in modes 1, 4 and 6 are used for verification experiments. The coincidence counting system is summarized in Figure 5.4 (b).

5.3 Experimental results

5.3.1 Interference of two EPR photon pairs at a PDBS

In our experiment, it is important to match the temporal and spatial modes of the photons in modes 2 and 3. In order to match the temporal modes of photons in 2 and 3, we

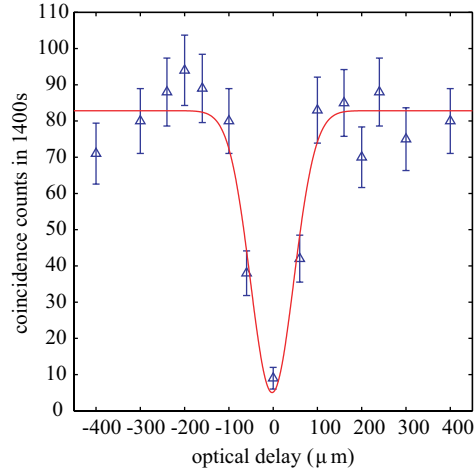


Figure 5.6: Observed two photon interference by recording four-photon coincidences as a function of the optical delay. PDBS works as a 50:50 BS for V-polarized photons. The best fit to the data is represented by the solid Gaussian curve which shows a coherence length of $l_c \simeq 110\mu\text{m}$. The visibility from the fitting curve is 0.885.

performed the Hong-Ou-Mandel (HOM) interference experiment.

The HOM interference observed in our experiment can be understood as follows: It is known that when two indistinguishable photons are incident on a 50:50 BS, these photons will go to only one of the outputs of the BS but never to both outputs at the same time due to destructive interference which leads to bunching effect. The PDBS used in our experiment acts as a 50:50 BS for V-polarized photons, and thus if the V-polarized photons in modes 2 and 3 arrive at the PDBS within their coherence times, photons will channel either to mode 2 or 3. Therefore, no coincidence detection will be observed.

In the experiment, we set the UV pulses to H-polarization so that in each pass of the UV pulses through the BBOs, V-polarized photon pairs were generated. The HWPs inserted in front of the detectors were adjusted so that only V-photons arrive at the detectors. One photon from each pair was then sent to the PDBS and four-fold coincidences were recorded while the optical delay experienced by the photons in modes 2 and 3 were changed using

the motorized stage M. When the temporal overlap of these two V-photons at the PDBS was achieved, HOM dip was observed as shown in Fig. 5.6. If we delay the photon from one source with respect to the other one, the time overlap of the photons is decreased. Then we lose temporal indistinguishability, and the destructive interference diminishes. In order to estimate how well the indistinguishability is achieved, namely, how identical the polarization, spatial, temporal and spectral modes of the photons are made, we applied a gaussian curve fitting to the experimentally obtained data using the function

$$G(x) = A(1 - Ve^{-\frac{(x-x_0)^2}{2\delta^2}}), \quad (5.15)$$

where $G(x)$ is the coincidence count rate when the distance between the paths of the two photons is x , A is the coincidence rate away from the HOM dip, V is the visibility of the HOM-dip, x_0 is the position of the minimum for zero time delay between the paths of the photons and δ is the width of the HOM-dip. The choice of a gaussian function is due to the fact that the transmission spectra of IFs are well-approximated by a gaussian function. From the fitting curve, the visibility of the interference curve was found as 0.885. Although the ideal value of the visibility of HOM dip is 1.0, the value obtained by this experiment is smaller than 1.0. The deviation from the ideal value is caused by temporal and spatial mode mismatch, multi-photon effects and dark counts in photodetectors.

5.3.2 Characterization of initial EPR photon pairs

Before we generate a final three-photon state, we characterized initial two EPR photon pairs from SPDC. We then estimated fidelity and entanglement of formation (EOF) of reconstructed density matrices by using the maximum likelihood method.

After setting the zero-delay time of fitting curve, we adjusted the UV pulses to diagonal polarization so that EPR pairs ρ_{12} and ρ_{34} were generated. Since the PDBS has different transmission coefficients for H and V polarizations, the measurement bases for the photons in modes 2 and 3 were selected by the HWPs and QWPs inserted before the PDBS. We finally measure the state projected by H-polarization using a PBS in front of each detector [see Fig. 5.7]. The QWP and HWPs in mode 6 and the set of glass plates in mode 1

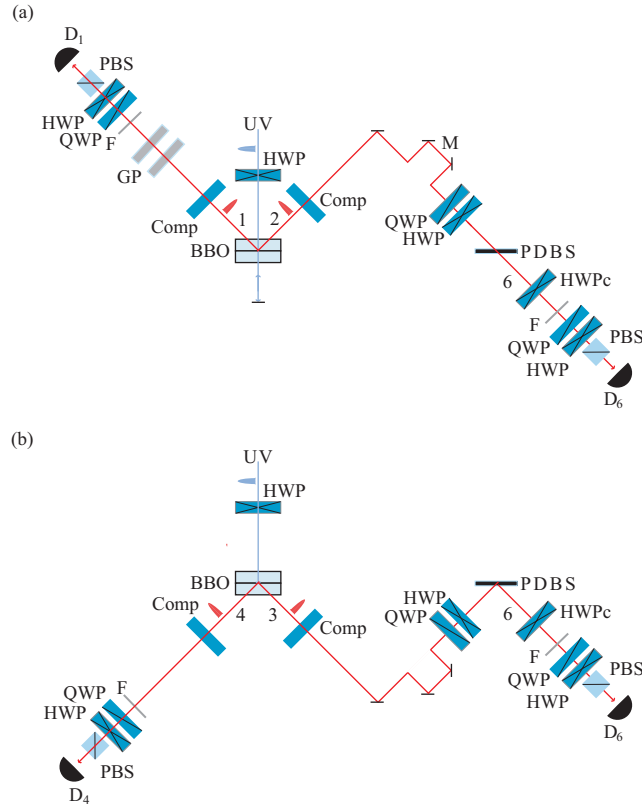


Figure 5.7: Measurement setup for the initial EPR pairs: (a) ρ_{12} and (b) ρ_{34}

were adjusted so that they did not affect the polarization of the incoming photons. Each pair was characterized by quantum state tomography (QST) using 16 different tomographic settings chosen from the combinations of the single photon projections, $|H\rangle$, $|V\rangle$, $|D\rangle = (|H\rangle + |V\rangle)/\sqrt{2}$, $|R\rangle = (|H\rangle - i|V\rangle)/\sqrt{2}$ and $|L\rangle = (|H\rangle + i|V\rangle)/\sqrt{2}$, on each photon [see Fig. C.1 in Appendix C]. Coincidences were recorded in modes 1 and 6 for ρ_{12} , and in modes 4 and 6 for ρ_{34} . From these measured polarization correlations, we estimated the fidelity $F_{ij} \equiv \langle \text{EPR} | \rho_{ij} | \text{EPR} \rangle$ of each pair to the ideal EPR pair as $F_{12} = 0.967 \pm 0.002$ and $F_{34} = 0.976 \pm 0.002$. Here and henceforth, uncertainties in the fidelities and the other quantities were calculated using a Monte Carlo routine assuming Poissonian statistics of errors. We further reconstructed their density matrices ρ_{12} and ρ_{34} , and calculated the amounts of entanglement using entanglement of formation (EOF) [53] as 0.922 ± 0.006 and

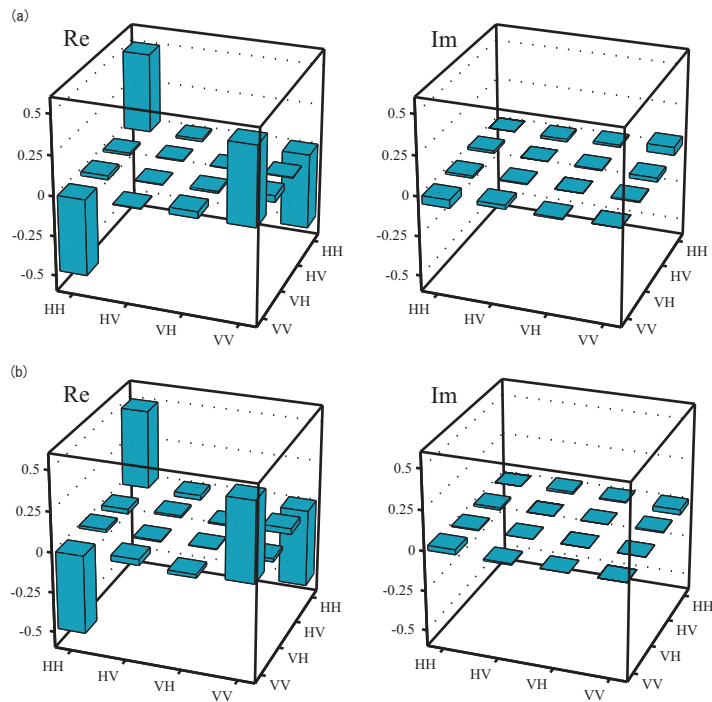


Figure 5.8: Real and imaginary parts of the reconstructed density matrices for the initial EPR pairs: (a) ρ_{12} and (b) ρ_{34} .

0.947 ± 0.004 . The density matrices estimated using the maximum likelihood method are shown in Fig. 5.8.

5.3.3 Characterization of the prepared three-photon W state

We characterized the prepared three-photon output state using quantum state tomography, fidelity estimation and entanglement witness, and confirmed that the prepared state is a genuine tripartite W state. In the tomographical reconstruction of density matrices, we used iterative maximum likelihood method (IML). We also evaluated marginal bipartite states of the prepared three-photon W state with entanglement of formation, concurrence and Peres-Horodecki criterion.

In the experiments, we adjusted the glass plates (GP) to induce the required loss on V-polarized photons in mode 1, and set the QWPs and HWPs in modes 2 and 3 such that

they only add a constant phase shift between H and V on the incoming photons. HWP in mode 5 was also adjusted so that only H-photons arrive at the detector. HWPC in mode 6 was set to swap H and V polarizations. We post-selected the successful events with four-fold coincidences. The final three-photon state ρ_{146} was characterized using 64 different tomographic settings [65] implemented by the sets of QWP, HWP and PBS in front of the detectors in modes 1, 4 and 6 [see Fig. C.2 in Appendix C]. We recorded coincidences for an acquisition time of 5800s at each tomographic setting. From the recorded correlations, we reconstructed the density matrix of ρ_{146} using iterative maximum likelihood (IML) method [68, 69]. This is shown in Fig. 5.9 together with the density matrix for the ideal $|W_3\rangle$. The density matrix for the ideal W state consists of only nine real nonzero terms, namely, the diagonal terms corresponding to $|HHV\rangle$, $|HVH\rangle$ and $|VHH\rangle$ and six off-diagonal elements corresponding to coherences among these terms. It is seen that the density matrix of the state prepared in our experiment has a similar structure with nine dominant elements.

Furthermore, from the reconstructed density matrix, we calculated the fidelity as $F \equiv \langle W_3 | \rho_{146} | W_3 \rangle = 0.778 \pm 0.043$. We also calculated the entanglement witness of this state using the operator $\mathcal{W}_W = \frac{2}{3}\mathbf{1} - |W_3\rangle\langle W_3|$ to distinguish it from separable and bi-separable states [62, 63]. For an ideal W state, the expectation value of this operator is $-1/3$. We find $\text{Tr}(\mathcal{W}_W \rho_{146}) = -0.111 \pm 0.043$ for the final state in our experiment, which confirms that ρ_{146} has a genuine tripartite entanglement. The achieved fidelity of 0.778 ± 0.043 is higher than the value of 0.684 ± 0.024 previously obtained via local transformation from a GHZ state [43], signifying the advantage of direct transformation that does not suffer from the fidelity-efficiency trade-off.

One of the distinct properties of the W state is the entanglement left in the marginal state of any pair of qubits after one qubit is removed. We confirmed this by reconstructing the density matrices ρ_{14} , ρ_{16} and ρ_{46} , corresponding respectively to Alice-Bob, Alice-Charlie, and Bob-Charlie marginal bipartite states. These density matrices are given in Fig. 5.10 together with the density matrix of the marginal bipartite state of the ideal W state. We evaluated the entanglement of the marginal bipartite state using EOF [53], the Peres-Horodecki criterion [55, 56] and concurrence [54]. The results of these analyses are

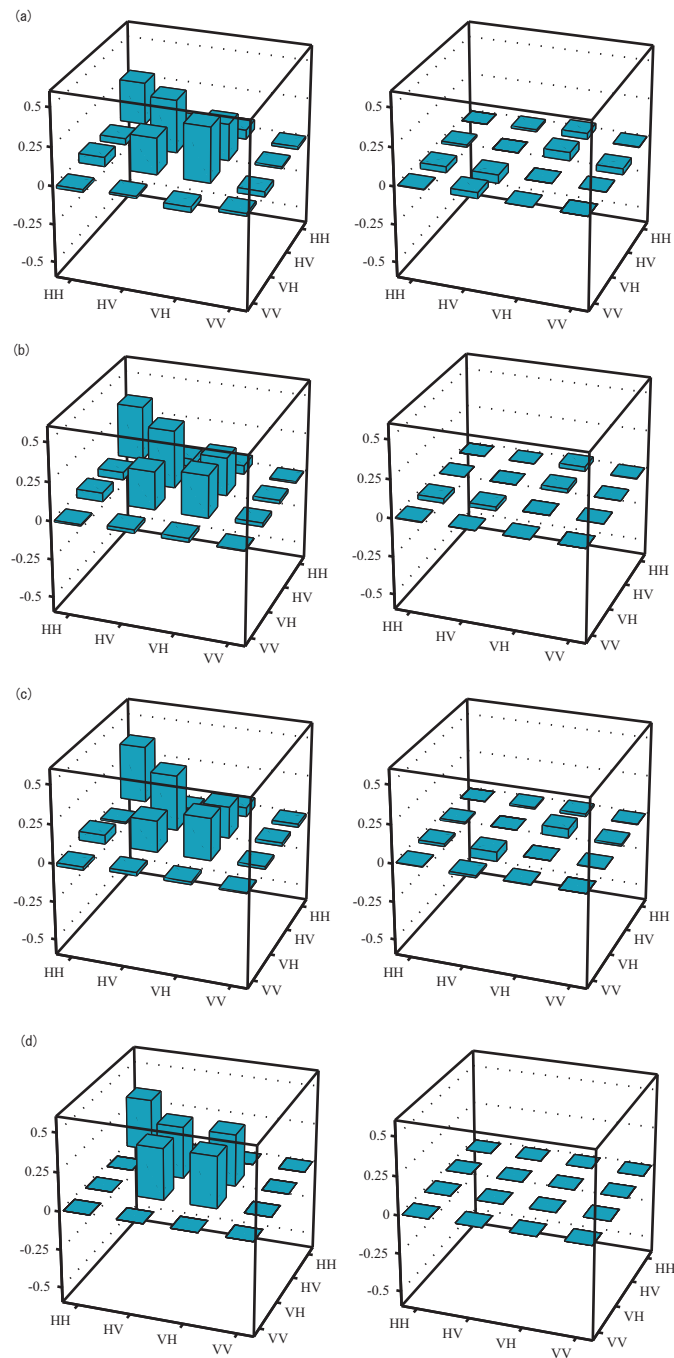


Figure 5.10: Real and imaginary parts of the reconstructed reduced density matrices of the experimentally obtained W state, (a) ρ_{14} , (b) ρ_{16} and (c) ρ_{46} . (d) Real and imaginary parts of the reduced density matrix of the ideal state $|W_3\rangle$ for which $\rho_{14} = \rho_{16} = \rho_{46}$.

	EOF	Concurrence	Peres-Horodecki criterion
ideal	0.55	0.667	-0.206
modes 1-4	0.244 ± 0.066	0.415 ± 0.068	-0.123 ± 0.027
modes 1-6	0.263 ± 0.065	0.421 ± 0.066	-0.143 ± 0.030
modes 4-6	0.195 ± 0.065	0.322 ± 0.073	-0.091 ± 0.026

Table 5.1: Entanglement of formation (EOF), Concurrence and Peres-Horodecki criterion of the prepared marginal bipartite states.

5.4 Discussion

The imperfection in the final W state produced in our experiment may be ascribed to the following causes. Let us assume that the initial EPR photon pairs are represented by

$$|\text{EPR}\rangle_{12} = \frac{1}{\sqrt{2}} \left[|H\rangle_1 |\varphi_{1H}\rangle_1 |H\rangle_2 |\varphi_{2H}\rangle_2 + |V\rangle_1 |\varphi_{1V}\rangle_1 |V\rangle_2 |\varphi_{2V}\rangle_2 \right] \quad (5.16)$$

and

$$|\text{EPR}\rangle_{34} = \frac{1}{\sqrt{2}} \left[|H\rangle_3 |\varphi_{3H}\rangle_3 |H\rangle_4 |\varphi_{4H}\rangle_4 + |V\rangle_3 |\varphi_{3V}\rangle_3 |V\rangle_4 |\varphi_{4V}\rangle_4 \right], \quad (5.17)$$

where $|\varphi_{jH(jV)}\rangle_j$ represents the state of each spatial mode. Furthermore, we assume that further points, transmission and reflection efficiency of a PDBS and local filtering, are ideal.

Considering that fidelities of the initially prepared states ρ_{12} and ρ_{34} to an EPR photon pair is also affected by the mode mismatches between the photons in modes 1 and 2, and photons in modes 3 and 4, we write the expression for their fidelities using the above assumption which leads to

$$\begin{aligned} F_{12} &= {}_p\langle \text{EPR} | \text{Tr}_s [|\text{EPR}\rangle_{12} \langle \text{EPR} |] | \text{EPR}\rangle_p \\ &= \text{Tr}_s [{}_p\langle \text{EPR} | \text{EPR}\rangle_{12} \langle \text{EPR} | \text{EPR}\rangle_p] \\ &= \frac{1}{4} \left(2 + 2 | \langle \varphi_{1H} | \varphi_{1V} \rangle_{12} \langle \varphi_{2H} | \varphi_{2V} \rangle_2 | \right), \end{aligned} \quad (5.18)$$

for the first EPR photon pair, where subscripts p and s stand for polarization modes and

spatial modes. Similarly, we have

$$F_{34} = \frac{1}{4} \left(2 + 2 | {}_3 \langle \varphi_{3H} | \varphi_{3V} \rangle_{34} \langle \varphi_{4H} | \varphi_{4V} \rangle_4 \right) \quad (5.19)$$

for the second EPR photon pair. For simplicity, we assume that ${}_1 \langle \varphi_{1H} | \varphi_{1V} \rangle_1 = {}_2 \langle \varphi_{2H} | \varphi_{2V} \rangle_2 = \eta_{12}$ and ${}_3 \langle \varphi_{3H} | \varphi_{3V} \rangle_3 = {}_4 \langle \varphi_{4H} | \varphi_{4V} \rangle_4 = \eta_{34}$. Then, from the estimated fidelities F_{12} and F_{34} , we have $\eta_{12} = 0.96$ and $\eta_{34} = 0.97$.

We also estimate the amount of the mode-mismatch from the visibility of the interference experiment in Sec. 5.3.1. Here we show the relation between the amount of the mode-mismatch and visibility. Under the current assumptions, V-polarized photons in modes 2 and 3 are written as $|V\rangle_2 | \varphi_{2V} \rangle_2$ and $|V\rangle_3 | \varphi_{3V} \rangle_3$. After the PDBS, which acts as 50: 50 BS for V-polarized photons, a coincidence counting at modes 5 and 6 will postselect the state

$$|\Gamma\rangle_{56} = \frac{1}{\sqrt{2}} |V\rangle_5 |V\rangle_6 [| \varphi_{2V} \rangle_5 | \varphi_{3V} \rangle_6 - | \varphi_{3V} \rangle_5 | \varphi_{2V} \rangle_6], \quad (5.20)$$

where the state is unnormalized. Then the probability of the coincidence detection is given by

$$\begin{aligned} M_s &= {}_{56} \langle \Gamma | \Gamma \rangle_{56} \\ &= 1 - | {}_5 \langle \varphi_{2V} | \varphi_{3V} \rangle_{56} \langle \varphi_{2V} | \varphi_{3V} \rangle_6 |. \end{aligned} \quad (5.21)$$

Since the visibility V measured in the experiment is $1 - V = M_s$, we have $\langle \varphi_{2V} | \varphi_{3V} \rangle = \sqrt{V} = 0.94$. We further assume that the mode-mismatch estimated from the visibility of the interference of V-polarized photons are the same for photons of various polarizations. That is, the mode-mismatch factor is the same regardless of the polarization of photons in modes 2 and 3. We set $\langle \varphi_{2V} | \varphi_{3V} \rangle = \langle \varphi_{2H} | \varphi_{3H} \rangle = \langle \varphi_{2H} | \varphi_{3V} \rangle = \langle \varphi_{2V} | \varphi_{3H} \rangle = \eta_V = 0.94$.

Using Eqs. (5.3), (5.16) and (5.17), and detecting H-polarized photon in mode 5, the output state is given by

$$\begin{aligned} |\theta\rangle &= |H\rangle_1 |V\rangle_6 |H\rangle_4 \left(\mu | \varphi_{2H} \rangle_5 | \varphi_{1H} \rangle_1 | \varphi_{3H} \rangle_6 | \varphi_{4H} \rangle_4 \right. \\ &\quad \left. + (\mu - 1) | \varphi_{3H} \rangle_5 | \varphi_{1H} \rangle_1 | \varphi_{2H} \rangle_6 | \varphi_{4H} \rangle_4 \right) \\ &+ \sqrt{\frac{1-\mu}{2}} |H\rangle_1 |H\rangle_6 |V\rangle_4 | \varphi_{2H} \rangle_5 | \varphi_{1H} \rangle_1 | \varphi_{3V} \rangle_6 | \varphi_{4V} \rangle_4 \\ &+ \sqrt{\frac{\mu}{2}} |V\rangle_1 |H\rangle_6 |H\rangle_4 | \varphi_{3H} \rangle_5 | \varphi_{1V} \rangle_1 | \varphi_{2V} \rangle_6 | \varphi_{4H} \rangle_4. \end{aligned} \quad (5.22)$$

Let us assume that we compensate amplitude imbalances by local filtering. Then the state is represented by

$$\begin{aligned}
|\Theta\rangle = \frac{1}{\sqrt{3}} & \left[|H\rangle_1 |V\rangle_6 |H\rangle_4 \left(\frac{\mu}{\nu} |\varphi_{2H}\rangle_5 |\varphi_{1H}\rangle_1 |\varphi_{3H}\rangle_6 |\varphi_{4H}\rangle_4 \right. \right. \\
& \left. \left. + \frac{\mu-1}{\nu} |\varphi_{3H}\rangle_5 |\varphi_{1H}\rangle_1 |\varphi_{2H}\rangle_6 |\varphi_{4H}\rangle_4 \right) \right. \\
& + |H\rangle_1 |H\rangle_6 |V\rangle_4 |\varphi_{2H}\rangle_5 |\varphi_{1H}\rangle_1 |\varphi_{3V}\rangle_6 |\varphi_{4V}\rangle_4 \\
& \left. + |V\rangle_1 |H\rangle_6 |H\rangle_4 |\varphi_{3H}\rangle_5 |\varphi_{1V}\rangle_1 |\varphi_{2V}\rangle_6 |\varphi_{4H}\rangle_4 \right]. \quad (5.23)
\end{aligned}$$

Where $\nu = \sqrt{2\mu^2 - 2\mu + 1 + 2\mu(\mu - 1)\eta_V^2}$. The expression for the fidelity of the prepared state to an ideal W state can be found using Eq. (5.23) in

$$\begin{aligned}
F_{W_3} &= {}_p\langle W | \text{Tr}_s[|\Theta\rangle\langle\Theta|] | W \rangle_p \\
&= \text{Tr}_p \left[(\text{Tr}_s[|\Theta\rangle\langle\Theta|]) | W \rangle_p \langle W | \right] \\
&= \text{Tr}_s[{}_p\langle W | \Theta \rangle \langle \Theta | W \rangle_p] \\
&= \frac{1}{9} \left\| \frac{\mu}{\nu} |\varphi_{2H}\rangle_5 |\varphi_{1H}\rangle_1 |\varphi_{3H}\rangle_6 |\varphi_{4H}\rangle_4 + \frac{\mu-1}{\nu} |\varphi_{3H}\rangle_5 |\varphi_{1H}\rangle_1 |\varphi_{2H}\rangle_6 |\varphi_{4H}\rangle_4 \right. \\
&\quad \left. + |\varphi_{2H}\rangle_5 |\varphi_{1H}\rangle_1 |\varphi_{3V}\rangle_6 |\varphi_{4V}\rangle_4 + |\varphi_{3H}\rangle_5 |\varphi_{1V}\rangle_1 |\varphi_{2V}\rangle_6 |\varphi_{4H}\rangle_4 \right\|^2 \\
&= \frac{1}{9} \left[\frac{2\mu^2 - 2\mu + 1}{\nu^2} + \frac{2\mu(\mu - 1)}{\nu^2} + \frac{2\mu(\eta_{34}^2 + \eta_V^2 \eta_{12})}{\nu} \right. \\
&\quad \left. + \frac{2(\mu - 1)(\eta_{12}^2 + \eta_V^2 \eta_{34})}{\nu} + 2\eta_V^2 \eta_{12} \eta_{34} + 2 \right]. \quad (5.24)
\end{aligned}$$

Substituting $\mu = (7 + \sqrt{17})/16$, $\eta_V = 0.94$ and $\eta_{12} = \eta_{34} = 1$, we obtain $F_{W_3} = 0.89$, which is considered to be coming from the mode mismatch between modes 2 and 3. If we include the imperfections in the initially prepared EPR photon pairs, $\eta_{12} = 0.96$ and $\eta_{34} = 0.97$, the fidelity further drops to $F_{W_3} = 0.87$.

Next, for amplitude imbalances of three diagonal terms of the final state observed in Fig. 5.9 (a), we consider how the prepared W state is improved by using local filtering. If we compensate the amplitude differences among the three diagonal terms in Fig. 5.9 (a), the fidelity of the prepared W state increases to 0.81. Furthermore, compensating the relative phase of the prepared W state $|W_3\rangle$ in Fig. 5.9 (a), the fidelity increases to 0.83. It is seen that the effect of the unequal weights of the diagonal elements of the density matrix of the

prepared state on the fidelity is much higher than that of the unwanted relative phase shift. Thus, we conclude that the residual imbalance explains further reduction from $F_{W_3} = 0.87$ by 0.04, arriving in the vicinity of the error bar of the observed fidelity, $F_{\text{exp}} = 0.778 \pm 0.043$.

In this chapter, we have proposed and experimentally demonstrated a method for converting two EPR photon pairs to a three-photon W state via LOCC, using a polarization dependent beamsplitter and post-selection. The achieved final state was shown to have various characteristics of the W state. This work extends our ability to manipulate multipartite entanglement, since our results imply that it is now possible to generate arbitrary three qubit states from a single resource of two EPR pairs via LOCC with a moderate success probability and with fidelity only limited by the imperfection of the apparatus.

Chapter 6

Conclusion and Future Prospects

6.1 Summary

In the first part of our work, we have proposed two optical gates for the preparation and expansion of photonic W states, and one optical gate for fusing two arbitrary size W state into a larger one. The gates work under the condition of local operations on a single site. The fusion gate also uses classical communication. In such a setting, there are two main difficulties in working with W states: One is that a W state cannot be expanded by a unitary operation. Another is that an added new qubit must form pairwise entanglement with the remaining qubits without direct interactions. A remedy for these difficulties is to allow probabilistic operations where successful events do not take place deterministically but once they take place the gate prepares the desired output with unit fidelity.

First, we have proposed a simple optical gate for expanding polarization entangled W states using a polarization dependent beamsplitter. This gate expands a state $|W_N\rangle$ into a state $|W_{N+1}\rangle$, and also prepares an arbitrary W state by cascading the gate. When an initial state is a photon from an EPR photon pair, this gate can prepare a three photon W state with a success probability of $3/10$ which is higher than all the previous schemes so far. Taking into account the imperfections encountered in practice, we analyzed its feasibility for the expansion of an EPR photon pair to the three photon W state. In addition, the gate

does not require stability of optical paths and does not require sub-wavelength adjustments. The gate used the beamsplitter which has different transmission/reflection characteristics for H- and V-polarized photons. On the other hand, next, we have proposed an elementary optical gate for expanding polarization entangled W state using two non-polarizing 50:50 beamsplitters. With a proper seeding, the gate can also be used for preparation of W states, and it has a larger success probability than other preparation methods for a four-photon W state. We showed that the gate is easy to demonstrate and feasible with the current experimental technologies. A fundamental characteristic of this gate is that polarization-dependent components play no essential role and two ancillary photons play a significant role. The gate has the property that just by modifying the state of the ancilla photons, a GHZ state can be prepared and expanded. These two gates have differences interestingly. For example, for the preparation of $|W_3\rangle$, the success probability $3/10$ of the former gate is higher than the success probability $3/16$ of the latter gate. If the gate is cascaded, the success probability of the former gate is smaller than that of the latter gate. Finally, we have proposed an optical fusion gate for polarization-entangled W states. The fusion gate takes the cost of preparing N -photon W states from an exponential overhead into a subexponential one; however, there are many open problems which needs a detailed analysis and consideration. For example, we do not know whether a polynomial scaling is possible or not, nor how much cost it takes for the preparation and the growth for a W state of desired size under various scenarios. Considering the obtained results, we believe that these gates will provide a simple and useful tool to probe interesting features of multipartite W states.

In the second part of our work, we proposed and experimentally demonstrated a transformation of two EPR photon pairs distributed among three parties into a three-photon W state using local operations and classical communication (LOCC). We showed that the proposed local transformation induced by a PDBS, polarization dependent loss and post-selection prepares a W state with high fidelity. We characterized the final state using quantum state tomography on the three-photon state and on its marginal bipartite states experimentally. The fidelity of the final state to the ideal W state is 0.778 ± 0.043 and

the expectation value for its witness operator is -0.111 ± 0.043 implying the success of the proposed local transformation. Considering the fact that entanglement is a quantum resource under LOCC, it is important to convert the common resource of entanglement, EPR photon pairs, into multi-qubit entangled states by using only LOCC. Our proposal and demonstration address this problem by proposing and demonstrating an effective method for direct conversion of two EPR photon pairs into a three-qubit W state via LOCC. Since the conversion of two EPR photon pairs to three-photon GHZ states has been already done, our achievement implies that we are now able to generate any state of three photons starting from a common resource of EPR photon pairs, which we believe is a significant advancement in our ability to manipulate quantum entanglement.

6.2 Future Outlook

During the studies which is the subject of this thesis, we proposed optical schemes for expanding and fusing W states, and experimentally demonstrated local transformation of two EPR photon pairs into a three-photon W state. With the techniques developed during this study, sharing tripartite and even larger W states among many distantly located parties has become within the reach of the current state-of-the-art quantum optics technologies. As a result of our work, we now know how to prepare one of the inequivalent classes of multipartite entanglement, namely the W state, from EPR pairs, which are one of the basic resources of quantum information science. Our toolbox to prepare inequivalent classes of tripartite entanglement using LOCC is now complete.

Although the recent studies including the present thesis have shown that parity checking gate plays an important role in fusing two GHZ states into a larger one, two W states into a larger W state, and two cluster states into a larger cluster, we still do not know whether parity checking gate can be used as a fusion gate for other classes of multipartite entanglement. This is partly due to the lack of complete understanding of the entanglement structure of those multipartite states. For example, fusion of two Dicke states, which are the equally weighted superposition of all permutations of H and V polarizations, into a

larger Dicke state is still an open problem. Indeed, at present there is only one proposal and demonstration for preparing a four-photon Dicke state [74].

There have been proposals to classify multipartite entangled states under various conditions [75, 76, 77]. Except for tripartite entanglement, multipartite entanglement is not well understood and there are few proposals for the preparation of multipartite entanglement of other classes so far. Thus we have many open questions to solve such as classification of the states, their efficient preparation using optical techniques, and their expansion. For a far future prospect, this direction sounds to be interesting, albeit a challenging task. We should keep in mind that it is such challenging tasks which are given us the advancement, and more innovative and surprising results in all of fields through science, technology and philosophy.

Appendix A

Expansion and fusion of polarization entangled GHZ states using a polarizing beamsplitter

We show the expansion and fusion for polarization entangled GHZ states using a polarizing beamsplitter.

The expansion gate for polarization entangled GHZ states is shown in Fig. A.1 (a). The gate is composed of a polarizing beamsplitter and a half wave plate (HWP) for compensating a phase shift. With the coincidence detection between modes 3 and 4, the successful gate operation is given by the following transformations

$$\begin{aligned} |1_H\rangle_1 |1_H\rangle_2 &\rightarrow -|1_H\rangle_3 |1_H\rangle_4, \\ |1_V\rangle_1 |1_V\rangle_2 &\rightarrow -|1_V\rangle_3 |1_V\rangle_4, \end{aligned} \tag{A.1}$$

where we have included the effect of the HWP in mode 4. If the input photon is one photon in a three-photon GHZ state $|\text{GHZ}_3\rangle = (|1_H\rangle_{0'} |1_H\rangle_0 |1_H\rangle_1 + |1_V\rangle_{0'} |1_V\rangle_0 |1_V\rangle_1) / \sqrt{2}$ and the new added photon is an equal superposition of H- and V- polarized photons,

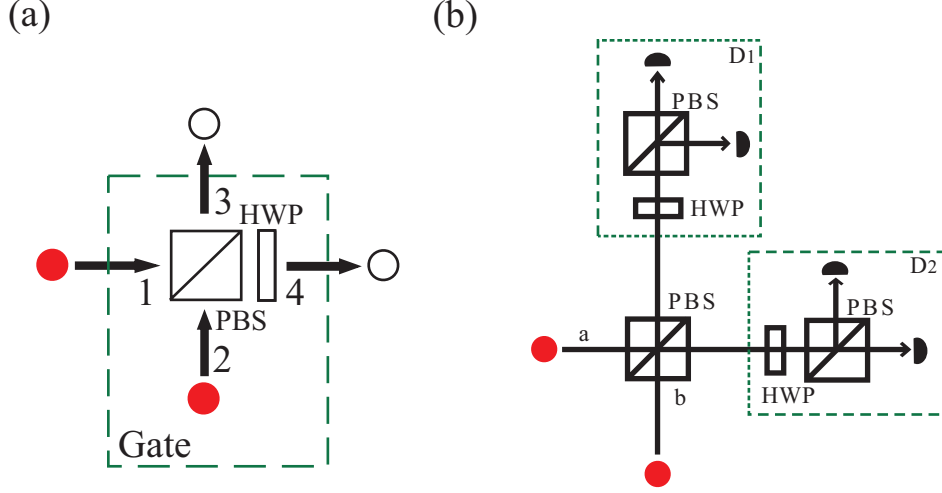


Figure A.1: (a) Expansion gate and (b) fusion gate for polarization entangled GHZ states. The expansion gate is composed of a polarizing beamsplitter (PBS) and a half wave plate (HWP) for compensating a phase shift. The fusion gate is composed of a PBS and two polarization discriminating detectors (D_1 and D_2). This discriminating detector is composed of a HWP, a PBS and two photodetectors.

$(|1_H\rangle_2 + |1_V\rangle_2)/\sqrt{2}$, the output state for the post-selected events are given by

$$\begin{aligned}
 |\text{GHZ}_3\rangle &\rightarrow -\frac{1}{2} [|1_H\rangle_{0'} |1_H\rangle_0 |1_H\rangle_3 |1_H\rangle_4 + |1_V\rangle_{0'} |1_V\rangle_0 |1_V\rangle_3 |1_V\rangle_4] \\
 &\rightarrow -\frac{1}{2} |\text{GHZ}_4\rangle,
 \end{aligned} \tag{A.2}$$

which means that the $|\text{GHZ}_4\rangle$ state is produced with probability $1/2$. From this result, It is also apparent that it expand any size of GHZ state $|\text{GHZ}_N\rangle$ to $|\text{GHZ}_{N+1}\rangle$ with the success probability $1/2$.

The fusion gate for polarization entangled GHZ states is shown in Figure A.1 (b). The gate is composed of a polarizing beamsplitter (PBS) and two polarization discriminating detectors (D_1 and D_2). This discriminating detector is composed of a HWP, a PBS and two photodetectors. If both polarization discriminating detectors (D_1 and D_2) have click events, it means that a GHZ state is fused with probability $1/2$. On the other hand, if

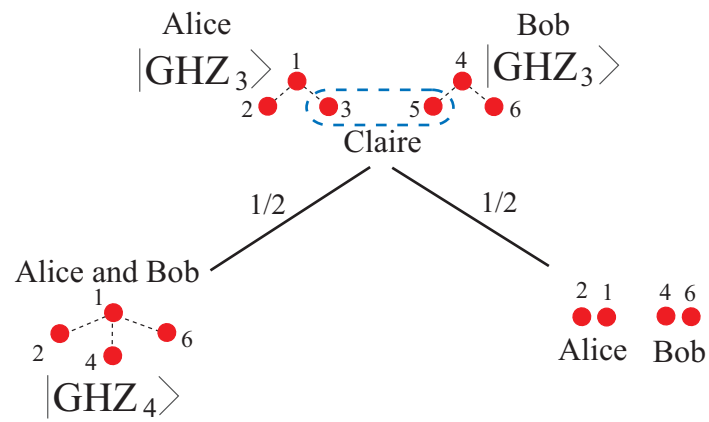


Figure A.2: Example of fusing two three-photon GHZ states.

either polarization discriminating detector D_1 or D_2 has a click events, it means that a fusion of the GHZ state is failed with probability $1/2$. Thus we can fuse any size of GHZ state $|\text{GHZ}_N\rangle$. We show the example of fusing two three-photon GHZ states $|\text{GHZ}_3\rangle$ in Fig. A.2.

Appendix B

Alignment

Here, we describe the methods we have employed for the alignment of beams for spontaneous parametric down conversion (SPDC) process. Since the single photons prepared by SPDC process cannot be seen by naked-eye, construction of the optical path along which they will travel and their efficient coupling to the detectors must be done using visible alignment beams. As the alignment beam for the construction of the optical paths, we use a part of the coherent light emitted from a mode-locked Ti:sapphire laser (wavelength 790nm; pulse width 90fs; repetition rate 82MHz).

In the first method, we send the alignment beam to a 50:50 BS such that the beam hits the BS at a slightly off center point. The transmitted and reflected portion of the beam are directed to right angle prisms, which are located on motorized stages, as shown in Fig. B.1 (a). The two beams return back to the beam splitter after travel along the prisms. These separated parallel beams (twin beams) are then directed to a system of two convex lenses with the first and second lenses, respectively, having focus lengths as $f = 80 \text{ mm}$ and $f = 90 \text{ mm}$. The parallel beams cross each other at the focus of the first lens and travels to the second lens (see Fig. B.1 (a)) that further directs them to a BBO crystal. If the twin beams spatially and temporally overlap on the BBO crystal, an ultraviolet (UV) pulse is generated by second harmonic generation (SHG). At the exit of the BBO, three beams are clearly seen. The UV beam has a wavelength of 395 nm, while the other two beams are residual twin beams with wavelengths of 790 nm. The intensity of the UV pulse

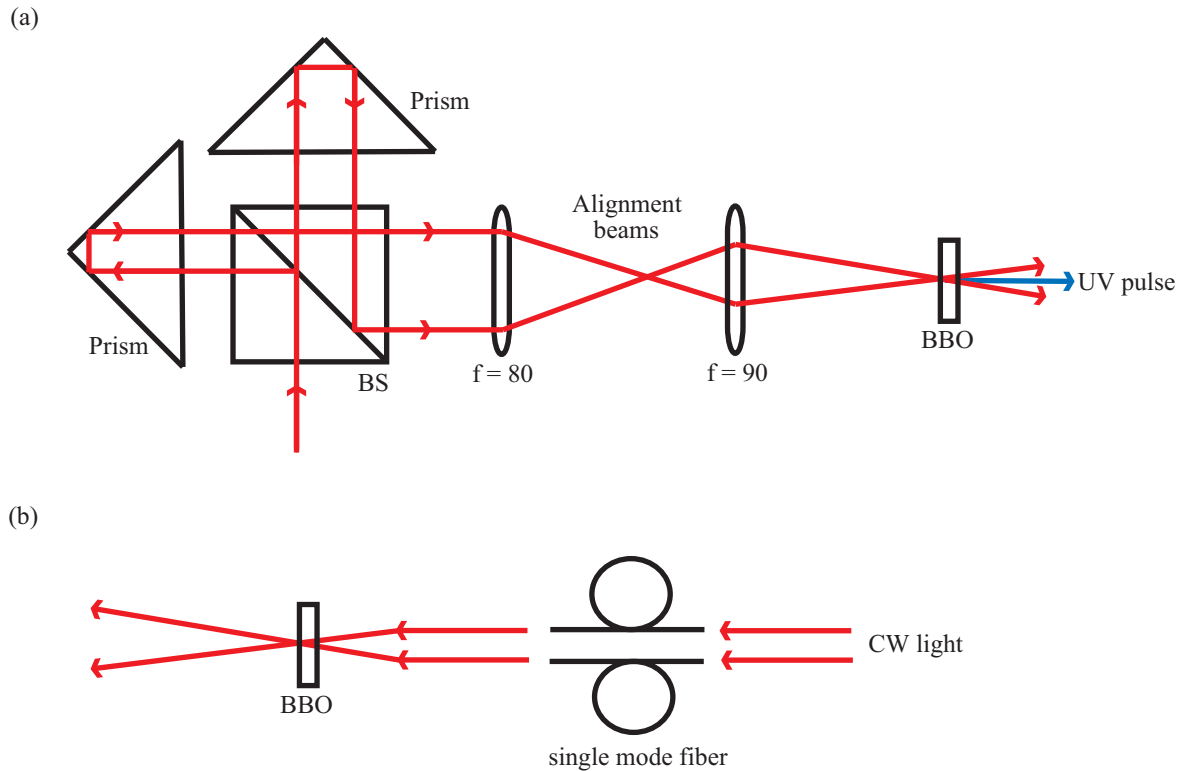


Figure B.1: (a) Preparation of the alignment beams and adjustment of the generation of UV pulse from BBO. (b) Alignment of backward optical paths

is then adjusted by properly focusing the twin beams on the BBO. One can check that the UV is due to the mixing of the twin beams on the BBO by blocking one of the twin beams and confirming that the UV beam disappears. After the maximization of the intensity of the UV beam, the two residual beams of the twin beams are used as the alignment beams to construct the optical paths between the BBO and the single-mode fiber (SMF) coupled single photon counter modules (SPCMs). Here, it is important that the maximal coupling into the SMF is achieved for both of the beams. The idea behind the efforts explained so far is that if the UV pulse used in the experiment of single photon pair preparation using BBO is overlapped with the UV pulse generated by the twin alignment beams, the idler and signal photons from the spontaneous parametric down conversion (SPDC) will be created in the direction of the twin alignment beams after the BBO. Thus, keeping the

twin alignment beams and the UV beam generated by mixing them on the BBO, we direct the UV pulse that will be used in the main experiment to the BBO in such a way that near-perfect overlap of the two UV beams are achieved both in size and the shape. After the maximal overlap is achieved, we block the twin beams, and use only the UV pump pulse for SPDC. By observing the count rates of the true idler and signal photons with SPCMs, we fine tune the fiber-coupler and the orientation of the BBO axis to maximize the detected signal and idler photons. This completes the process of constructing the forward optical paths.

In order to further optimize the optical paths and hence the coupling, we apply a backward optical path construction [see Fig. B.1 (b)]. In this method, we disconnect the SPCMs from the SMFs, and instead couple continuous-wave (CW) light (wavelength 790nm) from the same end of the fibers. The light beams coupled to SMFs then travel the optical paths back to the BBO and further. If the CW light beams, propagated past the BBO in backward direction, overlap with the twin alignment beams propagating in the forward direction, we accept the constructed paths. Otherwise, we fine tune the system until the overlap and photon count rate are maximized.

Appendix C

Measurement data

The measurement data for initial two EPR photon pairs using quantum state tomography is shown in Fig. C.1, and the measurement data for final prepared W state using quantum state tomography is also shown in Fig. C.2.

Base	Count
HH	6835
HV	86
VV	6744
VH	151
RH	3826
RV	2979
DV	3283
DH	3356
DR	3524
DD	181
RD	3922
HD	3002
VD	4142
VL	3460
HL	3586
RL	154

Base	Count
HH	7859
HV	173
VV	7879
VH	63
RH	3535
RV	4383
DV	4735
DH	3885
DR	4261
DD	99
RD	3071
HD	3785
VD	3383
VL	3672
HL	3911
RL	78

Figure C.1: Measurement data for initial two EPR photon pairs using quantum state tomography: (a) ρ_{12} and (b) ρ_{34} . One base measurement time 1 [s] and 2 [cycle].

Base	Count	Base	Count	Base	Count	Base	Count
HHH	2	HRD	30	RDH	46	DDR	34
HHV	69	VRD	16	RRH	64	DDV	26
HVV	4	VDD	17	RHH	31	DDH	70
HVH	82	HDD	73	RHV	39	DRH	37
VVH	0	HDR	37	RVV	1	DRV	11
VHH	54	VDR	13	RVH	30	LRV	9
VHV	1	VRR	11	DVH	36	LDV	15
VVV	0	HRR	65	DHH	36	LDR	13
VVR	0	HRH	45	DHV	37	LDD	33
VHR	36	HRV	27	DVV	1	LRD	14
HHR	37	VRV	0	DVR	18	LHD	26
HVR	43	VRH	22	DHR	35	LVD	16
HVD	24	VDH	31	DHD	54	LVL	20
VVD	1	VDV	1	DVD	13	LHL	53
VHD	30	HDV	37	DRD	46	LRL	9
HHH	39	HDH	39	DDD	65	DRL	19

Figure C.2: Measurement data for final prepared W state (ρ_{146}) using quantum state tomography. One base measurement time 20 [s] and 290 [cycle].

Publications

- 1 T. Tashima, Ş. K. Özdemir, T. Yamamoto, M. Koashi, and N. Imoto
“Elementary optical gate for expanding an entanglement web”
Phys. Rev. A. **77**, 030302(R) (2008).

- 2 T. Tashima, Ş. K. Özdemir, T. Yamamoto, M. Koashi, and N. Imoto
“An elementary optical gate for expanding symmetrically shared entanglement”
Theory of Quantum Computation, Communication, and Cryptography
Third Workshop TQC 2008 Tokyo, Japan, January/February 2008
Revised Selected Papers, Lecture Notes in Computer Science, Springer, pp70-82 (2008).

- 3 T. Tashima, Ş. K. Özdemir, T. Yamamoto, M. Koashi, and N. Imoto
“Local expansion of photonic W state using a polarization dependent beamsplitter”
New J. Phys. **11**, 023024 (2009).

- 4 T. Tashima, T. Wakatsuki, Ş. K. Özdemir, T. Yamamoto, M. Koashi, and N. Imoto
“Local transformation of two EPR photon pairs into a three-photon W state”
quant-ph/0812.3255.

Activities

International Conference

Oral presentation [1]

- 1 T. Tashima, Ş. K. Özdemir, T. Yamamoto, M. Koashi, and N. Imoto
“An elementary optical gate for expanding symmetrically shared entanglement”
3th Workshop on Theory of Quantum Computation, Communication, and
Cryptography, Japan,
January 30 -February 1 2008.

Poster presentation [4]

- 1 T. Tashima, Ş. K. Özdemir, T. Yamamoto, M. Koashi, and N. Imoto
“An optical gate for seeding large scale polarization entangled W-state”
3th Handai Nanoscience and Nanotechnology International Symposium, Japan,
September 26 - 28 2007.
- 2 T. Tashima, T. Wakatsuki, Ş. K. Özdemir, T. Yamamoto, M. Koashi, and N. Imoto
“Local transformation of two EPR photon pairs into a three-photon W state”
9th International Conference on Quantum Communication, Measurement and
Computing, Canada,
August 19 - 24 2008.
- 3 T. Tashima, Ş. K. Özdemir, T. Yamamoto, M. Koashi, and N. Imoto
“Local expansion of photonic W state using a polarization dependent beamsplitter”

4th Handai Nanoscience and Nanotechnology International Symposium, Japan,
September 29 - October 1 2008.

4 T. Tashima, T. Wakatsuki, Ş. K. Özdemir, T. Yamamoto, M. Koashi, and N. Imoto
“Preparation of a three-photon *W*-state from two EPR photon pairs by LOCC”
International Symposium on Physics of Quantum Technology, Japan,
November 25 - 28 2008.

Bibliography

- [1] E. Schödinger. "Die gegenwartige Situation in der Quantenmechanik", *Naturwissenschaften* **23**, 807 (1935).
- [2] A. Einstein, B. Podolsky and N. Rosen. Can Quantum-Mechanical Description of Physical Reality Be Considered Complete?, *Phys. Rev.* **47**, 777 (1935).
- [3] J. S. Bell. On the Einstein-Podolsky-Rosen paradox, *Physics* **1**, 195 (1964).
- [4] S. J. Freedman and J. F. Clauser, *Phys. Rev. Lett.* **28**, 938 (1972).
- [5] J. F. Clauser and A. Shimony, *Rep. Prog. Phys.* **41**, 1881 (1978).
- [6] A. Aspect, P. Grangier and G. Roger, *Phys. Rev. Lett.* **47**, 460 (1981).
- [7] C. H. Bennett, G. Brassard, C. Crepeau, R. Jozsa, A. Peres, and W. K. Wootters, *Phys. Rev. Lett.* **70**, 1895 (1993).
- [8] A. K. Ekert, *Phys. Rev. Lett.* **67**, 661 (1991).
- [9] M. A. Nielsen and I. L. Chuang, "Quantum Computation and Quantum Information", Cambridge university Press, (2000).
- [10] V. Giovannetti, S. Lloyd, L. Maccone, *Phys. Rev. Lett.* **96**, 010401 (2006).
- [11] M. Hillery, V. Bužek, and A. Berthiaume, *Phys. Rev. A.* **59**, 1829 (1999).
- [12] M. Murao, D. Jonathan, M. B. Plenio, and V. Vedral, *Phys. Rev. A.* **59**, 156 (1999).

- [13] J. Kempe, Phys. Rev. A. **60**, 910 (1999).
- [14] R. Raussendorf, D. E. Browne, and H. J. Briegel, Phys. Rev. A. **68**, 022312 (2003).
- [15] M. Bourennane, M. Eibl, S. Gaertner, C. Kurtsiefer, A. Cabello, and H. Weinfurter, Phys. Rev. Lett. **92**, 107901 (2004).
- [16] L. Xiao, G. L. Long, F. -G. Deng, and J. -W. Pan, Phys. Rev. A. **69**, 052307 (2004).
- [17] Z. Zhao, Y. -A. Chen, A. -N. Zhang, T. Yang, H. J. Bregel, and J. -W. Pan, Nature (London) **430**, 54 (2004).
- [18] E. D'Hondt, and P. Panangaden, Quant. Inf. and Comp. **6(2)**, 173 (2005).
- [19] P. Walther, K. J. Resch, T. Rudolph, E. Schenck, H. Weinfurter, V. Vedral, M. Aspelmeyer, and A. Zeilinger, Nature (London) **434**, 169 (2005).
- [20] N. Kiesel, C. Schmid, U. Weber, G. Tóth, O. Gühne, R. Ursin, and H. Weinfurter, Phys. Rev. Lett. **95**, 210502 (2005).
- [21] Y. Tokunaga, T. Yamamoto, M. Koashi, and N. Imoto, Phys. Rev. A. **71**, 030301(R) (2005).
- [22] S. Gaertner, C. Kurtsiefer, M. Bourennane, and H. Weinfurter, Phys. Rev. Lett. **98**, 020503 (2007).
- [23] N. Kiesel, C. Schmid, G. Tóth, E. Solano, and H. Weinfurter, Phys. Rev. Lett. **98**, 063604 (2007).
- [24] C. -Y Lu, X. -Q. Zhou, O. Gühne, W. -B. Gao, J. Zhang, Z. -S. Yuan, A. Goebel, T. Yang, J. -W Pan, Nature Physics (London) **3**, 91 (2007).
- [25] Y. Tokunaga, S. Kuwashiro, T. Yamamoto, M. Koashi, and N. Imoto, Phys. Rev. Lett. **10**, 210501 (2008).

- [26] T. Yamamoto, K. Hayashi, Ş. K. Özdemir, M. Koashi, and N. Imoto, *Nature Photonics*. **2**, 488 (2008).
- [27] D. M. Greenberger, M. Horne, and A. Zeilinger, in *Bell 's Theorem, Quantum Theory, and Conceptions of the Universe*, edited by M. Kafatos (Kluwer, Dordrecht, 1989); D. M. Greenberger, M. A. Horne, A. Shimony, and A. Zeilinger, *Am. J. Phys.* **58**, 1131 (1990).
- [28] M. Koashi, V. Bužek, and N. Imoto, *Phys. Rev. A*. **62**, 050302(R) (2000).
- [29] W. Dür, *Phys. Rev. A*. **63**, 020303(R) (2001).
- [30] H. J. Briegel and R. Raussendorf, *Phys. Rev. Lett.* **86**, 910 (2001).
- [31] R. H. Dicke, *Phys. Rev.* **93**, 99 (1954).
- [32] A. Zeilinger, M. A. Horne, H. Weinfurter, and M. zukowski, *Phys. Rev. Lett.* **78**, 3031 (1997).
- [33] D. Bouwmeester, J. -W. Pan, M. Daniell, H. W. Weinfurter, and A. Zeilinger, *Phys. Rev. Lett.* **82**, 1345 (1999).
- [34] J. G. Rarity, and P. R. Tapster, *Phys. Rev. A*. **59**, R35 (1999).
- [35] K. J. Resch, P. Walther, and A. Zeilinger, *Phys. Rev. Lett.* **94**, 070402 (2005).
- [36] Y. L. Lim and A. Beige, *Phys. Rev. A*. **71**, 062311 (2005).
- [37] P. Walther, M. Aspelmeyer, and A. Zeilinger, *Phys. Rev. A*. **75**, 012313 (2007).
- [38] A. Zeilinger, M. A. Horne, and D. M. Greenberger, *NASA Conf. Publ.* **3135**, 73 (1997).
- [39] T. Yamamoto, K. Tamaki, M. Koashi, and N. Imoto, *Phys. Rev. A*. **66**, 064301 (2002).
- [40] N. Kiesel, M. Bourennane, C. Kurtsiefer, W. Laskowski, and M. Zukowski, *J. Mod. Opt.* **50**, 1131 (2003).

- [41] M. Eibl, N. Kiesel, M. Bourennane, C. Kurtsiefer, and H. Weinfurter, Phys. Rev. Lett. **92**, 077901 (2004).
- [42] H. Mikami, Y. Li, K. Fukuoka, and T. Kobayashi, Phys. Rev. Lett. **95**, 150404 (2005).
- [43] P. Walther, K. J. Resch, and A. Zeilinger, Phys. Rev. Lett. **94**, 240501 (2005).
- [44] X. Zou, K. Pahlke, and W. Mathis, Phys. Rev. A. **66**, 044302 (2002).
- [45] B. -S. Shi, and A. Tomita, J. Mod. Opt. **52**, 755 (2005).
- [46] Y. Li, and T. Kobayashi, Phys. Rev. A. **70**, 014301 (2004).
- [47] T. B. Pittman, B. C. Jacobs, and J. D. Franson, Phys. Rev. A. **64**, 062311 (2001).
- [48] T. Tashima, Ş. K. Özdemir, T. Yamamoto, M. Koashi, and N. Imoto, New J. Phys. **11**, 023024 (2009).
- [49] T. Tashima, Ş. K. Özdemir, T. Yamamoto, M. Koashi, and N. Imoto, Phys. Rev. A. **77**, 030302(R) (2008).
- [50] T. Tashima, T. Wakatsuki, Ş. K. Özdemir, T. Yamamoto, M. Koashi, and N. Imoto, quant-ph/0812.3255.
- [51] B. Schumacher, Phys. Rev. A **51**, 2738 (1995).
- [52] A. Uhlmann, Rep. Mat. Phys. **9**, 273 (1976).
- [53] W. K. Wootters Phys. Rev. Lett. **80**, 2245 (1998).
- [54] V. Coffman, J. Kundu, and W. K. Wootters, Phys. Rev. A. **61**, 052306 (2000).
- [55] A. Peres, Phys. Rev. Lett. **77**, 1413 (1996).
- [56] M. Horodecki, P. Horodecki, and R. Horodecki, Phys. Lett. A **223**, 1 (1996).
- [57] M. Horodecki, P. Horodecki, R. Horodecki, Phys. Rev. Lett. **80**, 5239(1998).

- [58] W. Dür, G. Vidal, and J. I. Cirac, Phys. Rev. A. **62**, 062314 (2000).
- [59] Yu-xi Liu, A. Miranowicz, M. Koashi, and N. Imoto, Phys. Rev. A. **66**, 062309 (2002).
- [60] N. D. Mermin, Phys. Rev. Lett. **65**, 1838 (1990).
- [61] A. Acín, D. Bruß, M. Lewenstein, and A. Sanpera Phys. Rev. Lett. **87**, 040401(2001).
- [62] O. Gühne and P. Hyllus, Int. J . Theor. Phys. **42**, 1001 (2003).
- [63] M. Bourennane, M. Eibl, C. Kurtsiefer, S. Gaertner, H. Weinfurter, O. Guhne, P. Hyllus, D. Brus, M. Lewenstein, and A. Sanpera, Phys. Rev. Lett. **92**, 087902 (2004).
- [64] P. G. Kwiat, E. Waks, A. G. White, I. Appelbaum, and P. H. Eberhard, Phys. Rev. A. **60**, R773 (1999).
- [65] D. F. V. James, P. G. Kwiat, W. J. Munro, and A. G. White, Phys. Rev. A. **64**, 052312 (2001).
- [66] Y. Vardi and D. Lee, J. R. Statist. Soc. B **55**, 569 (1993).
- [67] Z. Hradil, J. Summhammer, H. Rauch , Phys. Lett. A **261**, 20 (1999).
- [68] J. Řeháček, Z. Hradil, and M. Ježek, Phys. Rev. A. **63**, 040303(R) (2001).
- [69] J. Fiurášek, Phys. Rev. A. **64**, 024102 (2001).
- [70] J.-. W. Pan, Z.-B. Chen, M. Zukowski, H. Weinfurter, and A. Zeilinger, quant-ph/0805.2853
- [71] Ş. K. Özdemir, A. Miranowicz, M. Koashi, and N. Imoto, Phys. Rev. A. **66**, 053809 (2002).
- [72] T. Yamamoto, M. Koashi, and N. Imoto, Phys. Rev. A. **64**, 012304 (2001).
- [73] Ş. K. Özdemir, A. Miranowicz, M. Koashi, and N. Imoto, Phys. Rev. A. **64**, 063818 (2001).

- [74] N. Kiesel, C. Schmid, G. Toth, E. Solano, and H. Weinfurter, *Phys. Rev. Lett.* **98**, 063064 (2007).
- [75] F. Verstraete, J. Dehaene, B. De Moor, and H. Verschelde, *Phys. Rev. A.* **65**, 052112 (2002).
- [76] L. Lamata, J. León, D. Salgado, and E. Solano, *Phys. Rev. A.* **74**, 052336 (2006).
- [77] L. Lamata, J. León, D. Salgado, and E. Solano, *Phys. Rev. A.* **75**, 022318 (2007).